POLITECNICO DI MILANO

SCHOOL OF INDUSTRIAL AND INFORMATION ENGINEERING

Master of Science in Chemical Engineering

Master Thesis

Computational Fluid Dynamics of Multiphase Flow Using ANSYS Fluent

Academic Supervisor

Prof. Alessio Frassoldati

Industrial Supervisor

Ing. Paolo Vergani

Candidate

Omar Elshawarby

ID Number

919480

Academic Year 2020-2021

DEDICATION

I would like to dedicate this thesis work to the soul of my father with much love and respect.

May your soul rest in peace.

ACKNOWLEDGEMENTS

I would like to express my gratitude to everyone who has helped me during this thesis work.

First, I would like to thank my academic supervisor in Politecnico di Milano Professor Alessio Frassoldati who did not keep any effort in advising me when I started my thesis. He always encouraged me to do a great job and provided me with many suggestions and guidelines with his knowledge and patience during the development of this thesis work.

Besides, I am very grateful to Tecnimont for giving me the possibility to do an internship for almost a year which greatly helped me in doing this work.

Special thanks to my company supervisor Mr Paolo Vergani for sharing his own experience which greatly improved my knowledge about the oil and gas industry. He guided me through many problems and was always patient in listening to my problems and giving me suggestions to complete my work. Moreover, I had the opportunity to meet and work with extraordinary people such as Mr Tafuri Gianlorenzo and my colleagues Davide and Andrea. They spent much time helping me and therefore, they deserve so much gratitude.

Huge gratitude is directed to my mother because of her endless love, prayers and support since I was born in which I would never become who I am without her. The hands that held me first are still the ones that hold me when I feel lost and I am forever grateful for you, my mom.

Moreover, I would never forget the love and support from my sister Norhan and my brother Ali. You were always beside me through thick and thin and nothing would be accomplished without being by my side. In addition, I would never forget the prayers from my grandparents that always supported me.

In addition, I would like to thank my best friends Bassam, Wagdy, Hisham and Zaki for the great moments shared with them during this exciting path and for being always very close to me.

Finally, I would like to thank my life partner, my fiancée Nada. We faced a lot since we came here that taught us how to overcome obstacles together. Moreover, no words can describe how much she supported me during this work, and I hope to continue our life together and be always supportive to each other.

ABSTRACT

In many industries, especially the oil and gas one, multiphase systems are very common and numerically simulating them is vital to both study them without the need to go to the lab and be able to even modify their phenomena. Computational fluid dynamics (CFD) is a relatively new technique, established in the second half of the 20th century and that can be used to simulate any fluid flow. However, since the numerical simulation of multiphase flow systems is particularly challenging due to their complexity, CFD has only started a few years ago to study these complex systems. Therefore, many areas related to the modelling of multiphase flow systems in CFD are still vague and need investigation. Phase interaction force is one of these vague areas as there are many forces of interaction between different phases (Drag, Lift, Wall lubrication,..etc) in which each one has multiple models to be used. The purpose of this thesis is to study all these forces and their available models in ANSYS Fluent to find which forces and what models should be considered to better simulate a multiphase flow system. Our first step was to perform a sensitivity analysis on all these forces and models using an experimental study (Case study 1) as a reference case. The analysis showed that adding the forces of Drag, Wall lubrication, turbulent dispersion with specifically selected sub-models increased the accuracy of the overall CFD simulation. On the other hand, Virtual mass and Lift forces were excluded because they made our model either diverge or predict wrong/unrealistic values of our parameters. After that, our selected model was then revalidated using another experiment with more complex geometry (Case study 2) and it accurately predicted the measured parameters. Finally, the model was tested on an industrial case study (Case study 3) in which the two-phase flow system had a problem of having asymmetric behaviour. The model was able to both predict this behaviour and solve it using a newly proposed geometry.

GLOSSARY

Notations

ρ	*Density*	a	*Acceleration*
λ, ψ	*Dimensionless Parameters in Baker Chart*	A	*Area*
μ	*Dynamic Viscosity*	B	*Birth of the Particle*
f_i	*Friction Coefficient*	D	*Death of the Particle*
n_i	*Number Density of Size Group (i)*	d	*Diameter*
β	*Particulate Loading*	Eo	*Eotvos Number*
σ_t	*Prandtl Number*	F	*Force*
λ_{RT}	*Rayleigh-Taylor Instability Wavelength*	g	*Gravitational Acceleration*
ω	*Specific Dissipation Rate*	G	*Growth*
σ	*Surface Tension*	R	*Interaction Force Between Different Phases*
η_t	*Turbulent Diffusivity*	K	*Interface Momentum Exchange Coefficient*
ε	*Turbulence Dissipation Rate*	$\dot{m}$	*Mass Flowrate*
τ	*Viscous Stress Tensor*	P	*Mean Pressure*
α	*Volume Fraction*	U	*Mean Velocity Field*
St	*Stokes Number*	Mo	*Morton Number*
t	*Time*	p	*Pressure*
u	*Velocity*	Re	*Reynolds Number*
		S	*Source term*

Abbreviations

BFD	*Block Flow Diagram*	QMOM	*Quadrature Method of Moments*
CPP	*Central Processing Plant*	RANS	*Reynolds Average Navier-Stokes*
CFD	*Computational Fluid Dynamics*	RSM	*Reynolds Stress Model*
DNS	*Direct Numerical Simulation*	SMM	*Standard Method of Moments*
LES	*Large Eddy Simulation*	SIMPLE	*Semi Implicit Method for Pressure Linked Equations*
PBM	*Population Balance Model*	3D	*Three Dimensional*
PDF	*Probability Density Function*	VOF	*Volume of Fluid Model*

TABLE OF CONTENT

ACKNOWLEDGEMENTS II

ABSTRACT III

GLOSSARY IV

TABLE OF CONTENT VI

1 INTRODUCTION 1

2 LITERATURE REVIEW 4

2.1 Multiphase Flow Definition 4

2.2 Multiphase Flow Regimes 4

2.2.1 Gas-Liquid Flow 4

2.2.2 Gas-Solid Flow 5

2.2.3 Liquid-Solid Flow 5

2.2.4 Three-Phase Flow 5

2.3 Gas-Liquid Multiphase Flow Patterns 5

2.3.1 Vertical Flow in Pipes 7

2.3.1.1 Bubbly Flow 7

2.3.1.2 Plug Flow (Slug) 8

2.3.1.3 Churn Flow 8

2.3.1.4 Annular Flow 8

2.3.2 Horizontal Flow in Pipes 9

2.3.2.1 Stratified Flow 9

2.3.2.2 Bubble Flow 9

2.3.2.3 Wavy Flow 9

2.3.2.4 Plug Flow (Elongated Bubble Flow) 10

2.3.2.5 Slug Flow 10

2.3.2.6 Annular Flow 10

2.3.3 Flow Pattern Maps 11
2.3.3.1 Vertical Flow in Pipes Map 12
2.3.3.2 Horizontal Flow in Pipes Map 13
2.4 Multiphase Modelling 14
2.4.1 Euler-Lagrange Approach 14
2.4.2 Euler-Euler Approach 17
2.4.2.1 Eulerian Model 18
2.4.2.2 Volume of Fluid Model 20
2.4.2.3 Mixture Model 21
2.4.3 Interaction Forces Between the Phases 22
2.4.3.1 Interface Exchange Coefficient (Kpq): 23
2.4.3.1.1 Schiller and Naumann Model 24
2.4.3.1.2 Morsi and Alexander Model 24
2.4.3.1.3 Symmetric Model 24
2.4.3.1.4 Grace et al. Model 25
2.4.3.1.5 Tomiyama et al. Model 27
2.4.3.1.6 Universal Drag Law 27
2.4.3.2 Lift Force 28
2.4.3.2.1 Saffman-Mei Model 29
2.4.3.2.2 Legendre-Magnaudet Model 29
2.4.3.2.3 Moraga Model 30
2.4.3.2.4 Tomiyama Model 31
2.4.3.3 Wall Lubrication Force 31
2.4.3.3.1 Antal et al. Model 32
2.4.3.3.2 Tomiyama Model 33
2.4.3.3.3 Frank Model 33
2.4.3.3.4 Hosokawa Model 34

2.4.3.4 Turbulence Dispersion Force 34
2.4.3.4.1 Lopez de Bertodano Model 35
2.4.3.4.2 Simonin Model 35
2.4.3.4.3 Burns et al. Model 36
2.4.3.4.4 Diffusion in VOF Model 36
2.4.3.4.5 Limiting Function in the Turbulence Dispersion Force 36
2.4.3.5 Virtual Mass Force 37
2.4.4 Population Balance Model (PBM) 38
2.4.5 How to Choose Between Different Multiphase Models 40
2.5 Turbulence Modelling 44
2.5.1 Reynolds Average Navier-Stokes Equations 46
2.5.2 Boussinesq Hypothesis for ($k-\varepsilon$) and ($k-\omega$) Models 47
2.5.3 Reynolds Stress Model (RSM) 47
2.5.4 Turbulence in Multiphase System 48
2.6 Solution Methods 50
2.6.1 Finite Volume Method 50
2.6.1.1 Centre Node Based Finite Volume Method 51
2.6.2 Coupled Versus Segregated Solvers 51
3 CASE STUDY 1 53
3.1 Experimental Work 53
3.1.1 Experimental Procedure 54
3.1.2 Experimental Results 57
3.2 Simulation Methodology 61
3.3 Results and Discussion 69
3.3.1 Sensitivity Analysis on Phase Interaction Force Models 69
3.3.1.1 Drag Force 69
3.3.1.2 Wall Lubrication Force 74

3.3.1.3 Turbulence Dispersion Force 76
3.3.1.4 Turbulence Interaction Force 79
3.3.1.5 Lift Force and Virtual Mass Force 81
3.3.2 Revalidation Using Other Experimental Cases 83
4 CASE STUDY 2 92
4.1 Experimental Work 92
4.2 Simulation Methodology 94
4.3 Results and Discussion 101
4.3.1 Phase Separation Phenomenon 101
4.3.2 Effect of Bubble Diameter 101
5 CASE STUDY 3 (INDUSTRIAL) 107
5.1 Introduction 107
5.2 Simulation Methodology 108
5.3 Results and Discussion 116
5.3.1 Monophase Flow (Water Only) 116
5.3.2 Multiphase Flow (Water-Air) 121
6 CONCLUSION 126
7 REFERENCES 129
8 APPENDICES 133
8.1 List of Figures 133
8.2 List Of Tables 137

1 INTRODUCTION

Multiphase flow is common in many industrial processes and unit operations including pipelines, evaporators, crystallizers, chemical reactors,…etc. One of the industries that strongly includes dealing with multiphase systems is the oil and gas industry. It is the leading industry in the chemical and energy sector, ranging from the ability to fulfil our energy needs to supplying raw materials for most of the chemical industries (petrochemical industry in particular).

Therefore, any slight enhancement in this sector would lead to a major revenue for the companies in these industries.

In my point of view, the first step in the enhancement of any process should be the ability to numerically simulate it. Through simulation, we can gain insight into the process, study its parameters and how they can impact the overall process without even the need to go to the lab. This can be a lifesaver in the case of studying a complex system in which the experimental characterization would require a lot of time and money to perform such experiments.

Computational fluid dynamics or CFD was developed during the second half of the 20th century and became an established analysis tool for process simulation of systems involving fluid flow, heat transfer and associated phenomena such as chemical reactions through computer-based simulation. The technique is very powerful and has a wide range of industrial applications with the development of some software like ANSYS Fluent that was used in this thesis. However, it became widely used just in the 1990s and the reason for this delay in its industrial applicability was the high complexity and computational cost, which required the availability of high-performance computing hardware.

In the last two decades and after the recent technological development in computing hardware and software, CFD was able to model complex systems such as systems with more than one phase (multiphase systems). Moreover, different multiphase models were developed in which each one of them has its approximations and specific

applications. However, this was a recent development and so dealing with multiphase flow using CFD is still new, and many areas of studies are still vague and need digging.

One of these areas that need studying is the interaction between different phases. There are several interaction forces between both primary and secondary phases in a multiphase system, such as:

- Drag Force
- Lift Force
- Wall lubrication force
- Turbulence dispersion force
- Virtual mass force

All these forces have several modelling options in the available CFD codes, including ANSYS Fluent, and each one has its application. In this thesis study, all these options were studied and validation using a multiphase experiment was done using these several options to find the best combination of these models that best fit the experiment results. Moreover, this combination was revalidated through a second experiment. Finally, this combination of models was used in an industrial application to find its ability to simulate the case, monitor any problem and design a modified solution using CFD.

This thesis is organised into eight chapters. After the introduction in Chapter 1, Chapter 2 is mainly focused on the theory of multiphase flow systems, multiphase models in ANSYS fluent and phase interaction force models. Moreover, some basic theories about the population balance models (PBM), turbulence models and solution methods are also added.

In Chapter 3, a sensitivity analysis for the phase interaction force models is presented in which the selection of the best models is done through the validation with experimental data and an overall multiphase model was selected. In Chapter 4, this selected model is revalidated through different experimental data, but in complex geometries and in Chapter 5, a real industrial case study is presented in which our

multiphase model was used to accurately predict different phenomena occurring in the multiphase system, identify the critical points and design solutions to overcome the problems.

Finally, the conclusions are drawn from the study in Chapter 6, references are stated in Chapter 7 and the appendices are present in Chapter 8.

2 LITERATURE REVIEW

2.1 Multiphase Flow Definition

Most of the flows encountered in any industrial application are a combination of phases. Physical phases can be defined for a matter as gas, liquid, and solid, however, the term “phase” used in the industry is more than that.

In multiphase flow, a phase is defined as an identifiable class of material that has a particular inertial response to and interaction with the flow and the potential field in which it is immersed.[1]

For example, completely different-sized solid particles of the same material can be treated as different phases as a result of having different responses for each class of material sizes to the flow field and so, it is not just solid versus liquid, gas versus solid,…etc.

2.2 Multiphase Flow Regimes

Among all the possible combination of phases and so a wide range of flow regimes, we can identify four basic categories (based on the type of phases encountered in the flow regime):

2.2.1 Gas-Liquid Flow

The motion of bubbles in a liquid, as well as liquid droplets suspended in a gas stream, are all examples of gas-liquid flows.

It is very common to encounter gas-liquid flow in the industry. For example, bubble columns are commonly used in several process industries. Spray atomization to generate small droplets for combustion is important in power generation systems. Oil-gas flow coming from the wells is a common example of handling gas-liquid flow. Another example is the steam-water flows in pipes and heat exchangers used in power systems such as fossil fuel plants and nuclear reactors. Gas-liquid flows in pipes can assume several different configurations (patterns) ranging from bubbly flow to annular flow[2]. These configurations will be discussed in detail in the next section.

2.2.2 Gas-Solid Flow

Gas–solid flows usually refer to gas with suspended solid particles. This category of flow can be found in fluidized beds, cyclones separators and electrostatic precipitators. The combustion of coal in fossil–fuel power systems depend on the dispersion and burning of coal particles and so gas-solid flow study is important in this part.

If the particles are motionless, the gas-solid flow is considered as a gas flow through a porous medium (packed solid particles) in which the viscous force on the particle surfaces is the primary mechanism affecting the gas flow; a pebble-bed heat exchanger is an example of this type of flow. In this case, even though one phase is not "flowing," it will be included as a type of multiphase flow.[2]

2.2.3 Liquid-Solid Flow

It is solid particles being carried by the liquid and it always referred to as "slurry flows". Slurry flows can be found in a wide range of applications such as the transport of coals and ores to the flow of mud. As gas-solid flows, the flow of liquid through a stationary solid is another example of porous media flow.[2]

2.2.4 Three-Phase Flow

A three-phase flow is a mix between any of the previous flow regimes. For example, bubbles in a slurry flow give rise to three phases flowing together. Oil-gas flow coming from the well accompanied by a significant amount of water is another example of a three-phase flow that should be separated using a three-phase separator to handle each phase individually. A large number of possibilities are found here. However, it is not our scope in this thesis to study three-phase flow and so it shall not be discussed in detail.[2]

2.3 Gas-Liquid Multiphase Flow Patterns

In Gas-Liquid flow, there are lots of configurations for the geometry of the flow named flow patterns. These different configurations affect the hydrodynamics, heat and mass transfer, pressure drop,.. etc. Moreover, studying these configurations is important

because it was proven that there is no single correlation that can model this multiphase flow for the whole range of gas/liquid flows from 100% liquid to 100% gas.

In the past, flow pattern identification was by visual observation of the flow in transparent tubes in which both liquid and gas at different flow rates were injected. One problem appeared, a lot of possible shapes were identified and so many reported flow patterns were inevitable. It was solved by considering only the patterns of practical use, and a small number of major patterns have been agreed in the scientific literature, as described below.

One more problem came into view, i.e. how to assign a given flow to one of the known flow patterns. In other words, how to say that a given flow is bubbly flow or any other type of pattern. In narrow tubes, at moderate fluid velocities, you can recognize the flow pattern by eye (as in the experiments), but this is not always possible as in the case of high flow velocities, wider tubes or at the shell side of heat exchangers. In all these cases, it is impossible to see anything.

One possible solution was to photograph with a high-speed flash or high-speed video study.

Another more objective and quantitative method was the measurements of time-varying cross-sectionally averaged void fraction at one cross-section in a pipe using X-ray and then plotting the Probability Density Function (PDF) of these measurements.

This PDF can be used as a fingerprint for each flow pattern. For example, bubbly flow gives a single peak at low void fractions, annular flow gives a single peak at high void fractions, and slug flow gives two peaks.

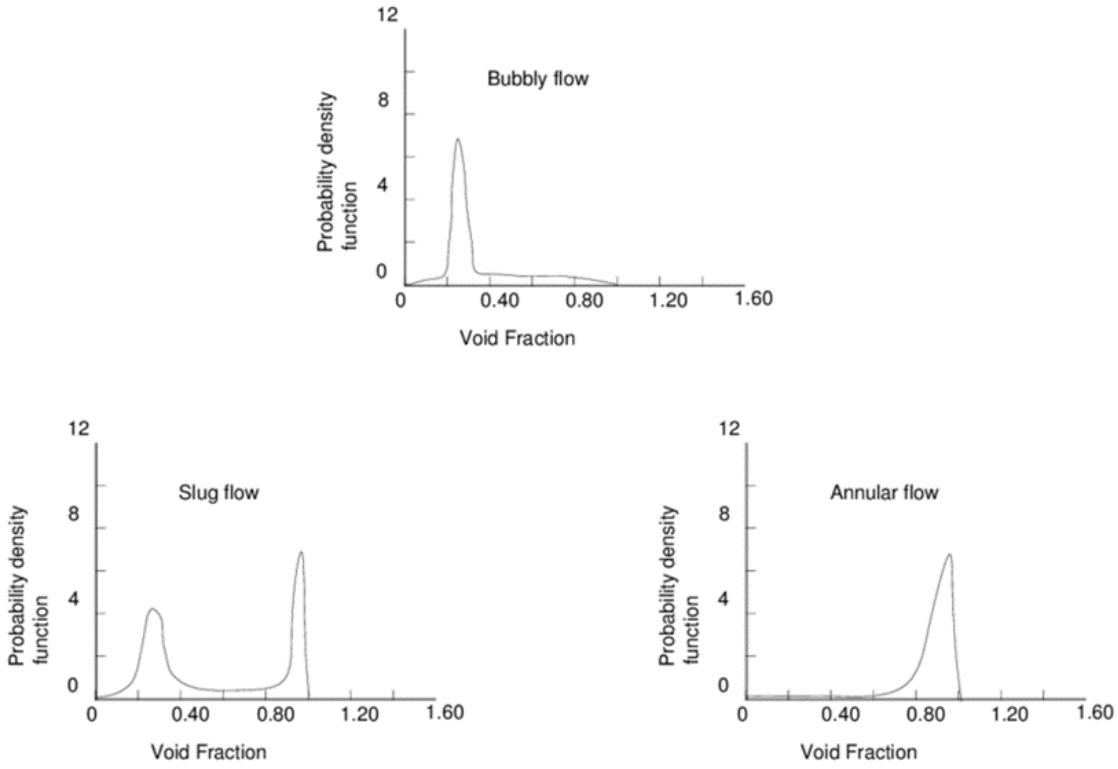

Figure 1: X-ray absorption Probability Density Functions of a void fraction by Jones and Zuber (1975)

Other approaches used more sophisticated statistical analyses than that of time-varying data.[4]

The major flow patterns for both vertical and horizontal flows are defined below:

2.3.1 Vertical Flow in Pipes

Four main flow patterns are considered in the vertical gas-liquid flow. They are shown in figure 2:

2.3.1.1 Bubbly Flow

It can be described as a continuous liquid phase with the gas phase being dispersed as bubbles within it and it usually arises when we are dealing with high liquid velocity compared to the gas one, discussed in section 2.3.3. These bubbles travel with a complex motion within the flow due to the liquid turbulence, maybe coalescing or breaking and are of non-uniform shapes and sizes. In some situations, they can gather at the pipe centre, in others, near the pipe walls.

2.3.1.2 Plug Flow (Slug)

It is often referred to as slug flow in vertical systems, and it occurs when coalescence between the bubble increases due to increasing the gas velocity and leading to having continuous large bubbles in the centre of the pipe. These characteristic bullet-shaped bubbles are called “Taylor bubbles” and they are surrounded by a thin film of liquid. In these thin liquid layers between the Taylor bubbles, there is a dispersion of smaller bubbles.

2.3.1.3 Churn Flow

It can be considered as an intermediate stage between the slug flow and annular flow, and it covers a wide range of gas flow rates. When velocities increase than that of the slug flow, the Taylor bubbles/liquid slugs in the plug flow break down into an unstable pattern in which there is a churning or oscillatory motion of liquid in the tube.

2.3.1.4 Annular Flow

Annular flow is characterized by liquid travelling as a thin layer film on the pipe wall and gas flowing as a continuous stream in the centre. Moreover, part of the liquid can also be carried as drops in the central gas core. It occurs when having a large gas flow rate compared to the liquid one. For certain flow rates, most of the liquid travels as drops and no thin film is formed on the walls, leading to the term “mist flow”. At very high liquid flow rates liquid droplets concentration in the gas core become so high that tendrils of liquid are observed instead of droplets, and this is called “wispy annular flow”.[4]

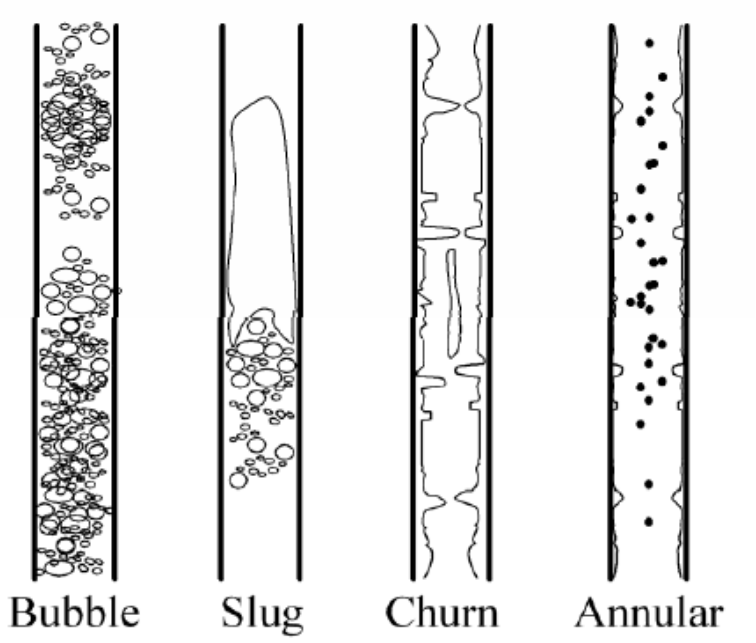

Figure 2: Flow patterns in vertical gas-liquid flow.[4]

2.3.2 Horizontal Flow in Pipes

Six main flow patterns are considered in the horizontal gas-liquid flow. They are shown in figure 3 and the increase of the number of patterns in the case of the horizontal flow is because of the gravity effect that acts perpendicular to the tube axis leading to the separation of phases and hence increases the pattern possibilities:

2.3.2.1 Stratified Flow

At both low liquid and gas velocities, there is a complete separation between the gas and liquid. The two phases are separated by an undisturbed horizontal interface in which the liquid is flowing over the bottom of the tube and the gas at the top (under normal gravity conditions).

2.3.2.2 Bubble Flow

Gas bubbles are dispersed in the continuous liquid flow (like the one in the vertical flow). This flow pattern occurs for high liquid velocity and small gas velocity.

2.3.2.3 Wavy Flow

When the gas velocity is increased in stratified flow, waves start to form on the liquid-gas interface. These waves travel in the direction of the flow and the amplitude of

these waves depends on the relative velocity between the phases and the properties of the fluids, such as their density and surface tension.

2.3.2.4 Plug Flow (Elongated Bubble Flow)

This flow pattern occurs at low gas flow rates and moderate liquid rates relative to the bubble flow. In this regime, liquid plugs, free of gas bubbles, are separated by zones of large (elongated) gas bubbles. The diameters of these elongated bubbles are smaller than the tube diameter which means that there is still a continuous liquid phase with no small bubbles flowing inside the tube.

2.3.2.5 Slug Flow

When the gas velocity is increased under plug flow conditions, the liquid flow becomes aerated and contains small gas bubbles beside the already existing elongated bubbles. The flow then becomes more chaotic compared to plug flow and the interface between the liquid slugs and the elongated gas bubbles is no longer sharp.

2.3.2.6 Annular Flow

Extremely high gas flow rates will cause the liquid to just form a continuous film around the perimeter of the tube and the gas is flowing continuously in the core (like the vertical flow). However, the film at the bottom of the tube may be much thicker than the film at the top because of the gravity.[3]

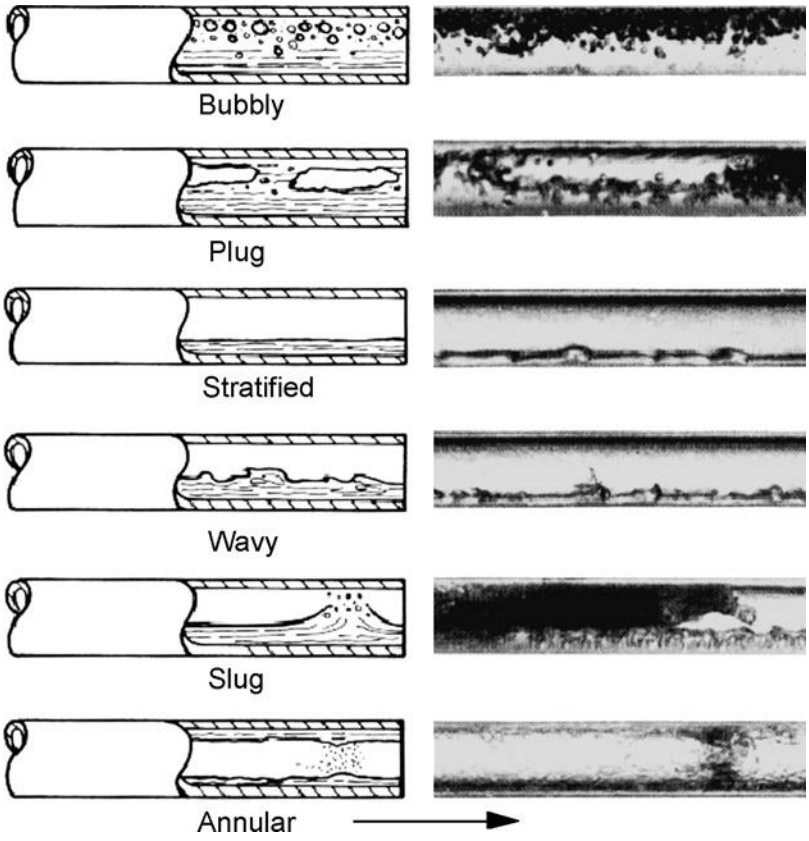

Figure 3: Flow patterns in Horizontal gas-liquid flow.[3]

2.3.3 Flow Pattern Maps

The most common variables used to identify the flow patterns are the liquid and gas superficial velocities (volumetric flow rate/cross-sectional area of the pipe) although there are other variables known to affect the flow pattern. This leads to having specific flow maps to a particular combination of fluids and geometry and no reliable universal flow map for all the fluids and geometries.

These maps are the result of flow pattern observation experiments. These experiments are carried out in a way that gas-liquid mixtures are injected in a tube at different velocities and the flow pattern is visually inspected and located on the map. When having a region of common velocity and more than one phase, the boundaries between the different flow type areas can be drawn.

Because of problems in correctly identifying flow patterns and especially the boundaries, it often happens that a few experimental points lie on the wrong side of these boundaries so that these lines would be better regarded as transition zones, of

indeterminate width. It is important to underline that these lines are just arbitrary lines for a transitional region between two distinct phases.[3]

2.3.3.1 Vertical Flow in Pipes Map

For vertical flow, flow pattern maps based on superficial velocities have been published since the 1960s and are still being produced. Some maps have been modified in which the superficial velocities are modified by factors of the actual physical properties so that it can be a more general map for different fluids (other than just water and air or oil and gas).

One popular approach, which tried to introduce some physical reality, is that of Hewitt and Roberts (1969), shown in figure 4.

The data were plotted as gas momentum flux ($\rho_g u_{gs}^2$) against liquid momentum flux ($\rho_1 u_{1s}^2$). Here the square root of those parameters, $u_{ls}\sqrt{\rho_1}$, $u_{gs}\sqrt{\rho_g}$ are employed.[4]

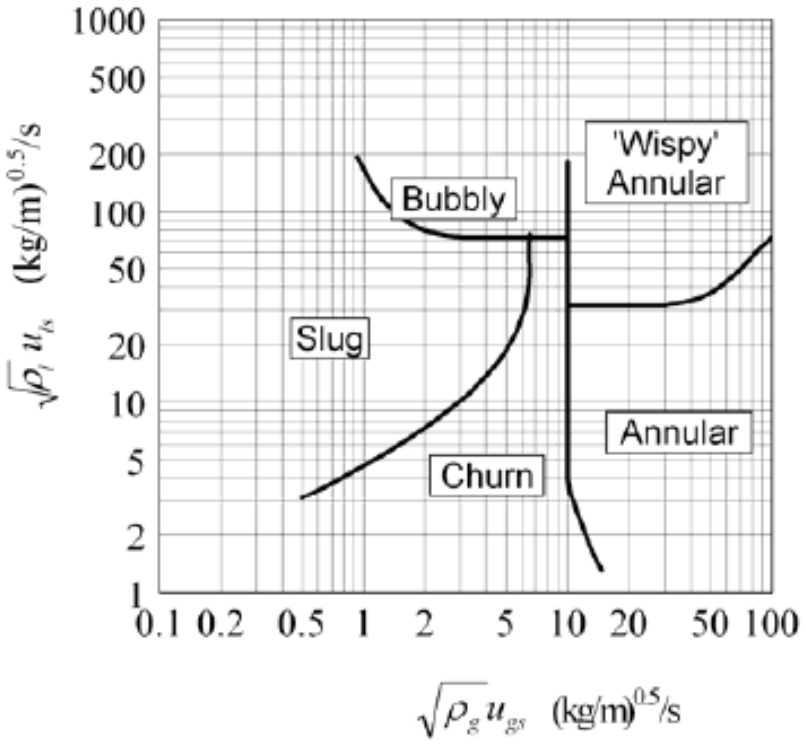

Figure 4: A modified form of the flow pattern map of Hewitt and Roberts (1969) – vertical flow.[4]

2.3.3.2 Horizontal Flow in Pipes Map

In horizontal flows, the flow pattern map of Baker (1954), shown in figure 5, is still being used although it is an old one. It is still famous because of its simplicity, based on industrially relevant data and accounts for the fluid properties.

In Baker flow regime map, the flow regime can be identified through the superficial mass velocity of the gas phase G and L/G, the ratio of superficial mass velocities of the liquid and gas/vapour phase.

Moreover, the dimensionless parameters λ and ψ were added so that the chart can account for the fluid properties and can be adopted for any gas/vapour–liquid combination different from the reference one (standard combination, at which both parameters λ and ψ equal unity, refers to water and air flowing under atmospheric pressure and at room temperature).

For any other flow conditions, appropriate values for λ and ψ could be assigned and so the general usage of the same map is enabled.[3]

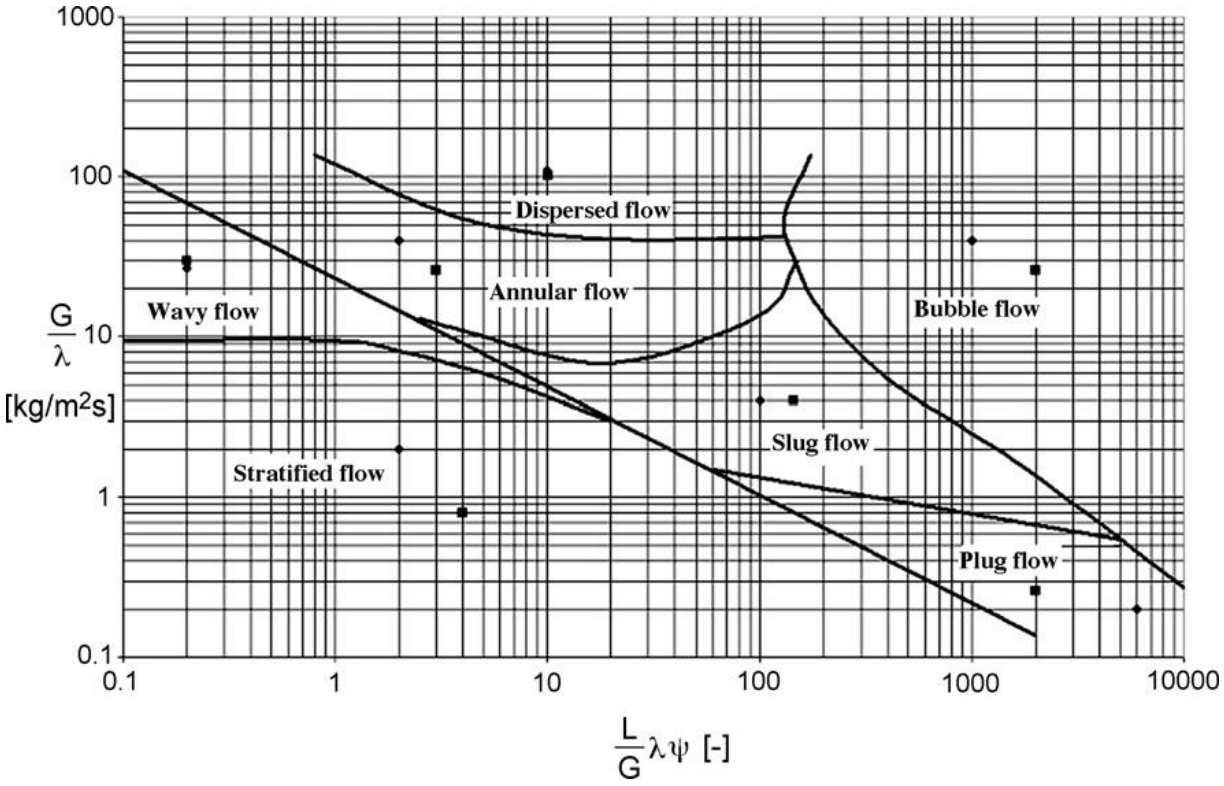

Figure 5: Baker Chart.[3]

2.4 Multiphase Modelling

To model any fluid flow (mathematically describe it), some main equations shall be used.

Two main equations are:

- **Continuity Equation:**

$$\frac{\partial \rho}{\partial t} + \nabla \cdot (\rho \mathrm{u}) = 0 \quad (1)$$

- **Momentum Equation (Navier-Stoke equation):**

$$\frac{\partial \rho \mathrm{u}}{\partial t} + \nabla \cdot (\rho \mathrm{uu}) = -\nabla p + \nabla \cdot \tau + \rho \mathrm{g} \quad (2)$$

In addition to these two main equations, other equations could be used to describe any additional phenomena coupled with the fluid flow such as energy equations and turbulence equations (if the flow is turbulent).

Here ρ is density, u is instantaneous velocity, p is pressure, τ is the viscous stress tensor and g is the gravity vector.[1]

Moreover, additional equations should be used to describe the multiphase flow system which adds more complexity to the modelling system. This is because we need to describe more than one flow, the interaction forces between them and how they affect each other, whether some parameters are shared between them or not,…etc. In addition, there are also limitations in time, and computational power when doing these numerical studies.

All these complications led to the development of more than one general model to describe the multiphase flow. Each of them has a different level of accuracy, suitable for different types of multiphase flow and can account for and provide different levels of information. Some of these modelling approaches are presented below.[5]

2.4.1 Euler-Lagrange Approach

In this approach, the primary phase is treated as a continuum, while the secondary phase is treated as moving particles being tracked inside the primary (continuous phase). These particles can either be a solid particle or a gas/fluid bubble/droplet.

Regarding the equations to be solved, conservation equations are needed for the continuous phase while equations of motion are needed to track the dispersed particles, see equations 3, 4 and 5 below.

$$\frac{\partial \alpha_f \rho_f}{\partial t} + \nabla \cdot \left(\alpha_f \rho_f \mathrm{u}_f\right) = \mathrm{S}_{\mathrm{mass}} \tag{3}$$

$$\frac{\partial \alpha_f \rho_f}{\partial t} + \nabla \cdot \left(\alpha_f \rho_f \mathrm{u}_f \mathrm{u}_f\right) = \alpha_f \nabla \mathrm{p} - \alpha_f \nabla \cdot \tau_f - \mathrm{S}_p + \alpha_f \rho_f \mathrm{g} = 0 \tag{4}$$

$$\frac{\partial \mathrm{u}_p}{\partial \mathrm{t}} = \sum \mathrm{F} \tag{5}$$

In which:

- α is the volume fraction (because we are dealing with a multiphase flow and so we need to account for the amount of each phase in our equations)
- S_{mass} is a mass source term, and it appears in the case of the exchange of mass between the phases.
- S_p is the momentum source term, and it appears in the case of the exchange of momentum between the phases.
- F is any force acting on the particles. These forces are like drag force, lift force, virtual mass force,…etc. It is up to the modeller to decide while forces will be added depending on their importance and effect. This is because adding all the possible forces to a model can increase the accuracy but also increases complexity, computational time and hence decrease the system stability (shall be discussed later in detail).
- Subscripts *f* and *p* refer to the fluid and particle phases, respectively.

Coupling is achieved between the continuous and dispersed phase equations through the source terms.

As this modelling approach resolves information on the level of a single particle it is quite computationally expensive, therefore Euler-Lagrange modelling is suitable for dilute dispersed flow (a maximum of about 10% volume fraction).[5]

When solving these model equations, you have two options: either to just include the effect of the continuous phase on the dispersed one and not the opposite (one-way

coupling) or also include the effect of the dispersed phase on the continuous one (two-way coupling).

- **Uncoupled way of solving (one-way coupling):**
  - Solve the continuous phase governing equations.
  - Solve the dispersed phase equation and evaluate the particle trajectories depending on the solution of the continuous one.
  - This is adequate when the discrete phase is of low quantity and so the continuous phase is not impacted significantly by the presence of the discrete phase.[1]

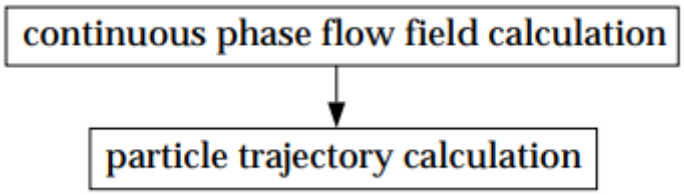

- **Coupled way of solving (Two-way coupling):**
  - Solve the continuous phase governing equations.
  - Solve the dispersed phase equation and evaluate the particle trajectories depending on the solution of the continuous one.
  - Re-solve the continuous phase governing equations, using the interphase exchange of momentum, heat, and mass determined during the previous particle calculation step.
  - Re-solve the dispersed phase trajectories using the modified values from the continuous phase flow field.
  - Repeat the previous two steps until a converged solution is achieved (no significant change in the parameters' values with each additional iteration).[1]

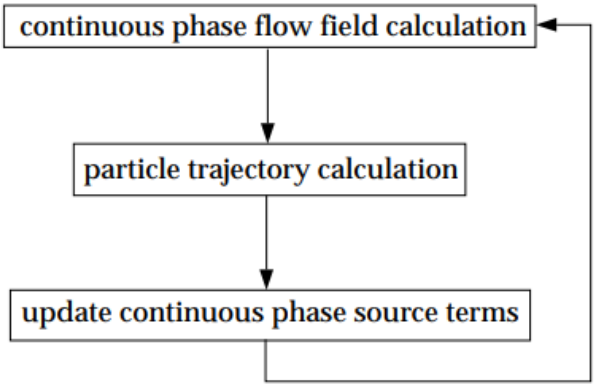

2.4.2 Euler-Euler Approach

What is different in this approach, other than the previous one, is that all phases are treated as interpenetrating continuous phases, and so it can also be called the "multi-fluid model".

The basic idea is simple: each phase shall be treated separately, and one set of conservation equations will be solved for each one. Moreover, coupling between the phases is to be achieved by having a shared pressure field and through the interphase exchange coefficients (like the forces found in the Euler-Lagrange approach). As in the Euler-Lagrange approach, the interphase exchange coefficients are numerous, and it is the modeller's choice to select which ones are more important and need to be included in the simulation.

The governing equations for each phase are shown below:

$$\frac{\partial \alpha_k \rho_k}{\partial t} + \nabla \cdot (\alpha_k \rho_k \mathrm{U}_k) = 0 \tag{6}$$

$$\frac{\partial \alpha_k \rho_k \mathrm{U}_k}{\partial t} + \nabla \cdot (\alpha_k \rho_k \mathrm{U}_k \mathrm{U}_k) = -\alpha_k \nabla \mathrm{P} + \alpha_k \nabla \cdot \tau_k + \alpha_k \rho_k \mathrm{g}_k + \mathrm{S}_k = 0 \tag{7}$$

$$\frac{\partial \alpha_k}{\partial t} + \nabla \cdot (\alpha_k \mathrm{U}_k) = 0 \tag{8}$$

Here U is the mean velocity field and P is the mean pressure shared by the phases. The subscript k refers to the k^{th} continuous phase.

As one can see, an additional transport equation is added regarding the volume fraction, and it is solved for each phase and their sum will be equal to one.

It is more appropriate to use this approach for separated flows because both phases are continuous ones. However, the Euler-Euler approach can also be used to model dispersed flows as well.

In the case of dispersed flow, the overall motion of particles is of interest rather than tracking individual particles and the dispersed phase equations are averaged in each computational cell to achieve average fields.

However, the volume fraction for the dispersed phase should be high enough so that it can be described as a continuous phase.[5]

Out of this general model, several models have been developed suitable for different flow types and have different levels of simplifications and approximations. In ANSYS Fluent, we have the Eulerian model, the Volume of fluid model and the Mixture model.

2.4.2.1 Eulerian Model

It is the most complete (accurate) model in which each phase is treated individually by solving a set of governing equations (as mentioned above).

The phases can be solid, liquid or gas (no limitations on the phases). Moreover, any number of phases can be included in which only the memory requirement and CPU time limit this number.

However, it is the most complex and the most computationally expensive model, so it is used only when other simplified models (discussed later) fail to give accurate predictions.

The governing equations are as follows (same as the ones mentioned above but in a detailed form):

- **Continuity Equation:**

  The continuity equation for phase q is:

$$\frac{\partial}{\partial t}\left(\alpha_q \rho_q\right) + \nabla \cdot \left(\alpha_q \rho_q \vec{v}_q\right) = \sum_{p=1}^{n} \left(\dot{m}_{\mathrm{pq}} - \dot{m}_{\mathrm{qp}}\right) + S_q \qquad (9)$$

  In which:

  - $\vec{v}_q$ is the velocity of phase q.

- $\dot{m}_{\mathrm{pq}}$ represents the mass transfer from phase p to phase q (if any).
- $\dot{m}_{\mathrm{qp}}$ represents the mass transfer in the opposite direction.
- S_q represents the source term (if any).[7]

- **Momentum Equation:**

For phase q, the momentum equation is as follows:

$$\frac{\partial}{\partial t}(\alpha_q \rho_q \vec{v}_q) + \nabla \cdot (\alpha_q \rho_q \vec{v}_q \vec{v}_q) = -\alpha_q \nabla p + \nabla \cdot \bar{\bar{\tau}}_q + \alpha_q \rho_q \vec{g} + \sum_{p=1}^{n} (\vec{R}_{pq} + \dot{m}_{pq}\vec{v}_{pq} - \dot{m}_{qp}\vec{v}_{qp}) + (\vec{F}_q + \vec{F}_{lift,q} + \vec{F}_{wl,q} + \vec{F}_{vm,q} + \vec{F}_{td,q}) \quad (10)$$

In which:

- p is the shared pressure between the phases.
- $\bar{\bar{\tau}}_q$ is the stress-strain tensor for the q[th] phase.
- $\vec{R}_{pq}$ is an interaction force between different phases. It depends on friction, pressure, and other effects. This force is mutual meaning that $\vec{R}_{pq} = -\vec{R}_{pq}$ and $\vec{R}_{pp} = 0$

  It can be simplified as follows:

$$\sum_{p=1}^{n} \vec{R}_{pq} = \sum_{p=1}^{n} K_{pq}(\vec{v}_p - \vec{v}_q)$$

  In which:

  - K_{pq} is the interface momentum exchange coefficient in which only drag force is included (shall be described later) and no other forces are included because they shall be included separately in their force terms.
- $\vec{v}_{pq}$ and $\vec{v}_{qp}$ are interfacial velocities and they are defined as follows:
  - $\dot{m}_{pq} > 0$ (Mass is being transferred from p to q), $\vec{v}_{pq} = \vec{v}_p$.
  - $\dot{m}_{pq} < 0$ (Mass is being transferred from q to p), $\vec{v}_{pq} = \vec{v}_q$.
  - Same for $\vec{v}_{qp}$.
- $\vec{F}_q$ is an external body force (if existed) acting on phase q.
- $\vec{F}_{lift,q}$ is the lift force.

- $\vec{F}_{wl,q}$ is the wall lubrication force.
- $\vec{F}_{vm,q}$ is the virtual mass force.
- $\vec{F}_{td,q}$ is the turbulent dispersion force (in the case of turbulent flows).[7]

- **Volume Fraction Equation:**

  It is the same as the one described in the general Euler-Euler model in which the sum of these volume fractions should be equal to one.[7]

2.4.2.2 Volume of Fluid Model

It is a surface tracking model which is designed for phases in which the interface between them is of interest, for example, stratified flow, slug flow,…etc.

It treats both phases as continuous phases but does not allow these phases to be interpenetrating. As a replacement, it uses a phase indicator function (called a colour function), to track the interface.

The extra function has a value between zero and one in which zero or one means only one phase is filling the control volume and if the value is between zero and one, it means an interface is present in the control volume. In other words, this phase indicator function is a volume fraction function.

Regarding the other governing equations "continuity equation, momentum equations,..etc), they are solved for the whole system (mixture) in which the physical properties are taken as an average between the phases.

It is also assumed that there is no velocity difference between the phases (no-slip velocity).

Volume of fluid governing equations are shown below:

$$\frac{\partial \rho_m}{\partial t} + \nabla \cdot (\rho_m \mathrm{u}) = 0 \quad (11)$$

$$\frac{\partial \rho_m \mathrm{u}}{\partial t} + \nabla(\rho_m \mathrm{uu}) = -\nabla P + \nabla \tau + \rho_m \mathrm{g} + \mathrm{S} = 0 \quad (12)$$

$$\frac{\partial \alpha}{\partial t} + \nabla(\alpha \mathrm{u}) = 0 \quad (13)$$

Subscript *m* refers to the mixture (average properties) which can be calculated as the following:

$$\rho_m = \sum \alpha_k \rho_k \quad (14)$$

To solve these equations, they should be discretized (transformed to algebraic equations in case of steady-state simulation) and because an accurate and sharp interface is needed, discretisation is crucial. Different discretization and interpolation methods were proposed like the Geometric reconstruction approach and Doner-Acceptor approach.

However, it is not our scope here to discuss these different techniques used in this model because we will not use them in our work.[5]

2.4.2.3 Mixture Model

It is a simplified form of the Euler-Euler approach in which governing equations for each phase are substituted with a single set of equations for the whole system (like the volume of fluid model) in which average properties are being used.

However, the difference between mixture model and the volume of fluid model is:

- It is not an interface tracking approach and so it allows phases to be interpenetrating as no sharp interface is required.
- It allows different velocities between phases and there is a relative velocity correlation that accounts for this velocity difference.

It can be considered as a good substitute for the full Eulerian model as it solves a smaller number of equations. This mixture approximation is reasonable when there is a uniform distribution of particles in the mixture (not being concentrated in certain regions) and so assuming a homogeneous mixture is acceptable. Eulerian model can be used, but it requires much higher computational time and may be numerically less stable.

To account for each phase, an extra volume fraction equation for each secondary phase is solved.

To account for the relative (slip) velocity, the following algebraic equation is used:

$$\vec{v}_{pq} = \frac{t_p}{f_{\text{drag}}} \frac{(\rho_p - \rho_m)}{\rho_p} \vec{a} \qquad (15)$$

In which:

- t_p is the particle relaxation time which represents the time needed by the particle to react to change in the fluid flow and it can be calculated as follows:

$$t_p = \frac{\rho_p d_p^2}{18\mu_q} \tag{16}$$

- d is the diameter of the particles (or droplets or bubbles) of secondary phase p.
- $\vec{a}$ is the secondary-phase particle's acceleration.

$$\vec{a} = \vec{g} - (\vec{v}_m \cdot \nabla)\vec{v}_m - \frac{\partial \vec{v}_m}{\partial t} \tag{17}$$

- f_{drag} is the drag function and can be calculated from different models (shall be discussed later).
- Subscripts *p* and *m* account for the secondary and mixture phases, respectively.

In the case of turbulent flow, a diffusion term should also be included in the relative velocity equation:

$$\vec{v}_{pq} = \frac{(\rho_p - \rho_m)d_p^2}{18\mu_q f_{\text{drag}}}\vec{a} - \frac{\eta_t}{\sigma_t}\left(\frac{\nabla\alpha_p}{\alpha_p} - \frac{\nabla\alpha_q}{\alpha_q}\right) \tag{18}$$

In which:

- σ_t is a Prandtl/Schmidt number set to 0.75
- η_t is the turbulent diffusivity.

Finally, if the relative (slip) velocity equation is not solved, our mixture model shall be reduced to a homogeneous multiphase model in which no velocity difference between the phases is assumed.[1]

2.4.3 Interaction Forces Between the Phases

When having multiphase fluid in which one of the phases is predominant, it can be considered as a continuous primary while the secondary phase can be assumed as bubbles or droplets. These bubbles/droplets should be affected by the primary phase through a number of forces like drag force, lift force, wall lubrication force, virtual mas force and turbulent dispersion force. Each of these forces has several possible models

in which each one is suitable for different cases. We will discuss these forces in detail and their different models.

2.4.3.1 Interface Exchange Coefficient (K_{pq}):

As we can see in equation (11), the interface exchange force can be simplified to a form that depends only on the interface exchange coefficient.

This exchange coefficient can be assumed to depend only on the drag force and so the other forces shall be excluded from this term and put in separate terms (as shown in equation 10).

Drag force is the force that opposes the motion of bubbles/droplets in the fluid as a result of both the viscous effect from the primary phase on the secondary one (skin drag) and the pressure difference caused by the shape of the bubble (form drag).[8]

The interface exchange coefficient is defined as follows:

$$K_{pq} = \frac{\rho_p f}{6 t_p} d_p A_i \tag{19}$$

In which:

- t_p is the particle relaxation time:

$$t_p = \frac{\rho_p d_p^2}{18 \mu_q} \tag{20}$$

- A_i is the interfacial area concentration and it is defined as the interfacial area between any two phases per unit total volume. It affects mass, momentum, and energy transfer and so it should be modelled, and its dedicated models will be discussed later.
- f is the drag function which depends on the drag coefficient C_D and the relative Reynolds number Re

$$f = \frac{C_D Re}{24} \tag{21}$$

Different models are available for calculating the drag coefficient C_D and it is up to the modeller to choose which model is suitable for the case of interest, as they are different in how they describe the secondary phase shape, the level of accuracy, the number of parameters to be considered,…etc.

The following models are available in ANSYS Fluent:

2.4.3.1.1 Schiller and Naumann Model

It is the default model and acceptable for all fluids. In this model, bubbles/droplets are assumed as rigid spheres and the drag coefficient depends on the relative Reynolds number between the primary phase q and secondary phase p[7][8][14]:

$$C_D = \begin{cases} 24(1 + 0.15Re^{0.687})/\,\mathrm{Re} & Re \leq 1000 \\ 0.44 & Re > 1000 \end{cases} \tag{22}$$

$$Re = \frac{\rho_q |\vec{v}_p - \vec{v}_q| d_p}{\mu_q} \tag{23}$$

2.4.3.1.2 Morsi and Alexander Model

This model is similar to Schiller-Naumann model in both being applicable only to rigid spherical bubbles/droplets and also having the drag coefficient depending only on the relative Reynolds number.

However, it uses a more complete correlation in which the range of Reynolds number is more detailed (divided into more regions than just two as the previous model). This makes the model more accurate but at the same time, less stable than the other models.[7][8][15]

$$C_D = a_1 + \frac{a_2}{\mathrm{Re}_b} + \frac{a_3}{\mathrm{Re}_b^2} \tag{24}$$

$$a_1, a_2, a_3 = \begin{cases} 0{,}24{,}0 & 0 < \mathrm{Re}_b < 0.1 \\ 3.69{,}22.73{,}0.0903 & 0.1 < \mathrm{Re}_b < 1 \\ 1.222{,}29.1667{,} -3.8889 & 1 < \mathrm{Re}_b < 10 \\ 0.6167{,}46.50{,} -116.67 & 10 < \mathrm{Re}_b < 100 \\ 0.3644{,}98.33{,} -2778 & 100 < \mathrm{Re}_b < 1000 \\ 0.357{,}148.62{,} -47500 & 1000 < \mathrm{Re}_b < 5000 \\ 0.46{,} -490.546{,}578700 & 5000 < \mathrm{Re}_b < 10000 \\ 0.5191{,} -1662.5{,}5416700 & 10000 \geq \mathrm{Re}_b \end{cases} \tag{25}$$

2.4.3.1.3 Symmetric Model

It is a special type of model that is suitable when calculating the drag coefficient between two secondary phases or when primary and secondary phases can exchange roles inside our domain. For example, if the air is injected into the bottom of a container half-filled with water, the air is considered as the secondary phase in the bottom of the container, while being considered as primary in the top.

The parameters such as viscosity, density and diameter are calculated as averages between the phases.

Interface exchange coefficient and drag coefficient for both phases p and q can be calculated as follows[7]:

$$K_{pq} = \frac{\rho_{\mathrm{pq}} f}{6 t_{\mathrm{pq}}} d_p A_{\mathrm{i}} \tag{26}$$

$$f = \frac{C_{\mathrm{D}} Re}{24} \tag{27}$$

$$\rho_{pq} = \alpha_p \rho_p + \alpha_q \rho_q \tag{28}$$

$$\mu_{pq} = \alpha_p \mu_p + \alpha_q \mu_q \tag{29}$$

$$d_{pq} = \frac{1}{2}(d_p + d_q) \tag{30}$$

$$t_{pq} = \frac{\rho_{\rho q}[d_{pq}]^2}{18\mu_{pq}} \tag{31}$$

$$Re = \frac{\rho_{pq}|v_\rho - v_q| d_{Pq}}{\mu_{pq}} \tag{32}$$

The drag coefficient can be calculated from equation (22).

2.4.3.1.4 Grace et al. Model

Bubbles/droplets are not always in sphere form. This assumption is only valid when moving in low velocities and having small sizes. When the dispersed phase velocity increases or its size increases, its shape can then be distorted and become elliptical or cap form.

To account for these shapes in our models, two-dimensional numbers are added, Eotvos number (Eo) and Morton number (Mo).[16]

Eotvos number is the ratio between buoyancy force and surface tension force:

$$Eo = \frac{g(\rho_q - \rho_p) d_p^2}{\sigma} \tag{33}$$

Morton number (Mo) considers the physical properties of the two phases:

$$Mo = \frac{\mu_q^4 g(\rho_q - \rho_p)}{\rho_q^2 \sigma^3} \tag{34}$$

In this model, each bubble shape has a specific drag coefficient relationship. They are all calculated and then be compared to each other according to the following equations[7]:

$$C_D = \alpha_q^{C_{\text{exp}}} \cdot max\left(min\left(C_{D_{\text{ellipse}}}, C_{D_{\text{cap}}}\right), C_{D_{\text{sphere}}}\right) \quad (35)$$

In which:

- α_q is the primary phase volume fraction.
- C_{exp} is the volume fraction correction exponent (For low dispersion, C_{exp} =0. For high dispersion, $C_{\text{exp}} \neq 0$.
- $C_{D_{\text{sphere}}}$ is the spherical drag coefficient and it depends only on the relative Reynolds number.

$$C_{D_{\text{sphere}}} = \begin{cases} 24/Re & Re < 0.01 \\ 24(1 + 0.15Re^{0.687})/Re & Re \geq 0.01 \end{cases} \quad (36)$$

$$Re = \frac{\rho_q \left|\vec{v}_p - \vec{v}_q\right| d_p}{\mu_q} \quad (37)$$

- $C_{D_{cap}}$ is the cap-shape drag coefficient and it is in a simple form:

$$C_{D_{cap}} = \frac{8}{3} \quad (38)$$

- $C_{D_{\text{ellipse}}}$ is the ellipse-shape drag coefficient that depends on both Evotos number and Morton number:

$$C_{D_{\text{ellipse}}} = \frac{4}{3}\frac{g d_p}{U_t^2}\frac{(\rho_q - \rho_p)}{\rho_q} \quad (39)$$

$$U_t = \frac{\mu_q}{\rho_q d_p} Mo^{-0.149}(J - 0.857) \quad (40)$$

$$J = \begin{cases} 0.94H^{0.757} & 2 < H \leq 59.3 \\ 3.42H^{0.441} & H > 59.3 \end{cases} \quad (41)$$

$$H = \frac{4}{3} EoMo^{-0.149}\left(\frac{\mu_q}{\mu_{ref}}\right)^{-0.14} \quad (42)$$

$$\mu_{ref} = 0.0009\ kg/(m.\text{s}) \quad (43)$$

- Subscripts *q* and *p* refer to primary and secondary phases, respectively.

2.4.3.1.5 Tomiyama et al. Model

Like the Grace et al. model, the Tomiyama et al. model accounts for bubbles/droplets having different shapes. The developed equations depend on bubble diameter, bubble shape, acceleration due to gravity, and the contamination degree of the fluid.[7][8][17]

$$C_D = max\left(min\left(\frac{24}{Re}(1+0.15Re^{0.687}), \frac{72}{Re}\right), \frac{8}{3}\frac{Eo}{Eo+4}\right) \quad (44)$$

2.4.3.1.6 Universal Drag Law

In a recent development, a new drag model was developed which is suitable for a variety of gas-liquid flow regimes. It can be applied to non-spherical bubbles/droplets with the constraint that the hydraulic diameter of the flow domain should be extremely larger than the average size of the particle. Moreover, the gas volume fraction is used instead of both Eotvos number and Morton number.[18]

In the case of bubble-liquid flow, three drag coefficients are calculated $C_{D_{vis}}$, $C_{D_{dis}}$, and $C_{D_{cap}}$ according to the following equations[7]:

$$C_{D_{vis}} = \frac{24}{Re}(1+0.1Re^{0.75}) \quad (45)$$

$$C_{D_{dis}} = \frac{2}{3\left(\frac{d_p}{\lambda_{RT}}\right)\left\{\frac{1+17.67f^{*\frac{6}{7}}}{18.67f^*}\right\}^2}; f^* = \left(1-\alpha_p\right)^{15} \quad (46)$$

$$C_{D_{cap}} = \frac{8}{3}\left(1-\alpha_p\right)^2 \quad (47)$$

In which subscripts *q* and *p* refer to primary and secondary phases, respectively.

- Re is the relative Reynolds number.
- α_p is the secondary phase volume fraction.
- λ_{RT} is Rayleigh-Taylor instability wavelength:

$$\lambda_{RT} = \left(\frac{\sigma}{g\Delta\rho_{pq}}\right)^{0.5} \quad (48)$$

- Any viscosity is replaced with an effective viscosity $\mu_e = \frac{\mu_q}{1-\alpha_p}$

After calculating each of these drag coefficients, the bubble regime is then chosen according to the following criteria:

- In the viscous regime, the following condition is satisfied: $C_{D_{dis}} < C_{D_{vis}}$, the drag coefficient $C_D = C_{D_{vis}}$.
- In the distorted bubble regime, the following condition is satisfied: $C_{D_{vis}} < C_{D_{dis}} < C_{D_{cap}}$, the drag coefficient $C_D = C_{D_{dis}}$.
- In the strongly deformed bubble regime, the following condition is satisfied: $C_{D_{dis}} > C_{D_{cap}}$, the drag coefficient $C_D = C_{D_{cap}}$.

2.4.3.2 Lift Force

When having bubbles/droplets in a continuous flow, the primary phase velocity field can affect the dispersed secondary phase by creating a resultant force called the lift force.

In the case of having a large diameter dispersed phase, it observes a higher velocity component on one side with a lower velocity component on the other side because of the continuous phase velocity profile which has a gradient across the pipe cross-section. According to Bernoulli's equation, the bubble side experiencing higher velocity shall have lower pressure and vice versa and so this leads to having unequal forces on both sides of the bubble. The resultant of these forces is called the lift force. Multiple models are suitable for lift force in which each one of them is applicable for certain flow conditions, but these models are computationally expensive, and they take a lot of time to converge. Hence, the inclusion of lift force is only helpful when having large bubbles where there is a significant pressure difference, while it can be neglected in case of small bubbles so as not to put extra complications in our system.

Lift force acting on a secondary phase *p* in a primary phase *q* can be calculated as follows[7][19]:

$$\vec{F}_{lift} = -C_l \rho_q \alpha_p \left(\vec{v}_q - \vec{v}_p\right) \times \left(\nabla \times \vec{v}_q\right) \quad (49)$$

In which C_l is the lift force coefficient.

This lift force term is added in both primary and secondary phase momentum equations ($-\vec{F}_{lift.q} = \vec{F}_{lift,p}$).

In the early models, lift force was calculated through an expression that only considered the pressure difference and so gave a positive lift coefficient C_l in the

direction of decreasing the primary phase velocity, i.e: towards the pipe wall in case of co-current pipe flow.

However, both numerical and experimental investigations showed that the direction of lift force can change its sign if more bubble deformation occurs.[8] In ANSYS Fluent manual, four lift force coefficient models are available.

2.4.3.2.1 Saffman-Mei Model

It is a suitable model for solid particles and liquid droplets that are not distorted plus having small velocity gradient in the primary phase[7][20][21]:

$$\mathrm{C}_l = \frac{3}{2\pi\sqrt{\mathrm{Re}_\omega}} C'_l \tag{50}$$

In which:

- $C'_l = 6.46$, this term was then modified by Mei-Klausner in which a mathematical expression was developed to calculate it.
- Re_ω is the vorticity Reynolds number:

$$\mathrm{Re}_\omega = \frac{\rho_q \left|\nabla \times \vec{V}_q\right| d_p^2}{\mu_q} \tag{51}$$

- Re_p is the particle Reynolds number (the same Reynolds number used before, but subscript *p* is added to differentiate between it and vorticity Reynolds number):

$$\mathrm{Re}_p = \frac{\rho_q \left|\vec{V}_q - \vec{V}_p\right| d_p}{\mu_q} \tag{52}$$

- It is valid for low-velocity fields:

$$0 < \mathrm{Re}_p < \mathrm{Re}_\omega < 1$$

2.4.3.2.2 Legendre-Magnaudet Model

What is different between this model and the previous one is that it can be applied to bubbles, besides liquid drops, and solids. However, these particles should not be distorted and have spherical shapes.

Here, two lift force coefficients are calculated for both low and high Reynolds numbers and then the total lift force coefficient is calculated through the following equation:[7][8][22]

$$C_l = \sqrt{\left(C_{l,\,\text{lowRe}}\right)^2 + \left(C_{l,\,\text{highRe}}\right)^2} \tag{53}$$

$$C_{l,\,\text{lowRe}} = \frac{6}{\pi^2}\left(\text{Re}_p\ Sr\right)^{-0.5}\frac{2.55}{\left(1+0.2\frac{\text{Re}_p}{S_r}\right)^{1.5}} \tag{54}$$

$$C_{l,\,\text{highRe}} = \frac{1}{2}\frac{1+16\text{Re}_p^{-1}}{1+29\text{Re}_p^{-1}} \tag{55}$$

In which:

- $Sr = 2\beta, \quad \beta = 0.5\left(\text{Re}_\omega\ /\text{Re}_p\right).$
- The validity of this model is:

$$0.1 < \text{Re}_p < 500$$

$$Sr = 2\beta \leq 1$$

2.4.3.2.3 Moraga Model

This model (as the Legendre-Magnaudet model) is applicable mainly on spherical solid particles, and undistorted liquid droplets/bubbles.

Here, the lift coefficient combines two opposite factors:

- Classical aerodynamic lift due to the interaction between the dispersed particles and the primary phase shear.
- Vorticity-induced lift due to the interaction between the particles and vortices from particles wakes.

Therefore, the lift force coefficient depends on both particle Reynolds number and vorticity Reynolds number:[7][23]

$$C_l = \begin{cases} 0.0767 & \varphi \leq 6000 \\ -\left(0.12 - 0.2e^{\frac{\varphi}{3.6}\times 10^{-5}}\right)e^{\frac{\varphi}{3}\times 10^{-7}} & 6000 < \varphi < 5\times 10^7 \\ -0.6353 & \varphi \geq 5\times 10^7 \end{cases} \tag{56}$$

In which $\varphi = \text{Re}_\omega.\text{Re}_p$

2.4.3.2.4 Tomiyama Model

In all the previous modes, nothing accounted for the distortion in the bubbles/droplets. So Tomiyama developed a model that can account for different shapes like the ellipsoid and cap shapes, same as the drag force model.

In the same way, the model depends on the Eotvos number (Eo) as follows:

$$C_l = \begin{cases} min\left[0.288\tanh\left(0.121\mathrm{Re}_p\right), f(Eo')\right] & Eo' \leq 4 \\ f(Eo') & 4 < Eo' \leq 10 \\ -0.27 & 10 < Eo' \end{cases} \quad (57)$$

$$f(Eo') = 0.00105Eo^3 - 0.0159E\sigma^2 - 0.0204Eo' + 0.474 \quad (58)$$

In which:

- Eo' is the modified Eotvos number:

$$E\sigma' = \frac{g\left(\rho_q - \rho_p\right)d_h^2}{\sigma} \quad (59)$$

- d_h is the long axis of the deformed/distorted bubble:

$$d_h = d_b(1 + 0.163Eo^{0.757})^{1/3} \quad (60)$$

According to this model, the bubbles maintain a spherical shape and move towards the wall at a low Eotvos number.

At higher values, distortion occurs leading to having slanted vortices that move the bubbles towards the pipe centre and hence change the lift force sign. This sigh change happens at Eo > 10.[7][8][24][25]

2.4.3.3 Wall Lubrication Force

It is a type of force acting on the bubbles/droplets because of the velocity gradient in the continuous phase field between the pipe centre and the wall. Similar to the lift force, this velocity gradient creates a pressure gradient across the particles that leads to moving these particles away from the pipe wall.

The difference between this force and the lift one is that it is strictly related to the velocity gradient between the pipe centre and the wall, while it is any velocity gradient in the case of the lift force.

For any secondary phase *p* found in a primary phase *q*, wall lubrication force can be calculated according to the following expression:[7]

$$\vec{F}_{wl} = C_{wl}\rho_q\alpha_p \left|\left(\vec{v}_q - \vec{v}_p\right)_{\parallel}\right|^2 \vec{n}_w \quad (61)$$

In which:

- C_{wl} is the wall lubrication coefficient.
- ρ_q is the primary phase density.
- α_p is the secondary phase volume fraction.
- $\left(\vec{v}_q - \vec{v}_p\right)_{\parallel}$ is the phase relative velocity component tangential to the wall surface.
- $\vec{n}_w$ is the unit normal vector pointing away from the wall.

To calculate the wall lubrication coefficient, four models are available in ANSYS Fluent:

2.4.3.3.1 Antal et al. Model

According to this model, wall lubrication force can be calculated according to the following expression:

$$C_{wl} = max\left(0, \frac{C_{w1}}{d_b} + \frac{C_{w2}}{y_w}\right) \quad (62)$$

In which:

- C_{w1} and C_{w2} are non-dimensional coefficients has default values of -0.01 and 0.05, respectively.
- d_b is the bubble diameter.
- y_w is the distance from the wall.

According to this equation, C_{wl} will not have a zero value ($\frac{C_{w1}}{d_b} + \frac{C_{w2}}{y_w} > 0$) only in the area close to the wall:

$$y_w \leq \left(\frac{C_{w2}}{C_{w1}}\right) d_b$$

This means that this model is only active when the bubble becomes extremely close to the wall, so a very fine mesh is required to be able to use this model.[7][26]

2.4.3.3.2 Tomiyama Model

This model modified the wall lubrication force found in Antal et al. according to an experiment with the flow of air bubbles in glycerin in a pipe.

According to this model:

$$C_{wl} = C_w \frac{d_b}{2}\left(\frac{1}{y_w^2} - \frac{1}{(D-y_w)^2}\right) \tag{63}$$

In which:

- D is the pipe diameter.
- C_w is a constant that depends on Eotvos number (same as any Tomiyama model proposed in other forces):

$$C_w = \begin{cases} 0.47 & Eo < 1 \\ e^{-0.933Eo+0.179} & 1 \le Eo \le 5 \\ 0.00599Eo - 0.0187 & 5 < Eo \le 33 \\ 0.179 & 33 \le Eo \end{cases} \tag{64}$$

This model is to be considered more accurate than that of Antal et al. model as it was a modification on it. However, it is restricted to flow in pipes because it was based on an experiment in a pipe).[7]

2.4.3.3.3 Frank Model

This model removed the pipe dependency that is present in the Tomiyama model and proposed a new correlation:[7]

$$C_{wl} = C_w max\left(0, \frac{1}{C_{wd}} \cdot \frac{1 - \frac{y_w}{c_{wc} d_b}}{y_w \left(\frac{y_w}{c_{wc} d_b}\right)^{m-1}}\right) \tag{65}$$

In which:

- C_w is a constant that depends on the Eotvos number (calculated from equation 64).
- C_{wd} is the damping coefficient that determines the relative magnitude of the force.
- c_{wc} is the cut-off coefficient that determines the distance from the wall where the wall lubrication force should be active.
- m is the power-law constant should be between 1.5 and 2.

- These constants (C_{wd}, C_{wc} and m) should have values of 6.8, 10 and 1.7 respectively to give the best agreement with the experimental data.[8]

2.4.3.3.4 Hosokawa Model

This model proposed a mathematical expression for calculation of wall lubrication force that depends on both Eotvos number and the phase relative Reynolds number other than just Eotvos number as Tomiyama and Frank models:[7][27]

$$C_w = max\left(\frac{7}{\mathrm{Re}_d^{1.9}}, 0.0217Eo\right) \tag{66}$$

2.4.3.4 Turbulence Dispersion Force

When having turbulence in a multiphase system, the flow can be affected by the presence of turbulence in two ways:

- Fluctuation in liquid velocity due to the vortices created by the turbulence.
- How these fluctuations affect the dispersed phase (bubbles) by scattering them.

This turbulence mutual effect between both phases is called turbulence dispersion force.

During the drag force term calculation (interface exchange force), we considered the mean (time-averaged) velocities of the continuous and dispersed phases and not the instantaneous ones. The difference between the instantaneous-velocity-based and average-velocity-based exchange forces represents the exchanged momentum, but due to turbulence.

So, for primary phase *q* and secondary phase *p*, instantaneous interface exchange force can be calculated as follows:

$$K_{pq}\left(\vec{\tilde{v}}_p - \vec{\tilde{v}}_q\right) = K_{pq}\left(\vec{v}_p - \vec{v}_q\right) - K_{pq}\vec{v}_{dr} \tag{67}$$

The first term on the left side is the instantaneous exchanged momentum and the first term on the right side is the average exchanged momentum, while the last term is the turbulent dispersion force as described above.

Therefore, turbulence dispersion force can be calculated as follows:

$$\vec{F}_{tdq} = -\vec{F}_{td,p} = -f_{td,\,\text{limiting}}\, K_{pq}\vec{v}_{dr} \tag{68}$$

In which $\vec{v}_{dr}$ is the drift velocity and accounts for the secondary phase dispersion due to turbulence and $f_{td,\text{ limiting}}$ is a limiting function that restricts the application of this force to certain places in our domain (shall be discussed below).

Four models were developed to model this force in ANSYS Fluent, and we shall see that the driving force in all these models will be the volume fraction gradient of the dispersed phase volume fraction as it acts as diffusion force for the dispersed phases.[7][8]

2.4.3.4.1 Lopez de Bertodano Model

Instead of using equation (68) and modelling the drift velocity, this model proposed a different formula to calculate the turbulence dispersion force:[28]

$$\vec{F}_{td,q} = -\vec{F}_{td,p} = C_{TD}\rho_q k_q \nabla\alpha_p \tag{69}$$

In which:

- ρ_q is the primary phase density.
- $\nabla\alpha_p$ is the secondary phase volume fraction gradient (the driving force).
- k_q is the turbulent kinetic energy for the primary phase associated with the vortices and it is considered a basic quantity in modelling any turbulent flow.
- C_{TD} is the turbulence dispersion force constant which can have a value between 0.5 and 0.1 for medium-size bubbles and ellipsoidal bubbles (distorted and large bubbles) and can reach 500 the for small bubbles. By default, it $C_{TD} = 1$.

2.4.3.4.2 Simonin Model

In this model, drift velocity $\vec{v}_{dr}$ is modelled and added to equation (68) to have:[7][29]

$$\vec{F}_{td,q} = -\vec{F}_{td,p} = C_{TD}K_{pq}\frac{D_{t,pq}}{\sigma_{pq}}\left(\frac{\nabla\alpha_p}{\alpha_p} - \frac{\nabla\alpha_q}{\alpha_q}\right) \tag{70}$$

In which:

- C_{TD} is the turbulence dispersion force constant=1.
- $D_{t,pq}$ is liquid bubble dispersion scalar that describes the turbulence model.
- σ_{pq} is Prandtl number = 0.75

2.4.3.4.3 Burns et al. Model

This model is like Simonin model, but the dispersion scalar $D_{t,pq}$ is estimated by the turbulent viscosity leading to the following model:[7][30]

$$\vec{F}_{td,q} = -\vec{F}_{td,p} = C_{TD} K_{pq} \frac{\mu_{tq}}{\sigma_{pq} . \rho_q} \left(\frac{\nabla \alpha_p}{\alpha_p} - \frac{\nabla \alpha_q}{\alpha_q} \right) \quad (71)$$

In which:

- μ_{tq} is the continuous phase turbulent viscosity.
- ρ_q is the continuous phase density.
- σ_{pq} is Prandtl number = 0.9

This model is said to be valid for any Reynolds-averaged turbulence model, any number of phases with any morphology.[8]

2.4.3.4.4 Diffusion in VOF Model

Instead of having the turbulence dispersion force as a term in the momentum equation, we can instead consider it as a turbulent diffusion term (because the volume fraction gradient is the driving force) and so adding to the continuity equation instead of the momentum one:[7][31]

$$\frac{\partial}{\partial t}(\alpha_q \rho_q) + \nabla \cdot (\alpha_q \rho_q \vec{v}_q) = \nabla(\gamma_q \nabla \alpha_q) + \sum_{p=1}^{n} (\dot{m}_{pq} - \dot{m}_{qp}) + S_q \quad (72)$$

In which γ_q is the diffusion coefficient of the continuous phase and it is related to the turbulent viscosity. It should satisfy the following correlation for all the phases:

$$\sum_{q=1}^{n} \nabla(\gamma_q \nabla \alpha_q) = 0 \quad (73)$$

2.4.3.4.5 Limiting Function in the Turbulence Dispersion Force

In some modelling systems, turbulence dispersion force can be applied to certain parts of our domain only. This is because it is unrealistic to apply this force in a system where the two phases are continuous (stratified flow for example). Therefore, a limiting function should be applied to account for the secondary phase volume fraction and hence decrease its impact on our system when having large volume fractions.

As seen in equation (68), $f_{td,\,\text{limiting}}$ is the limiting function that can have a value between zero and one.

- Zero means that no turbulence dispersion force should be applied.
- One means that no limiting is performed on this force.

In ANSYS Fluent, this limiting function can be calculated according to the following equation:

$$f_{t\ \text{d.limiting}}(\alpha_p) = max\left(0, min\left(1, \frac{\alpha_{p,2} - \alpha_p}{\alpha_{p,2} - \alpha_{p,1}}\right)\right) \quad (74)$$

In which $\alpha_{p,1}$ and $\alpha_{p,2}$ can have values of 0.3 and 0.7, respectively.[7]

2.4.3.5 Virtual Mass Force

When a bubble flows through a continuous liquid stream, this bubble can carry a portion of this liquid on its surface. This portion has the mass of the liquid, but the velocity of the gas. This shall lead to the increase of the total bubble mass and add extra force due to the bubble acceleration. This extra mass is called the virtual mass and the added force due to acceleration is called virtual mass force.

The same can happen in the case of having liquid droplets/solid particles moving in a gas stream. However, the gained mass is then negligible compared to the original mass of the droplet or particle. Therefore, the virtual mass should only be considered when the continuous phase density is much higher than the dispersed phase.

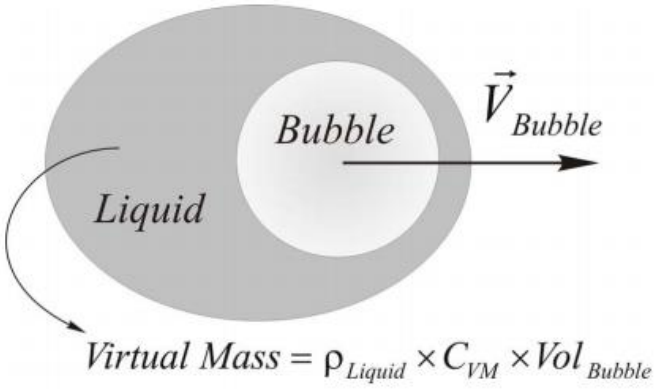

Figure 6: The concept of virtual mass.[10]

The virtual mass force can be calculated as follows:[32]

$$\vec{F}_{vm} = C_{vm}\alpha_p\rho_q\left(\frac{d_q\vec{v}_q}{dt} - \frac{d_p\vec{v}_p}{dt}\right) \quad (75)$$

In which C_{vm} is the virtual mass coefficient and it is the ratio between the mass carried by the bubble and the bubble volume. Typically, it has a value of 0.5. However, for higher volume fractions, dispersed phases (for example bubbles) can interact leading to an increase in the virtual mass carried by them. So, various models, based on volume fraction, have been proposed to calculate the virtual mass coefficient.[7][10]

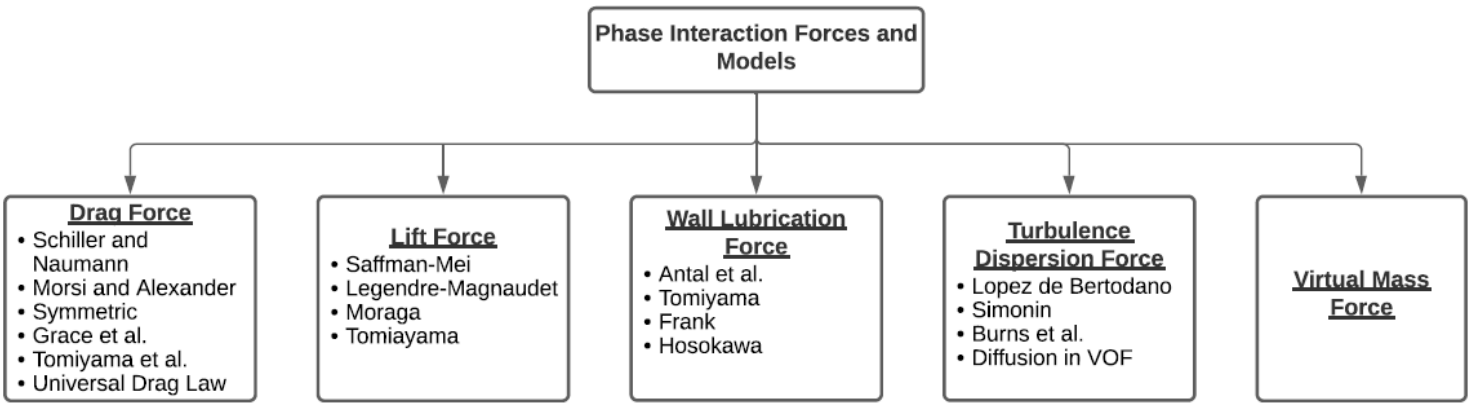

Figure 7: Flowchart representing the phase interaction forces and their available models.

2.4.4 Population Balance Model (PBM)

In any multiphase model, one of the parameters that need specification is the dispersed phase particle size. The most common and simple approach assumes that all the particles have the same size (diameter). However, this is not always realistic as there are several applications involving a secondary phase with a size distribution.

This particle size distribution can be important in many cases like crystallization, bubble columns, gas sparging,..etc where the assumption of having a constant particle size is unrealistic because it ignores a basic parameter in these cases.

Thus, in multiphase flows involving a size distribution, an additional model is needed to describe this particle size distribution. This model is called the “Population Balance Model” and it accounts for, not only particle size distribution”, but also predicts phenomena of how these sizes are interacting with each other (coalescence, nucleation and breakage of these particles).

When using the Population balance model, an additional equation is added to the dispersed phase governing equations called "Population Balance Equation" which describes the change in the dispersed phase particle size:

$$\frac{\partial n_i}{\partial t} + \nabla \cdot \left(\mathbf{u}_g n_i\right) = B_B + B_C - D_B - D_C + G \quad (76)$$

In which:

- n_i is the number density of size group (i) and it can be related to the dispersed phase volume fraction α_g according to the following relationship:

  $$\alpha_g f_i = n_i V_i \quad (77)$$

  Where f_i is the volume fraction of group size (i) and V_i is the volume of group size (i).

- $\mathbf{u}_g$ is the dispersed phase velocity.
- $B_B, B_C, D_B \; and \; D_C$ are terms representing the birth (B) and death (D) of the particles due to breakage (b) and coalescence (c).
- G is the growth term.

Various models have been proposed to both solve the population balance equation and model nucleation, coalescence, breakage, and growth of the dispersed phase.

To solve equation (76), ANSYS Fluent proposed three methods:

- **Discrete Method:**

  In this method, the particle size population is discretized (divided) into a certain number of intervals called bins. Each bin has its population balance equation, and they are all solved to find the particle size distribution.

  This method is suitable when the range of particle size is previously known, and it can be divided into a limited number of bins (not too many bins) and it has the advantage of directly finding the particle size distribution. However, it is computationally expensive as it solves a lot of additional equations.[33][34][35]

- **The Standard Method of Moments (SMM):**

  The difference between this method and the discrete one is that the moments of our distribution are simulated instead of directly simulating the bins and so the population balance equation is transformed into a set of transport equations for these moments.

  When doing this, the total number of added equations shall be lower as we shall have between three to six moment equations instead of solving ten or twenty bin equations as in the discrete method. This significantly decreases the computational time.

  However, the disadvantage here is that both coalescence and breakage of the dispersed particles cannot be written in the moment equations which add limits to its usage.[36]

- **The Quadrature Method of Moments (QMOM):**

  The quadrature method of moments (QMOM) is like the standard method of moments, but with no limitations in using both coalescence and breakage in the moment equations.[1][5][37]

2.4.5 How to Choose Between Different Multiphase Models

Choosing between all the previous multiphase models is quite challenging because they shall all work in most of the applications, but their results can sometimes be unreliable. Moreover, the computational time and the system stability can also affect our choice.

Therefore, we should have some basic criteria about how to choose between these models that shall help us in having a preliminary decision about what model should we use.

Our first step is to determine the flow regime we are dealing with (stratified, slug, annular, bubbly,…etc).

After determining our flow regime, we can choose between the models according to the following:

- **Volume of Fluid Model (VOF):**

  Choosing this model is very straightforward, it is used when we would like to track the interface between different phases. Therefore, it is used when having a sharp interface like in stratified flow, slug flow and free surface flow.

- **Discrete Phase Model (Euler-Lagrange Approach), Mixture Model and Eulerian Model:**

  Choosing between these models is less straightforward than the Volume of fluid model because they can handle the same applications (VOF was unique because it tracks the interface).

  However, one direct case in which we can easily decide which model to use is when dealing with very low dispersed phase volume fraction. In this case, discrete model is the best option.

  Other than this case, some parameters should be used to help us determine which model is more suitable:

  - **Particulate Loading:**

    The particulate loading (β) can be defined as the mass density ratio of the dispersed phase (d) to that of the carrier phase (q):

    $$\beta = \frac{\alpha_d \rho_d}{\alpha_c \rho_c} \tag{78}$$

    The ratio between dispersed phase density (d) and the carrier density (q) is called material density ratio (γ):

    $$\gamma = \frac{\rho_d}{\rho_c} \tag{79}$$

    The average distance between the dispersed phase particles relative to their diameter can be estimated according to the following equation:

    $$\frac{L}{d_d} = \left(\frac{\pi}{6}\frac{1+\kappa}{\kappa}\right)^{1/3} \tag{80}$$

    In which $k = \frac{\beta}{\gamma}$.

    Depending on the particulate loading, the degree of interaction between the phases can be predicted and so decide which model shall be used:

    - Very low particulate loading means that the dispersed particles are away from each other (isolated), and so the coupling between the

phases is one-way (the carrier phase affects the dispersed phase via drag and turbulence, but the particles do not affect the carrier). In this case, discrete model, mixture model and Eulerian model can be used. Since the Eulerian model is the most computationally expensive, discrete model and mixture model are recommended.

- Intermediate particulate loading means that the dispersed particles are no longer isolated and so the coupling is now *two-way* (the carrier affects the dispersed phase particles via drag and turbulence and in return, the dispersed phase particles affect the carrier via the reduction in mean momentum and turbulence). Here, you can also choose any of the three models. However, the decision is not complete and so other parameters should be considered such as Stokes number.
- In the case of very high particulate loading, there is *two-way* coupling plus particle pressure and viscous stresses due to particles (four-way coupling). Therefore, only the Eulerian model can handle this extremely high level of detail.

- **Stokes Number:**

  When having intermediate particulate loading, the loading number is not sufficient to decide which model is more appropriate and so an extra parameter "Stokes Number") shall be considered.

  Stokes number can be defined as the ratio between the particle response time (particle relaxation time τ_d) and the available system response time (t_s):

$$\mathrm{St} = \frac{t_d}{t_s} \tag{81}$$

  In which:

  - τ_p is the particle relaxation time which represents the time needed by the particle to react to change in the fluid flow and it can be calculated as follows:

$$t_p = \frac{\rho_p d_p^2}{18\mu_q} \tag{82}$$

- t_s is the available response time in our system and it can be calculated based on the characteristic length (L_s) and the characteristic velocity (V_s):

$$t_s = \frac{L_s}{V_s} \tag{83}$$

- Very low Stokes number means that the dispersed particles can easily respond to any change in the flow and so they strictly follow it. In this way, all the three models are acceptable and so the least computational expensive one will be desired (Mixture model or Dispersed Model).
- A very high Stokes number means that it is difficult to change the state of our dispersed particles and they shall take a long time to change (larger if compared to the available system time). So, these particles will move independently of the flow. Therefore, it is important to study the particles in detail with no averaging and so Eulerian or Dispersed Models are reliable.
- For intermediate Stokes number, both dispersed phase particles response time and the system time are comparable with nothing extreme. Therefore, any of the three models can be acceptable and so our choice will be based on the least computationally expensive one.[1]

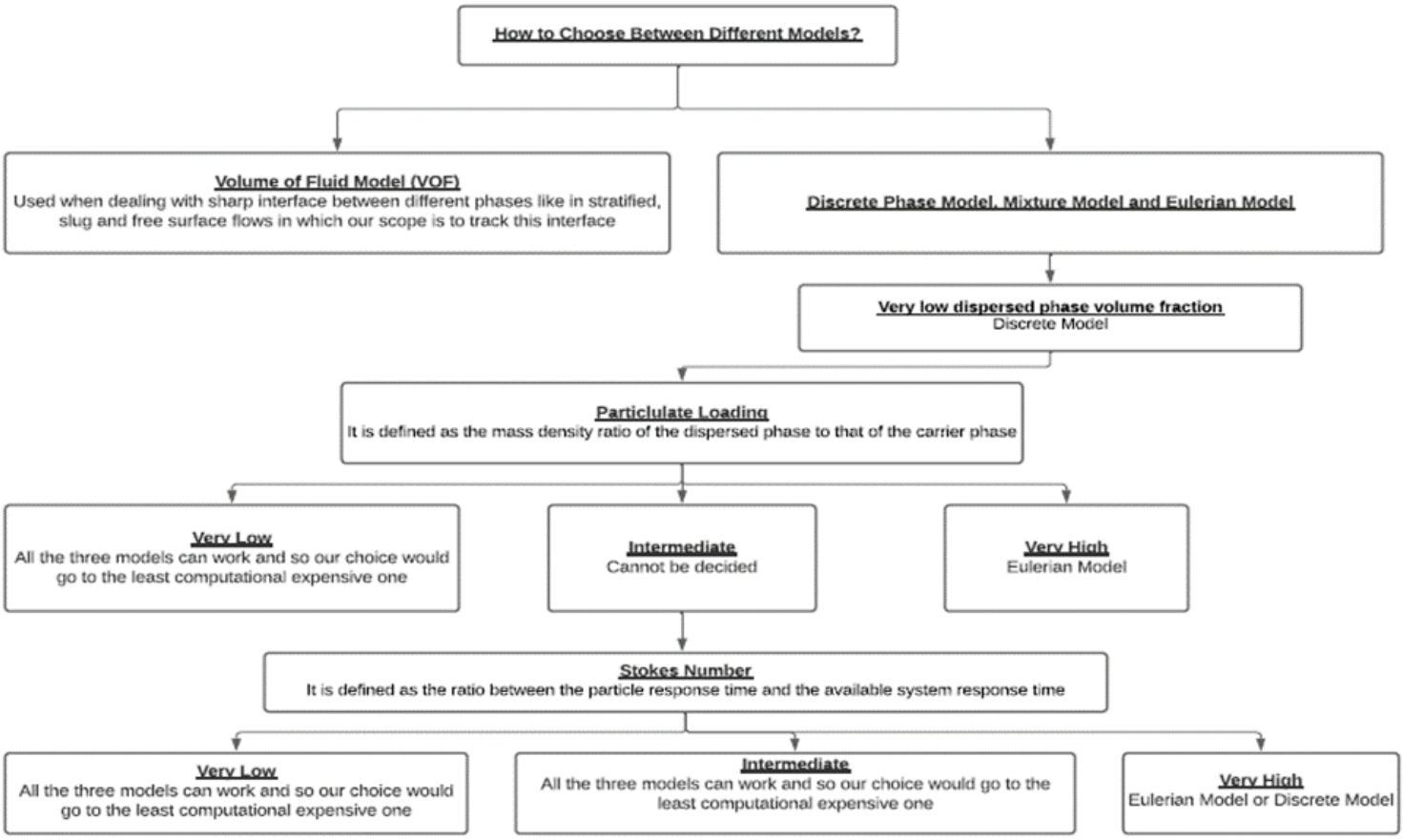

Figure 8: Flowchart representing how to choose between different multiphase models.

2.5 Turbulence Modelling

Turbulence means the chaotic motion of fluid flows. At low velocities, our fluid will flow in an orderly manner, and this called “Laminar flow”. However, this orderly manner flow changes when the speed or characteristic length of the flow is increased, leading to what is called “Turbulent flow”. Turbulent flow is characterized by having a large range of vortical structures at different scales, both in time and space, which interact with each other and exchange energy. The parameter that determines which flow type we are dealing with is the Reynolds number which is the ratio between inertial force and viscous force.[46]

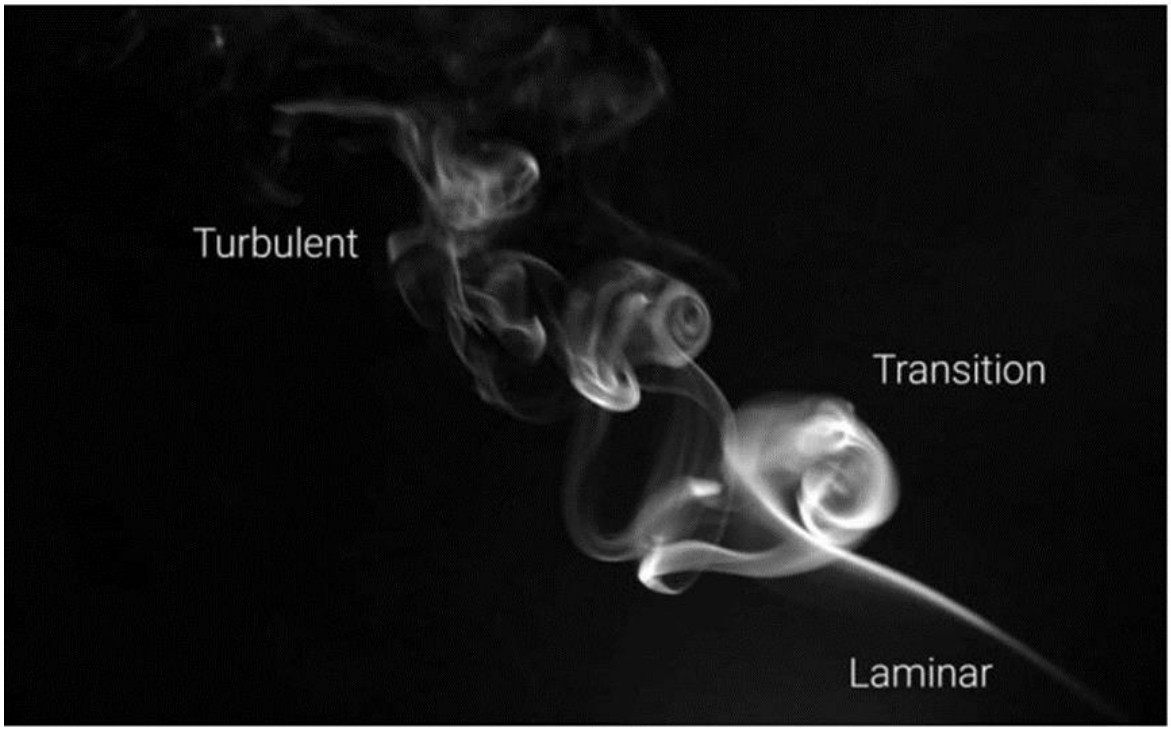

Figure 9: Laminar, Transitional and Turbulent flow

Since we are always dealing with turbulent flow in the industry, we shall always deal with this type of flow in any CFD simulation.

One way of dealing with turbulence is to solve directly the governing equations, especially Navier-Stokes's equation, without any modelling assumptions. This means we shall directly deal with the fluctuations in our parameters that are caused by the turbulence. This approach is called "Direct numerical simulation (DNS)".

It can accurately describe turbulence as it deals with the flow without any approximations. However, it requires extensively small mesh and large computational time and so it cannot be used in any industrial application.[46]

Another way of dealing with turbulent flows is to divide the eddies into large and small ones. Large eddies are then solved directly as the DNS while the small eddies are being modelled. This is because the flow structures at small scale turbulence tend to be similar to each other and so can be easily approximated to one model. This model is called "Large Eddy Simulation (LES).[7][46]

LES is considered a better modelling choice other than DNS. However, the main disadvantage of LES is the high meshing resolution required in the wall boundary

layers. This is because all the eddies, even the large ones, become relatively small near the wall and so direct simulation is then required.

Therefore, the need to have models for all the possible sizes is a necessity. Therefore, Reynolds Average Navier-Stokes Equations (RANS) approach is then developed to model the turbulence in an industrially acceptable way regarding both accuracy and computational time.

2.5.1 Reynolds Average Navier-Stokes Equations

When having turbulence in our system, there are fluctuations in our parameters (for example velocity, pressure,..etc). These parameters are found in each fluid governing equation (continuity and momentum equations) and if we would like to account for the turbulence in our model, we should then separate these fluctuations and find specific models for these new fluctuating parameters.

This separation process is called Reynolds averaging in which variables in the instantaneous (exact) Navier-Stokes governing equations are decomposed into average component and fluctuating component. For the velocity components:

$$u_i = \bar{u}_i + u_i' \tag{84}$$

In which:

- u_i is the instantaneous velocity.
- $\bar{u}_i$ is the average velocity.
- u_i' is the velocity fluctuations due to turbulence.

For any other variable, it can be decomposed in the same way as the velocity:

$$\varphi = \bar{\varphi} + \varphi' \tag{85}$$

After this decomposition, these terms are then substituted in the instantaneous Navier-Stokes equations with taking a time average. Finally, arranging the new equations and separating any fluctuation term.

The new equations are then called Reynold-averaged Navier-Stokes equations (RANS) and they have the same form as the instantaneous ones, but with averaged parameters instead of the instantaneous ones with additional terms that represent turbulence.

RANS equations can be written as follows (the overbar on the mean velocity $\bar{u}_i$ will be removed for simplicity):

$$\frac{\partial \rho}{\partial t} + \frac{\partial}{\partial x_i}(\rho u_i) = 0 \tag{86}$$

$$\frac{\partial}{\partial t}(\rho u_i) + \frac{\partial}{\partial x_j}(\rho u_i u_j) = -\frac{\partial p}{\partial x_i} + \frac{\partial}{\partial x_j}\left[\mu\left(\frac{\partial u_i}{\partial x_j} + \frac{\partial u_j}{\partial x_i} - \frac{2}{3}\delta_{ij}\frac{\partial u_l}{\partial x_l}\right)\right] + \frac{\partial}{\partial x_j}\left(-\rho\overline{u_i' u_j'}\right) \tag{87}$$

In which $\left(-\rho\overline{u_i' u_j'}\right)$ is the Reynolds stress which accounts for the turbulence and therefore, it needs to be modelled separately.[7]

2.5.2 Boussinesq Hypothesis for ($k-\varepsilon$) and ($k-\omega$) Models

Several models are used for Reynold's stress simulation like $k-\varepsilon$ model, $k-\omega$ model and Reynold's stress model. The main difference between them is the way of treating the Reynolds stresses.

In both $k-\varepsilon$ and $k-\omega$ models, Boussinesq hypothesis is used to relate the Reynolds stresses to the average velocity gradients:

$$-\rho\overline{u_i' u_j'} = \mu_t\left(\frac{\partial u_i}{\partial x_j} + \frac{\partial u_j}{\partial x_i}\right) - \frac{2}{3}\left(\rho k + \mu_t\frac{\partial u_k}{\partial x_k}\right)\delta_{ij} \tag{88}$$

Then, two additional transport equations are added to calculate the turbulent kinetic energy (K) and either turbulence dissipation rate (ε) or specific dissipation rate (ω). Then, μ_t (turbulent viscosity) is calculated as a function of these turbulence parameters.

The advantage of this approach is the relatively low computational time because only two equations are added to our system. However, its disadvantage that it is not very accurate because they are getting some average values representing the turbulence instead of modelling each stress term.[7]

2.5.3 Reynolds Stress Model (RSM)

In the case of having highly swirling flows and stress-driven secondary flows (complex turbulence systems). An alternative approach, called Reynolds Stress Model, can be

more accurate because our system needs a more rigorous way of modelling other than one or two equations.

In this approach, transport equations are to be solved for each Reynolds stress term. In addition, an extra equation representing the dissipation is required.

One advantage of this model is the accuracy and the ability to simulate complex turbulence conditions. However, it is computationally expensive because it adds seven transport equations to our system.

The general transport equation of the Reynolds stresses $\overline{u_i' u_j'}$ (for simplicity, R_{ij}) can be written as follows:

$$\frac{DR_{ij}}{Dt} = P_{ij} + D_{ij} - \epsilon_{ij} + \emptyset_{ij} + \theta_{ij} \tag{89}$$

In which:

- $\frac{DR_{ij}}{Dt}$ is the summation of both local time derivate of the Reynolds stress and its transport by convection.
- P_{ij} is the production rate of the Reynolds stress and can be calculated according to the following equation:

$$P_{ij} = -\left(\overline{u_i' u_k'} \frac{\partial U_j}{\partial x_m} + \overline{u_j' u_k'} \frac{\partial U_i}{\partial x_k}\right) \tag{90}$$

- D_{ij} is the diffusion transport term and it can be related to the Reynolds stress gradient according to the following equation:

$$D_{ij} = \frac{\partial}{\partial x_k}\left(\frac{\mu_t}{\sigma_k} \frac{\partial R_{ij}}{\partial x_k}\right) \tag{91}$$

- is the dissipation rate of the Reynolds stress.
- ϵ_{ij} , $\emptyset_{ij}$ and θ_{ij} are dissipation rate, pressure strain term and production by system rotation term, respectively. Each of them can be modelled but it is not our scope here to discuss in detail these terms and how to model them.[7][9][38][39][40]

2.5.4 Turbulence in Multiphase System

When having more than one phase in our system, describing the turbulence can be more challenging. This is because all the previous added equations to describe the

turbulence shall be doubled as we need to model each phase. This can be extremely complex and time-consuming. Moreover, it can be more difficult when using the Reynolds stress model (RSM) as we shall then add 14 equations to our system.

Therefore, ANSYS Fluent provides different approaches when dealing with the multiphase flow and we shall only discuss the option available for the RSM because this is the model to be used in our thesis.

For Reynolds Stress Model (RSM), turbulence model options are:[41]

- **Dispersed Turbulence Model:**

  It is used when having a low amount of the secondary phase (diluted secondary phase) in which the transport equations for turbulence (equation 86, 87 and 89) are only solved for the primary phase, while the predictions of turbulence quantities for dispersed phases are obtained using the Hinze-Tchen model.[45] According to Hinze-Tchen's model, particle fluctuation should be always weaker than the fluid fluctuation and the larger the particle size, the weaker the particle fluctuation. Hence larger particles should diffuse slower than smaller particles.

  Moreover, an extra term should be added in the momentum equation that represents the interaction between both phases.

- **Mixture Turbulence Model:**

  Here, it is assumed that both phases share the same turbulence field which is true when having comparable amounts of both phases in our system.

  Turbulence transport equations are normally solved, but for mixture properties that can be taken as an average of both phases.

When using any of these models, extra modelling is needed to simulate the turbulence interaction between primary and secondary phases.

In ANSYS Fluent, three models are proposed to simulate this interaction term:

- **Simonin et al. Model:**

  In this model, the turbulence interaction is modelled by adding a source term in the turbulence transport equation. However, it is suitable only for the dispersed turbulence model.[42]

- **Troshko-Hassan Model:**

  It is similar to Simonin et al. model in the way of including the interaction term in the transport equation but in an alternative way. Moreover, it is suitable for both dispersed turbulence model and mixture turbulence model.[43]

- **Sato Model:**

  Unlike the Simonin et al. and Troshko-Hassan models, the Sato model does not add an explicit turbulence interaction term in the transport equation. Instead, it adds the effect of the random primary phase motion induced by the dispersed phase and related it to the secondary phase through equations.[7][44]

2.6 Solution Methods

The previous governing equations can be solved analytically for very simple cases.

Practically, only numerical solutions are available for these equations and so they should be transformed, in the case of steady-state simulations, first to algebraic ones (discretization) and then these algebraic equations can be solved for our domain.

A lot of solution methods (discretization) are available, but we shall only discuss the ones that are found in ANSYS Fluent software and used in this thesis study.

2.6.1 Finite Volume Method

In this method, our domain is divided into cells (control volumes) and the differential governing equations are applied to each cell.

This method ensures the conservation in each cell and the whole domain and allows for the use of unstructured grids which decreases the computational time.

There are types of this solution method, and we shall only discuss the one that shall be used here.

2.6.1.1 Centre Node Based Finite Volume Method

- The computational domain is divided into a mesh where each cell is considered as a small control volume.
- The governing equations are integrated over each control volume and then discretised to obtain one set of algebraic equations for each control volume/cell.
- The value of each variable is stored in the node centre (that is why it is called centre node-based). However, the algebraic discretised equations should also include values for the cell faces and that is the role of interpolation to obtain approximate values at these faces.[5]

The interpolation is accomplished using an upwind scheme (for example First-Order upwind, Second-Order upwind, Quick,…etc) and choosing between these methods is up to the modeller as it has an impact on numerical stability, convergence rate and accuracy.[1]

2.6.2 Coupled Versus Segregated Solvers

After having the discretised algebraic form of the governing equations, pressure and velocity are strongly coupled (meaning that they are connected) and they should be solved at the same time (we cannot solve one and get the other).

This is because pressure gradient appears in the momentum equations and hence the pressure distribution is needed to solve these equations. If the pressure is known, the momentum equations can be also used to solve for the velocities, but the continuity equation cannot be used directly to obtain the pressure field if the velocity is known and here is the problem.

To solve this problem, two main types of solvers exist:

- **Segregated Solver:**

  It is based on using a pressure correction equation.

  - Firstly, the momentum equations are solved after guessing a certain pressure to obtain velocities.
  - Secondly, the obtained velocities are then checked through the continuity equation.

- If they satisfy the continuity equation, problem solved.
- If not, a pressure correction equation is solved to update the pressure field and then used again in the momentum equations to obtain new velocities and so on.
- There are several pressure corrections schemes. The most widely used one is the SIMPLE (Semi Implicit Method for Pressure Linked Equations).
- This process is repeated till the obtained velocity fields satisfy both the momentum equations and the continuity ones.

One advantage of this method is that the equations are solved subsequently (steps and not simultaneously) and so only one equation needs to be stored at a time which means low memory requirement. However, due to the iterative nature of the solution algorithm, the convergence rate is often slower as it needs a lot of iterations.[11]

- **Coupled Solver:**

  Momentum and continuity equations are solved simultaneously to obtain both pressure and velocities which is the basic difference between this solver and the previous one.

  This means that all the equations need to be stored at the same time and so larger memory requirement.

  However, in return for taking more time for each iteration due to the coupling, the total number of iterations to achieve convergence is usually lowered.[11]

3 CASE STUDY 1

3.1 Experimental Work

In bubble flow systems, some local parameters like local void fraction, interfacial area, interfacial velocities, and bubble diameters are extremely important in characterizing the flow. For example:

- Local void fraction shows how the dispersed phase is distributed inside our flow, which is basic in both hydrodynamic and thermal calculations.
- Interfacial area represents the available area between both phases, and it plays an important role in both mass and heat transfer between phases.

However, most of the information is about the average values of these properties and not local ones (average void fraction instead of local void fraction).

In the research paper named “Experimental Study on Local Interfacial Parameters in a Horizontal Bubbly Two-Phase Flow” conducted by “G. Kocamustafaogullari and Z. Wang”, these local parameters were measured in a horizontal bubbly two-phase (water-air) flow using a double-sensor electrical resistivity probe. Moreover, the dependence of these local parameters on other flow variables was also studied.

The double-sensor resistivity probe is shown in figure 10. It consists of two identical stainless-steel wire sensors which are completely insulated from the environment except at their tips. These tips are sharpened to minimize bubble deformation contacting these sensors and they are placed next to each other but insulated from each other.

When an air-water system flows across these sensors and both water and air contact them, they can electrically behave differently because air can be considered as electrically insulating, whereas water is electrically conducting.

- When contacting water (a good conductor of electricity), the circuit is closed.
- When contacting air (a bad conductor of electricity), the circuit is open.

Since the circuit is open or closed depending on whether the sensor is in contact with gas or liquid, the voltage drop across each sensor fluctuates between minimum and

maximum. These values were calibrated using previous experiments for each local parameter and so each voltage drop represents a certain value for each parameter.[11]

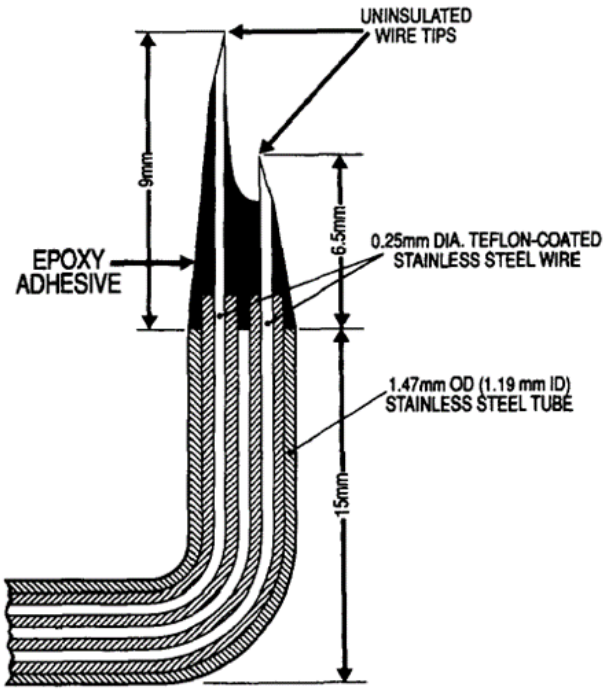

Figure 10: Double-Sensor Electrical Resistivity Probe Design.[11]

3.1.1 Experimental Procedure

- The experiment is conducted in a circular Pyrex glass tubing flow loop as shown below in figure 11. This loop is of 50.3 mm inner diameter and a total length of 15.4 m, and it is made of glass (a transparent material) to better visualize the flow and its local parameters.

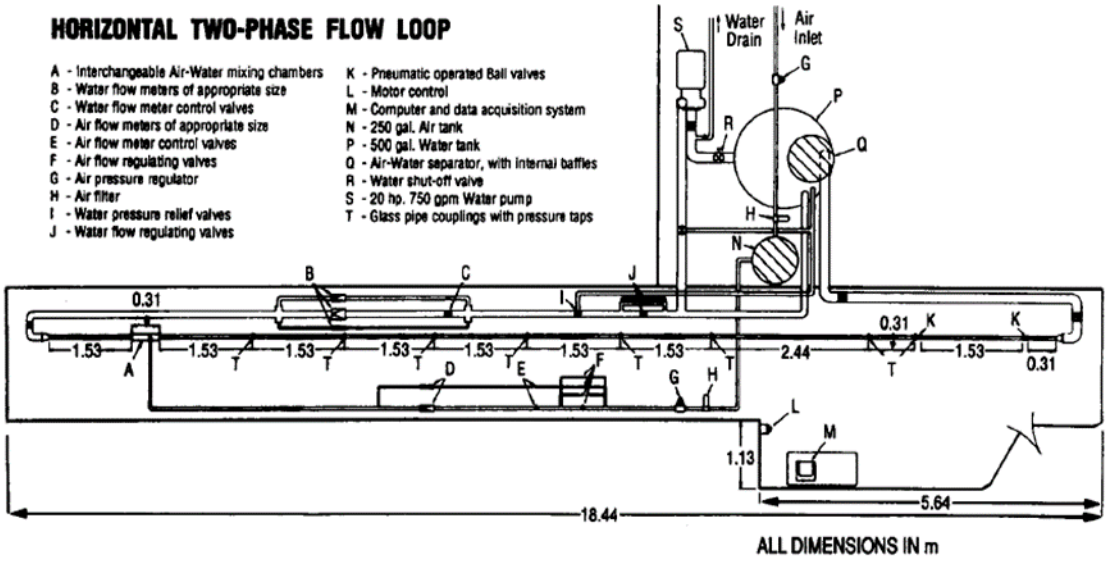

Figure 11: Schematic of the experimental flow loop.[11]

- Both water and air were supplied from two different sources and so mixing between them is essential before entering the flow loop. In the mixing chamber, air enters from a 90° vertical leg and is injected into the water flow through a porous cylindrical to achieve a uniform distribution of bubbles before entering the flow lop and so have a fast fully developed flow.

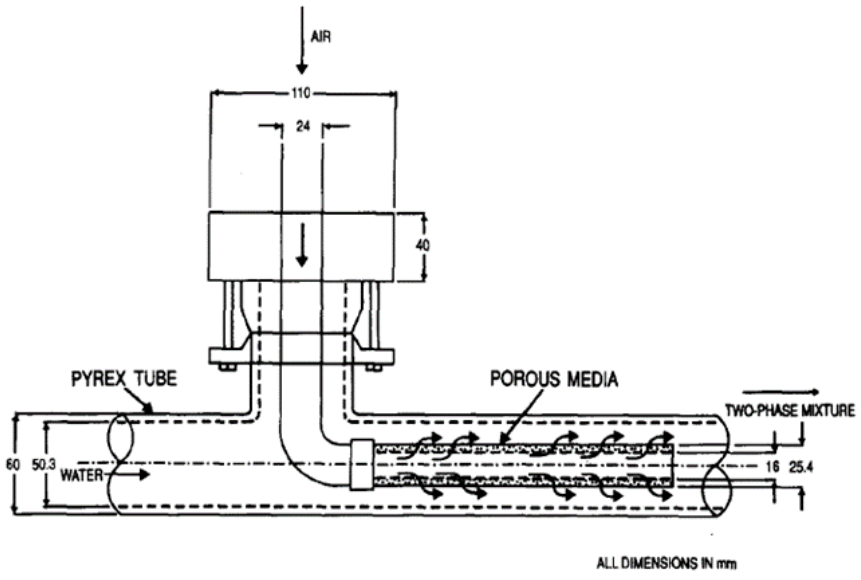

Figure 12: Air-Water mixing chamber.[11]

- Several experiments were carried out through the variations in both liquid and gas flow rate in which liquid superficial velocities ranged from 3.74 to 5.71 m/s

(Liquid Reynolds number is from 1.99×10^5 to 3.2×10^5), and gas superficial velocities ranged from 0.25 to 1.37 m/s (Superficial velocity means the velocity of any fluid in a multiphase flow if it found alone in the pipe). Details of these experimental conditions are summarized in table 1.

Number	Liquid Superficial Velocity (m/s)	Gas Superficial Velocity (m/s)	Void Fraction (%)
1	3.74	0.25	5.7
2	3.74	0.51	10.5
3	3.83	0.72	15.18
4	3.74	1.03	18.3
5	4.05	0.26	6.48
6	4.05	0.51	10.7
7	4.05	0.76	15.4
8	4.06	1.04	18.7
9	4.05	l.34	21
10	4.45	0.24	4.7
11	4.36	0.51	10.3
12	4.36	0.78	14.1
13	4.36	1.31	21.5
14	4.36	1.59	22.5
15	4.78	0.25	4.3
16	4.67	0.53	8.7
17	4.7	0.79	14.3
18	4.77	1.19	18.25
19	5.1	0.24	4.34
20	5.1	0.48	8.02
21	4.98	0.8	13.9
22	4.98	1.34	20.4
23	5.29	0.8	12.5
24	5.29	1.35	20.8
25	5.71	0.71	10.6
26	5.6	1.37	21.8

Table 1: Experimental conditions in G. Kocamustafaogullari and Z. Wang experiment.[11]

- For any fixed liquid superficial velocity, the gas superficial velocity was increased as long as the flow pattern was still bubbly.
- For each gas superficial velocity, our limit for the liquid velocity is the allowed pressure in the Pyrex glass tube.
- Local parameters were measured at the end of the flow loop using the double-sensor resistivity probe in which the sensor tip position is changed vertically across the pipe diameter (figure 13) to have readings about the local

parameters along the tube cross-section and thus reveal their patterns vertically.[11]

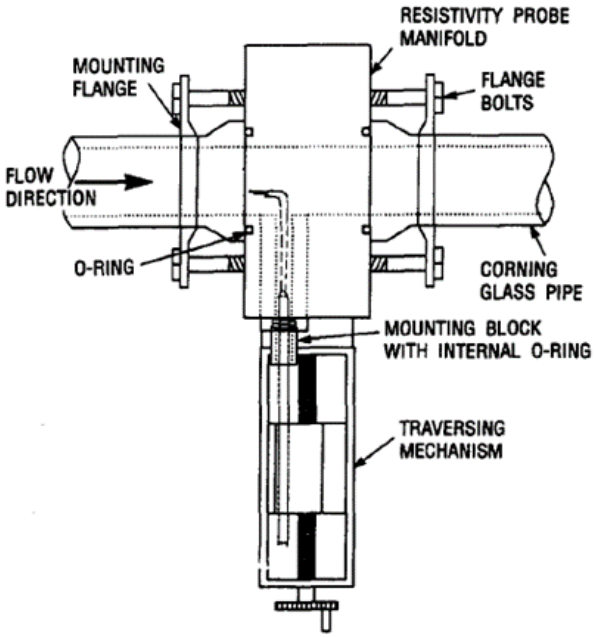

Figure 13: Mounting and traversing in double-sensor resistivity probe.[11]

3.1.2 Experimental Results

- Local void fraction results are shown in figures 14 and 15 for different gas and liquid superficial velocities.

  According to figures 14 and 15, we can see larger void fractions at the top of the pipe, which is reasonable because of the effect of buoyancy. This increase reaches a maximum at about r/R = 0.8 to 0.9 in which the peak value changes for each case according to the inlet velocities. However, a sharp decrease at the upper pipe wall happens because the bubbles start to collapse and so local gas fraction decreases. Moreover, peak value increases with increasing gas superficial velocity (gas flow rate) and decreases with decreasing the liquid velocity.

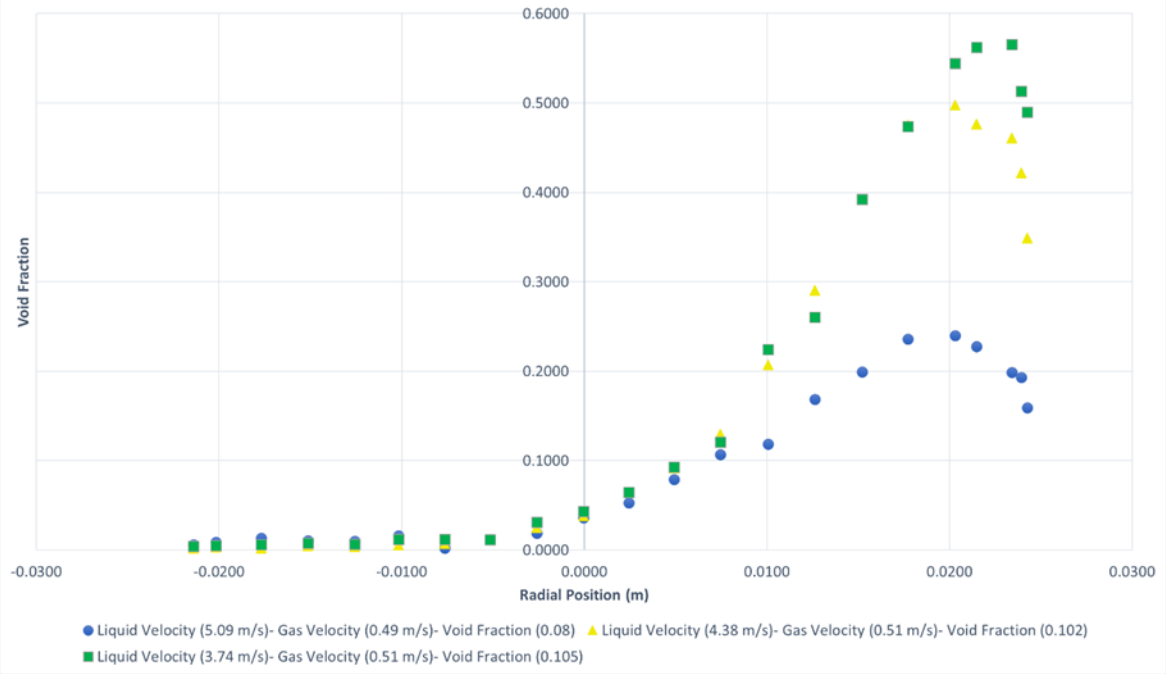

Figure 14: Gas Void fraction versus radial position for different gas flow rates at a constant liquid velocity.[11]

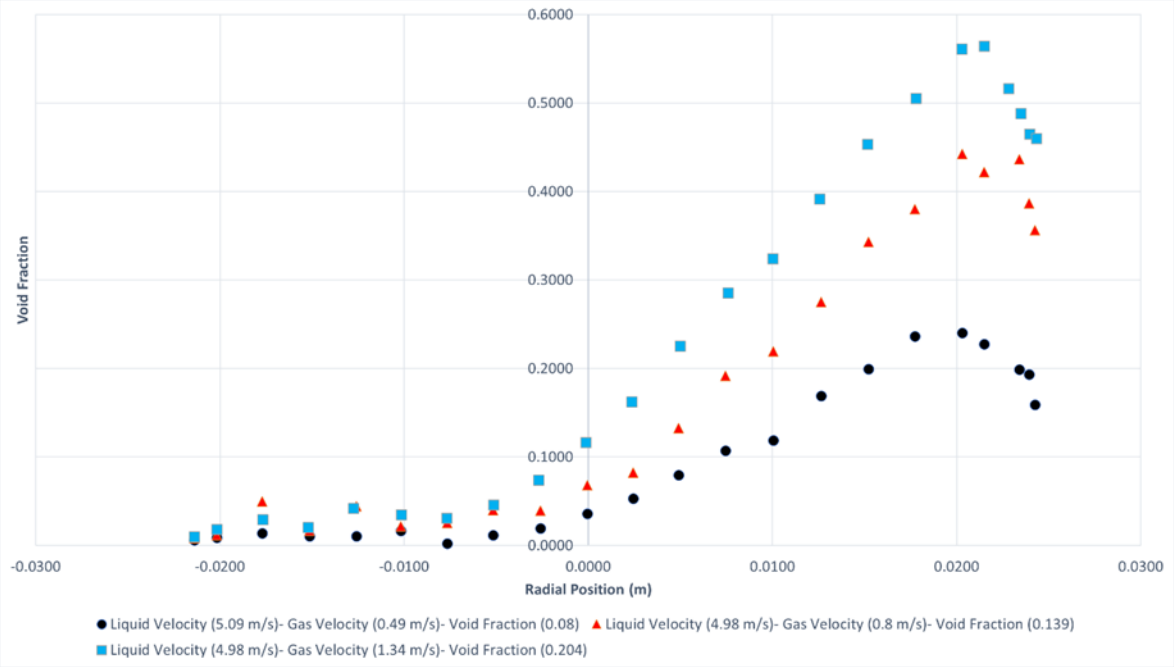

Figure 15: Gas Void fraction versus radial position for different liquid flow rates at a constant gas velocity.[11]

- Air bubble diameter was another local parameter to be reported as shown in figures 16 and 17 in which bubble diameter was estimated according to both measured local void fractions and interfacial area concentrations. It may be

observed that the local bubble diameter for each case is slightly uniform across the tube with a sharp decrease near the walls due to bubbles break up due to the shear rate near the wall[47]. Decreases with either decreasing gas flow rate or increasing liquid flow rate and vice versa with a range of 2-5 mm.

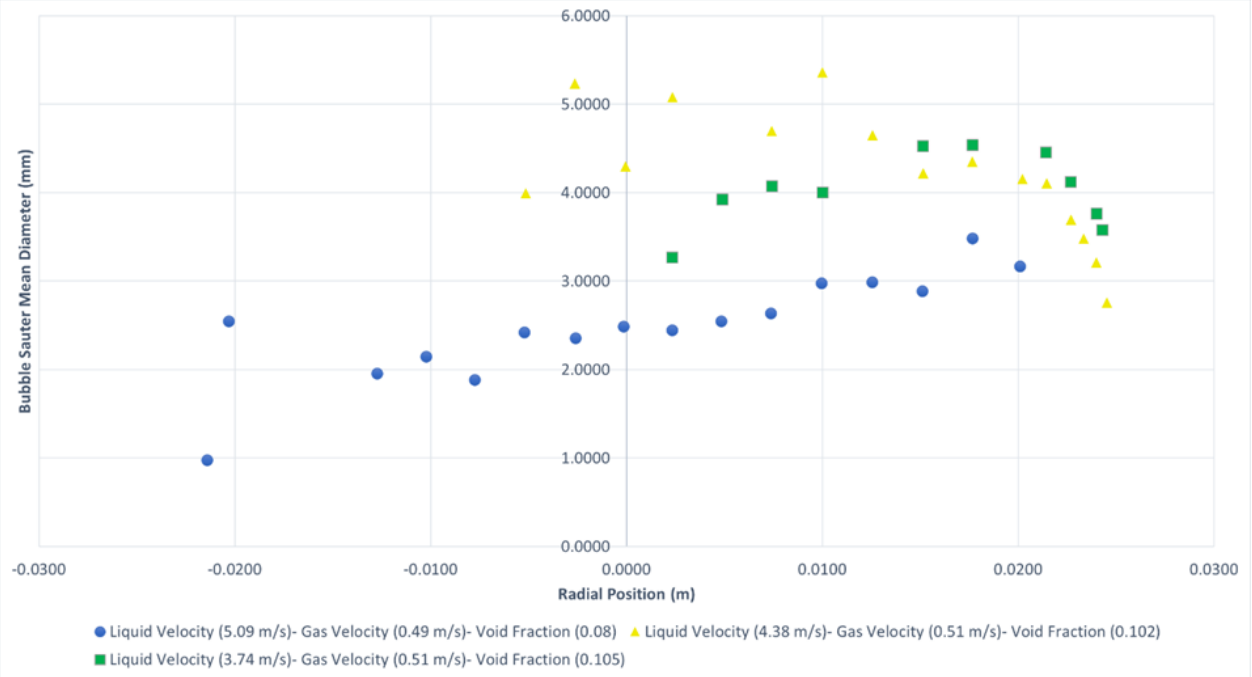

Figure 16: Bubble diameter versus radial position for different liquid flow rates at a constant gas velocity.[11]

Figure 17: Bubble diameter versus radial position for different gas flow rates at a constant liquid velocity.[11]

- Local bubble interface velocity was one last parameter to be measured as shown in figures 18 and 19. It can be observed that an increase in either liquid or gas flow rates increases the bubble velocity. Moreover, it shows a profile of having the biggest value in the pipe centre and almost no velocity near the wall.[11]

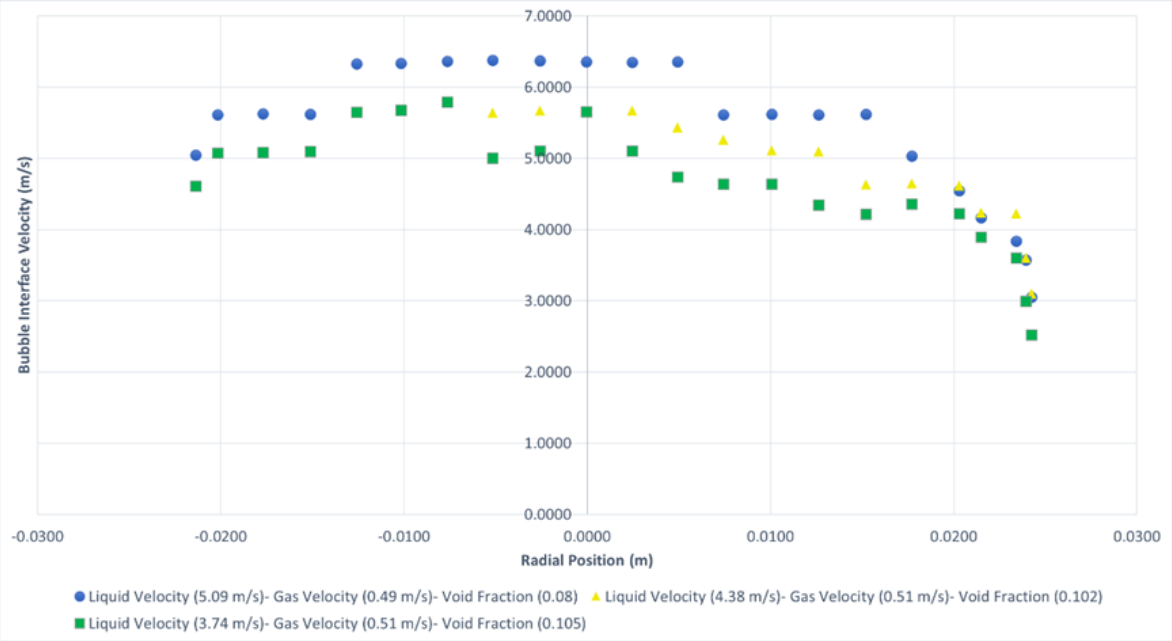

Figure 18: Local bubble interface velocity versus radial position for different liquid flow rates at a constant gas velocity.[11]

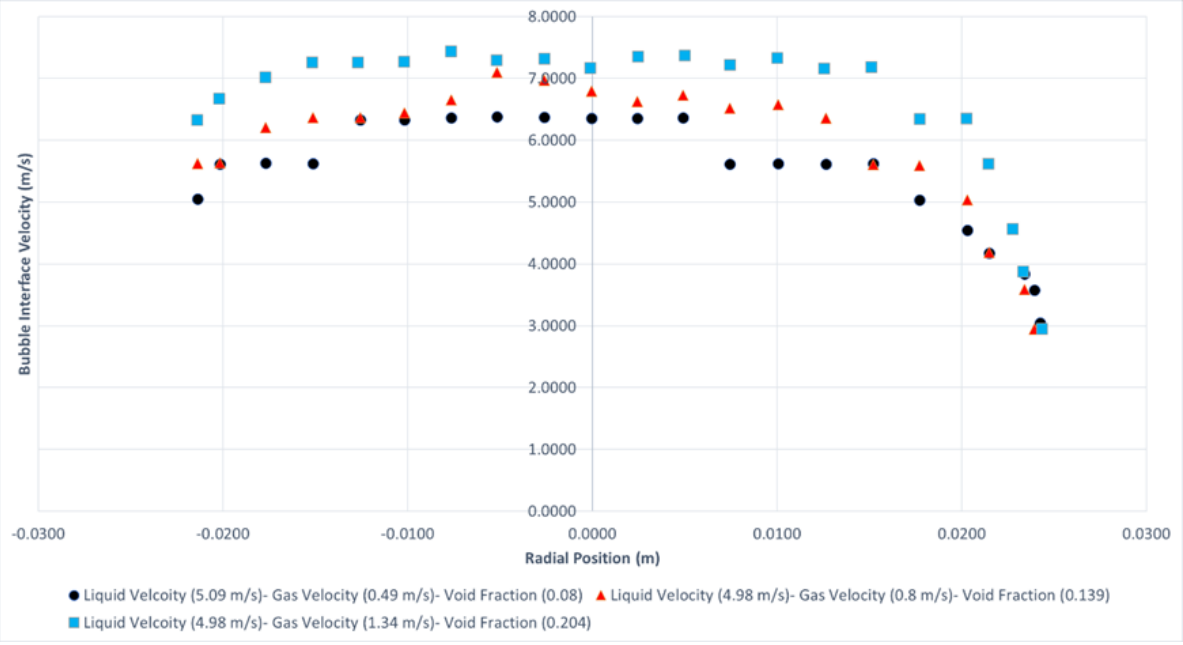

Figure 19: Local bubble interface velocity versus radial position for different gas flow rates at a constant liquid velocity.[11]

3.2 Simulation Methodology

The scope of this thesis work is to study different multiphase models and find the best one that can simulate bubbly gas-liquid flow.

Our study of multiphase flow will be focused on studying the interaction forces between different phases such as drag force, lift force, wall lubrication force,…etc (refer to section 2.4.3) in which we should answer two basic questions:

- What forces (out of all the possible interaction forces) should be included in our simulation model that can both accurately and stably describe our system.
- Out of all the possible models for each force, what model should be selected to describe bubble gas-liquid flow?

To do so, a sensitivity analysis shall be done on each force and each model using the experimental work done by G. Kocamustafaogullari and Z. Wang according to the following:

- Firstly, we took one experiment out of the 26 done experiments as a first case study to be used in doing the sensitivity analysis on the phase interaction forces.
- In the beginning, only the drag force was included as an interaction force between gas and liquid.
- Different sub-cases were investigated using all the 6 available models representing the drag force in ANSYS Fluent (Schiller and Naumann Model[14], Morsi and Alexander Model[15],…etc).[7]
- We ran these six sub-cases until they converged and used some parameters (local void fraction and bubble interface velocity) to compare both experimental and numerical results.
- Out of these six sub-cases, we chose the best drag force model in which its sub-case has both the most accurate results compared to the experimental one and the most stability.
- This selected drag force model shall be then fixed in all the successive sub-cases.

- After that, the lift force was analysed and another four sub-cases were investigated by including the four lift force models (Saffman-Mei Model[20][21], Legendre-Magnaudet Model[22], Moraga Model[23] and Tomiyama Model[24][25]).[7]The previously selected drag force model was adopted for all these sub-cases.
- Another sensitivity analysis was done for these four cases using the experimental data and allowed to choose the best lift force model that can accurately describe the system.
- After choosing the best lift force model, it shall be fixed beside the already fixed drag force model in all the coming sub-cases.
- The remaining phase interaction forces and their models were investigated using the same way as the drag and lift forces were analysed in which each chosen model was fixed in the next steps and so on.
- These steps were repeated for all the possible interaction forces until finding the best combination of models that can both accurately and stably describe any gas-liquid multiphase system.
- Finally, after having selected the best set of interaction force models, we applied it to other cases of the same experimental dataset to validate it and make sure that it can work in different simulation conditions.

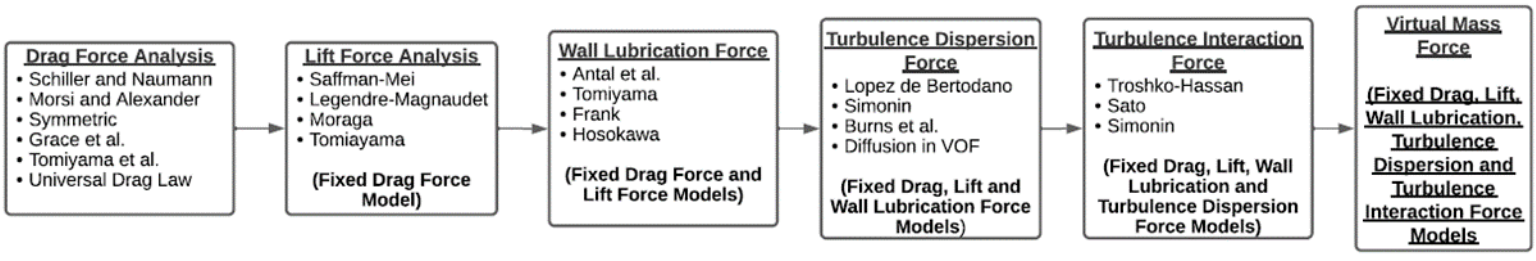

Figure 20: The sensitivity analysis methodology

Note: In this sensitivity analysis, all the other simulation settings (like the turbulence model, general multiphase model, solution methods,…etc) was kept fixed as we were mainly focused on studying the interaction force terms and so do not make our analysis extremely complicated.

- **Geometry and Meshing:**

Our computational domain was drawn using DesignModeler software (a drawing software coupled with ANSYS Fluent program in ANSYS workbench). According to figure 11, our computational domain should be the glass tubing (after the air-water mixing chamber) in which both air and water flow simultaneously. It is a horizontal cylinder having an inner diameter of 50.3 mm and a total length of 15.4 m. However, it would take a long computational time if we considered all the cylinder length (15.5 m) in our domain. This is because it is a horizontal cylinder in which our gas-liquid mixture is moving with no interference from the environment. Therefore, we considered only a part of it that secured having no change in the system flow. The minimum length to be considered should be the entrance region length in which the fluid reaches fully developed conditions (a constant continuous flow profile) and a length of 50D is used as a preliminary guess for this entrance region length (Wasp et al.). According to previous numerical studies done on this experiment, a tube length of 9 m must be considered (figure 21).[6][9]Moreover, full 3D geometry was used in describing our computational domain instead of having a 2D geometry with the central symmetry plane because of the buoyancy effect on the gas phase and due to having more complex geometries in most of the coming cases which are not axis-symmetric and so having a full 3D in doing our sensitivity analysis is essential.

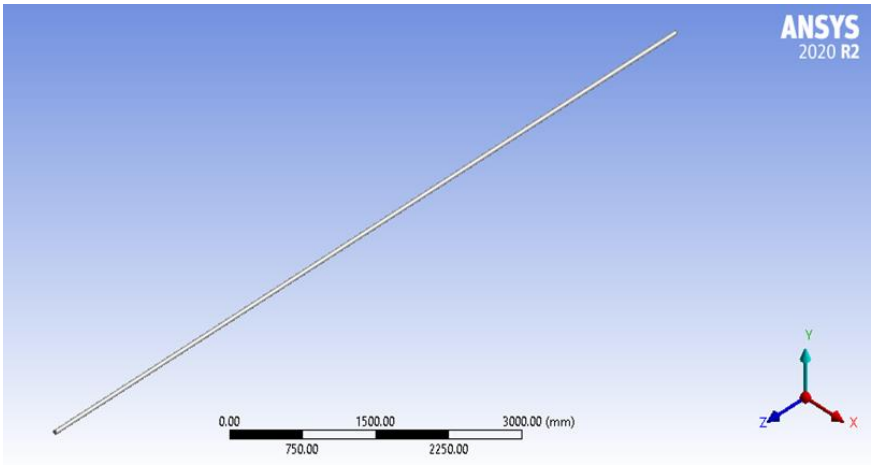

Figure 21: Case Study 1 (Computational Domain)

For meshing, an unsymmetrical mesh was done for our computational domain in which our cross-section has 15 inflation layers near the wall, with a growth rate of 20% and a total thickness of 13 mm (about half of the pipe radius).

The addition of these inflation layers was to increase the accuracy of our simulation accuracy near the wall due to the large number of phenomena taking place near the pipe wall (for example water velocity gradient, lift force, wall lubrication force,..etc).

To determine our mesh element size in the rest of our domain (Other than the inflation layers), a mesh independence analysis was done using different element sizes as shown in figure 22. Note that this mesh independence analysis was done using arbitrary phase interaction force models as the sensitivity analysis was still not performed till doing this mesh analysis. Moreover, it was done using an experimental case study of inlet superficial liquid velocity, inlet superficial gas velocity and inlet void fractions of 5.1 m/s, 0.24 m/s and 0.043, respectively.

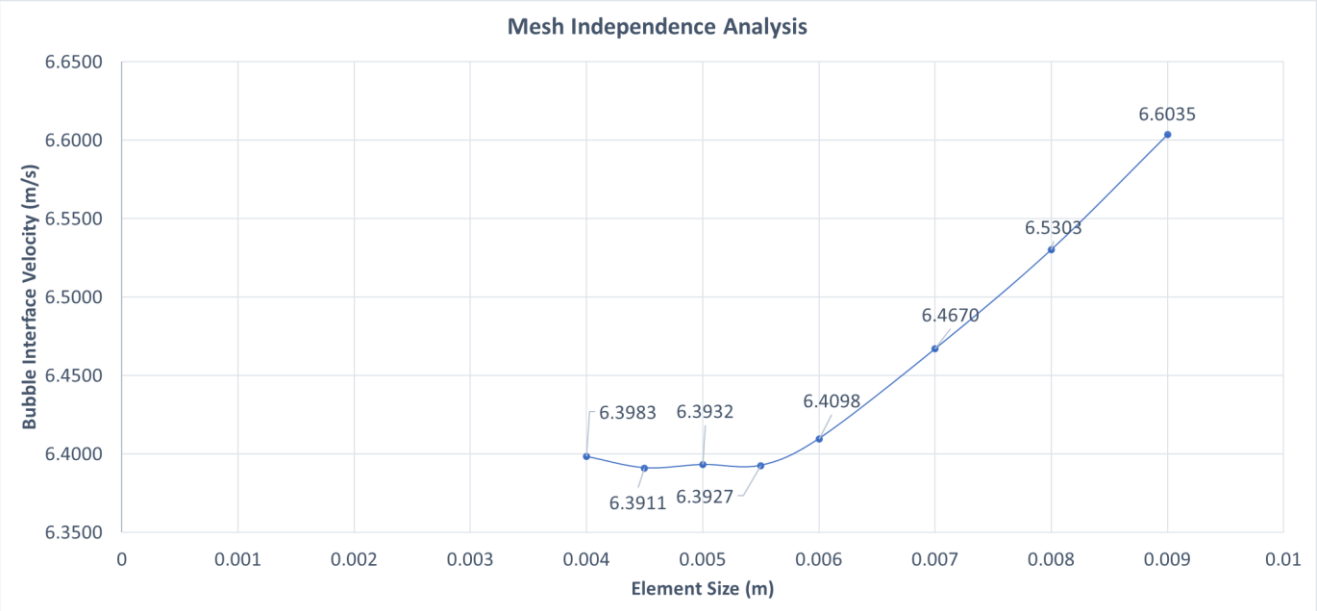

Figure 22: Mesh independence analysis of case study 1

As one can see, the bubble interface velocity value became almost constant after having an element size of 5.5 mm and so this element size shall be used in all our coming simulation cases.

Our mesh, using 5.5 mm as an element size with 15 inflation layers of a total thickness of 13 mm, is shown in figure 23.

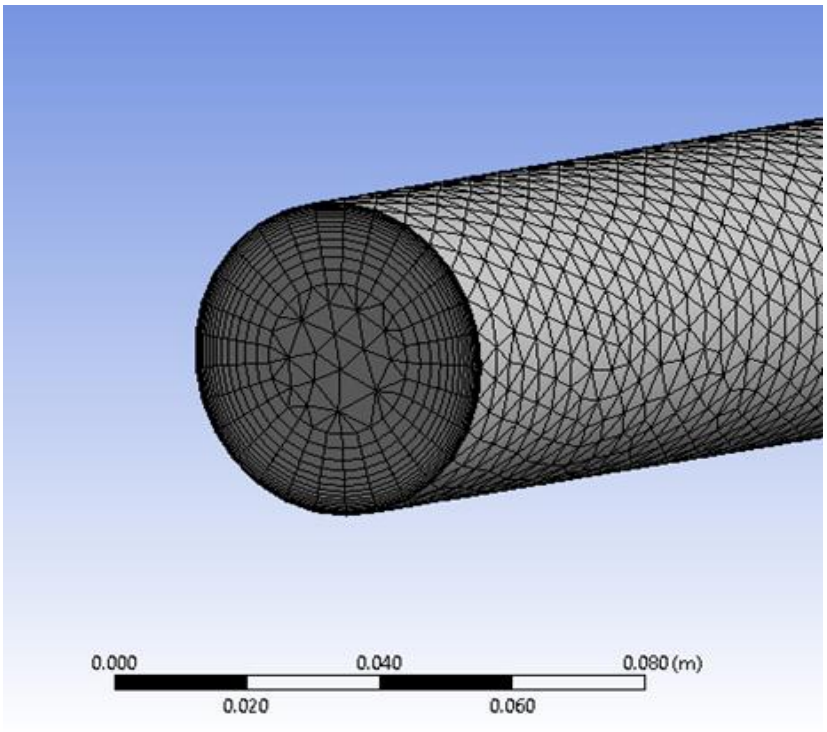

Figure 23: Mesh Distribution of case study 1 (using 5.5 mm element size)

- **Simulation Settings:**

  As mentioned before, all the simulation settings (other than the interaction forces between phases) should be fixed when setting up our simulation settings. These fixed settings are as follows:

  - **Solver Type:**

    Pressure based (as we are dealing with incompressible flow" water"). Although part of our domain was air (compressible), the presence of water makes the density-based option not available.

- **Time Formulation:**

  Steady State simulation because the experiment reached average steady conditions and the steady-state simulation is significantly less time consuming than a transient one.

- **Multiphase Model:**

  Eulerian model (refer to section 2.4.2.1) is used because it is the most accurate model used in dealing with the multiphase flow and so it does not involve other approximations (when using other multiphase models) that can affect our sensitivity analysis.

- **Turbulence Model:**

  Reynolds Stress Model (RSM) was used because it is the most accurate RANS model to describe the turbulence since it has 7 equations describing all the Reynolds stresses in our system other than having only 2 equations as in both k-ε and k-ω models (refer to section 2.5.3). Moreover, the Dispersed turbulence model will be used when applying RSM in our multiphase flow because these experiments are characterized by a low amount of air (less than 25%) in the water and so turbulence equations are solved only for water and air turbulence can be obtained using Hinze-Tchen theory.[45]

- **Boundary Conditions:**

  As already said, out of all the 26 runs found in the experimental work which differ in inlet superficial velocities and so differ in void fractions, we selected only six cases. Three of these cases have a constant gas superficial velocity and a decreasing superficial liquid velocity while the other three have a constant liquid velocity with increasing gas velocity. Their inlet boundary conditions are as follows:

Case Number	Inlet Superficial Liquid Velocity (m/s)	Inlet Superficial Gas Velocity (m/s)	Inlet Gas Void Fraction	Bubble Diameter (mm)
1	5.09	0.49	0.08	2.8
2	4.38	0.51	0.102	4.2
3	3.74	0.51	0.105	4

Table 2: Case studies having constant gas superficial velocity.

Case Number	Inlet Superficial Liquid Velocity (m/s)	Inlet Superficial Gas Velocity (m/s)	Inlet Gas Void Fraction	Bubble Diameter (mm)
4	5.09	0.49	0.08	2.8
5	4.98	0.8	0.139	4.2
6	4.98	1.34	0.204	4.5

Table 3: Case studies having constant liquid superficial velocity.

Case 6 will be the only case used in our sensitivity analysis of the interaction forces between phases, while the rest of the cases will be used in validating our generated model and making sure that it works in different simulation conditions.

In ANSYS Fluent, we cannot directly use these inlet velocities because they are superficial ones meaning that they represent the velocity of each fluid (liquid, gas) assuming that it is alone inside the pipe. To convert them to actual velocities, we should use the following relation:

$$Actual\ Phase\ Velocity = \frac{Superficial\ Phase\ Velocity}{Phase\ Volume\ Fraction} \quad (92)$$

Moreover, atmospheric pressure was used as an outlet pressure boundary condition and a stationary wall was assumed with standard roughness of 0.0001 m. This value was based on the Pyrex glass material roughness that was used in the experimental setup and on the research paper entitled "Validation of CFD Model of Multiphase Flow through Pipeline and Annular Geometries." done by Rasel A Sultan

- **Bubble Diameter:**

  As seen in tables 2 and 3, constant bubble diameters were assumed instead of using the population balance model because of simplicity, thus avoiding making our system too complex when performing the sensitivity analysis. Bubble diameters for our cases were extracted as an average from the experimental results (Figures 16 and 17).

- **Pressure-Velocity Coupling:**

  Phase coupled SIMPLE is used which is based on an extension of the SIMPLE algorithm for multiphase flow.

- **Discretization Scheme:**

  Second-order Upwind and QUICK discretization schemes were used because of their high accuracy.

- **Under Relaxation Factors:**

  Under-Relaxation factors always help in reaching solution stability. After each iteration, a new value for variable U in cell (i) is updated according to the following equation:

  $$U_i^{NEW,USED} = U_i^{OLD} + \alpha\left(U_i^{NEW,PREDICTED} - U_i^{OLD}\right) \quad (93)$$

  In which α is the under-relaxation factor. When having α =1, it means that no under-relaxation is included and the new predicted value from the new iteration is used. On the other hand, our system is relaxed when having α < 1 meaning that only a part of the predicted value is used in the next iteration, and not the whole predicted value. This slows down the speed of convergence but increases the stability of the computation because it decreases the possibility of divergence or oscillations in the solution.

  In our case study, ANSYS Fluent default values of under-relaxation factors were sufficient.

- **Solution Initialization:**

  Hybrid initialization is used because it solves a few iterations, usually 10, of a simplified equation system and thereby gets usually a better initial guess for the flow variables, for the pressure field.

- **Convergence Criteria:**

  Scaled residuals for momentum, continuity, turbulence, and volume fraction equations are monitored and our solution is considered converged when they all reach a value below 10^{-5}. However, this criterion alone is not always reachable because it might never be fulfilled even though the solution is valid in some cases. Therefore, some parameters are being monitored besides the scaled residuals (for example local void fraction peak in the pipe, average velocity,..etc) and when both scaled residuals and our parameters reach constant values over a large number of iterations, our solution can be considered converged.

- **Evaluation Criteria:**

  Results from a numerical simulation can be judged based on the following three different criteria:

  - Accuracy: it means how our different models succeeded in predicting some parameters like void fraction, phase velocities,…etc.
  - Computational time: It evaluates how much time is needed by a certain model to converge.
  - Stability: It measures how difficult it was to obtain a converged solution using a certain model.[5]

3.3 Results and Discussion

3.3.1 Sensitivity Analysis on Phase Interaction Force Models

To perform the sensitivity analysis on the phase interaction forces and find what forces and models should be included to better describe the bubbly gas-liquid flow, one case study, out of all the experimental cases, was used as a validation tool.
In our analysis, case study 6 (refer to table 3) was used in which:

- Inlet liquid superficial velocity: 4.98 m/s
- Inlet gas superficial velocity: 1.34 m/s
- Inlet void fraction: 0.204
- Inlet bubble diameter: 4.5 mm

In this case study, both local void fraction and local bubble interface velocity profiles across the pipe outlet cross-section were used as validation tools by comparing them in both the experiment and the model.

3.3.1.1 Drag Force

According to section 2.4.3.1, six models are available in ANSYS Fluent that can be used to describe the drag force between both primary and secondary phases:

- Schiller and Naumann Model[14]
- Morsi and Alexander Model[15]
- Symmetric Model[7]

- Grace et al. Model[16]
- Tomiyama Model[17]
- Universal Drag Law[18]

And so, six sub-cases were conducted in which each one uses one of these drag force models while having no other interaction forces in these sub-cases.

Figures 24 and 25 represent the comparison between different drag force models and the experiment concerning both local void fraction and bubble interface velocity.

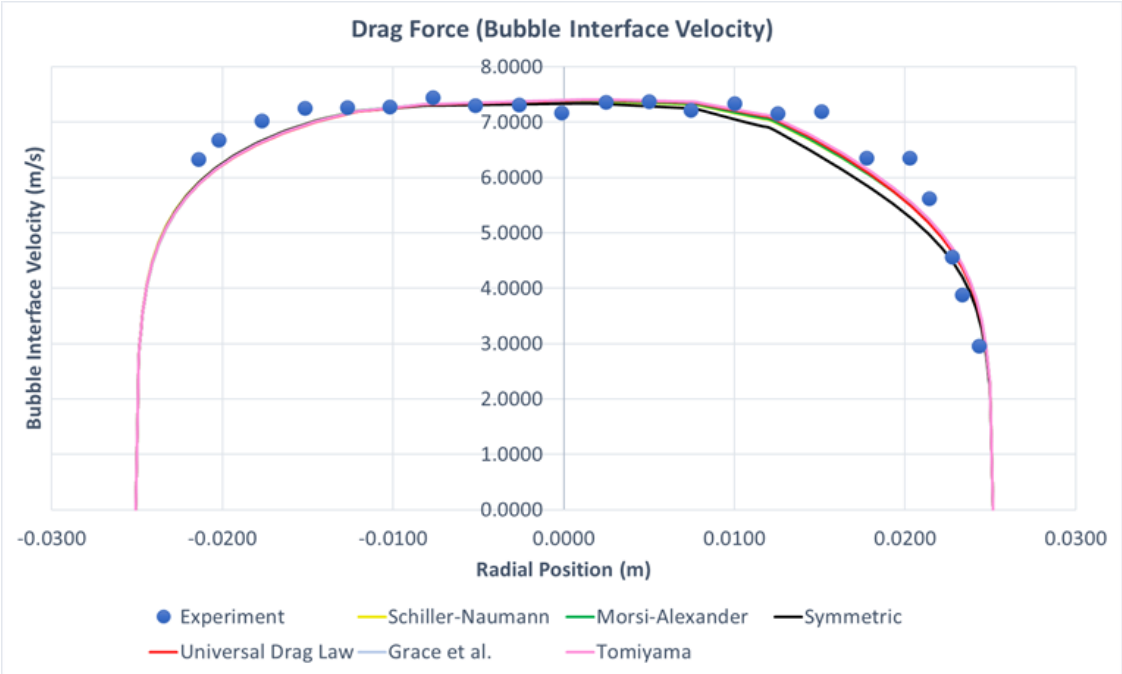

Figure 24: Comparison between drag force models and the experimental measurements concerning local void fraction.

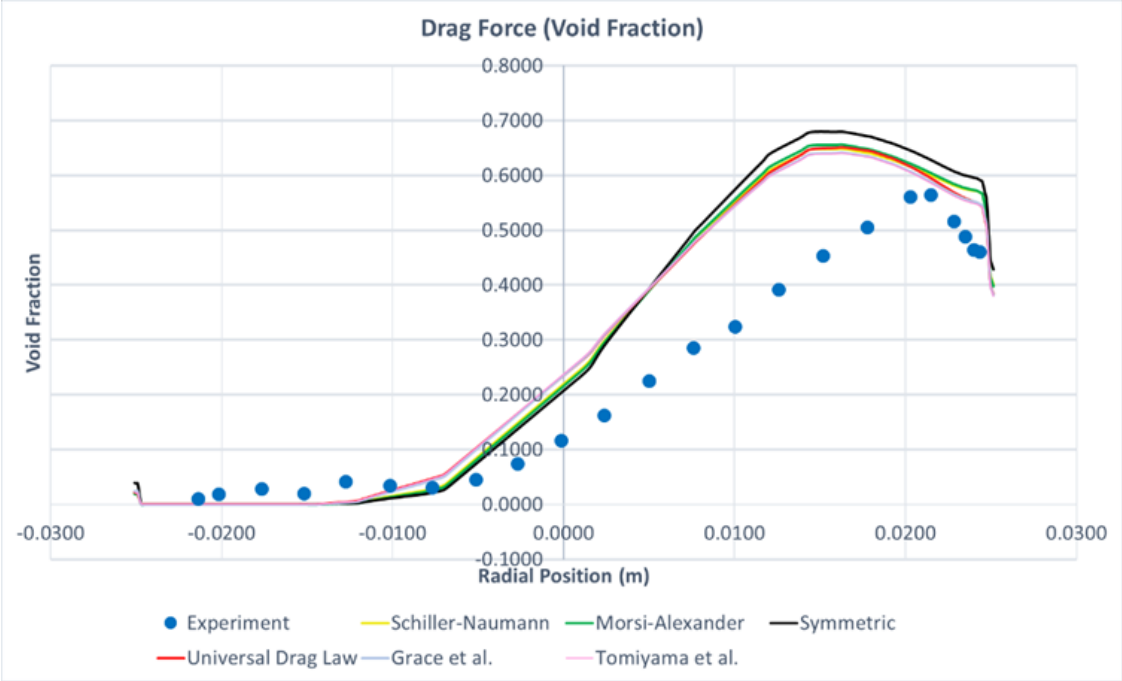

Figure 25: Comparison between drag force models and the experimental measurements concerning bubble interface velocity.

According to figures 24 and 25:

- Local void fraction: All the models showed similar results of having over predictions compared to the experiment.
- Local bubble interface velocity: They all showed similar results when comparing each other or with respect to the experiment and so there is no difference between drag force models in terms of accuracy.

Our next step was comparing these models in both stability and computational time. So, we investigated the scaled residual curves of their governing equations for the first 1300 iterations (take into consideration that the final results of these simulations were obtained after a larger number of iterations):

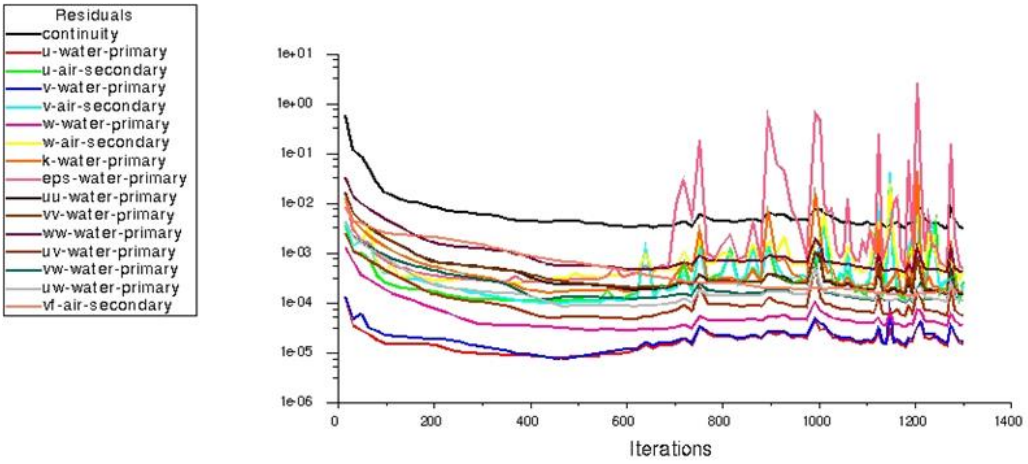

Figure 26: Schiller-Naumann Model Scaled Residual Curves

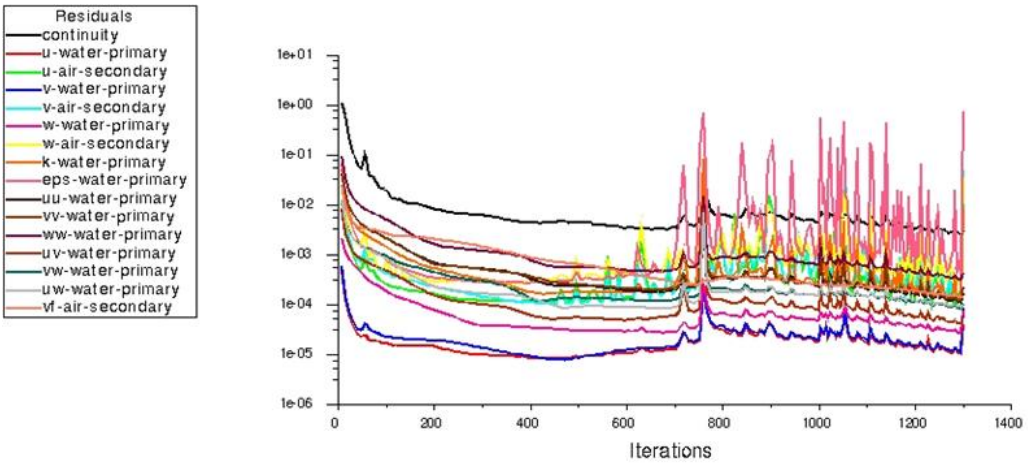

Figure 27: Morsi-Alexander Model Scaled Residual Curves

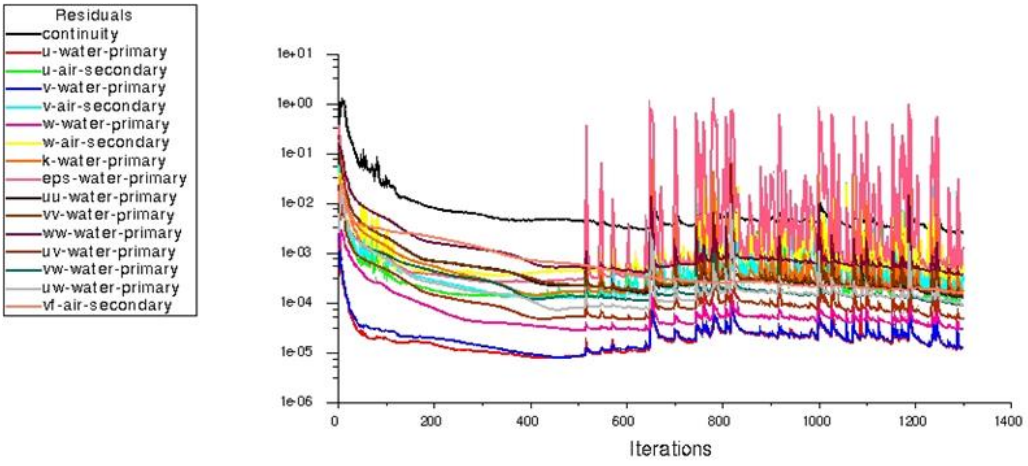

Figure 28: Symmetric Model Scaled Residual Curves

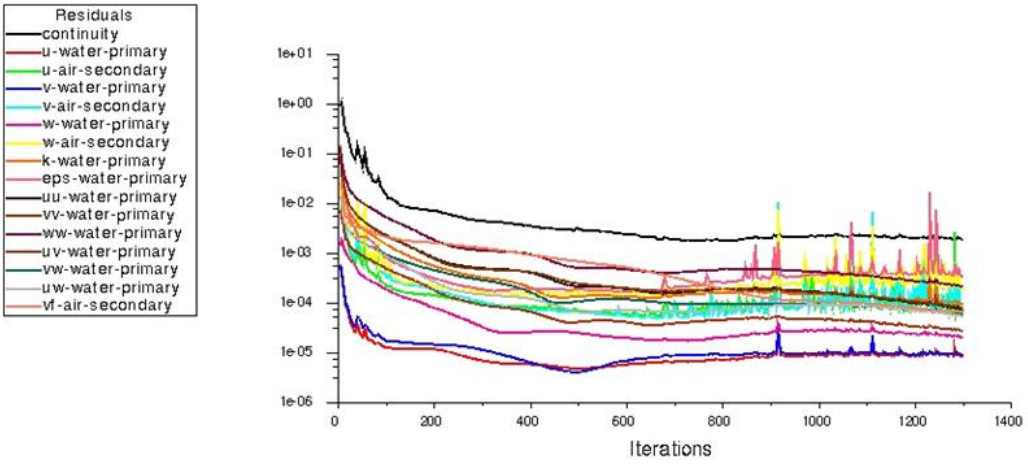

Figure 29: Grace et al. Model Scaled Residual Curves

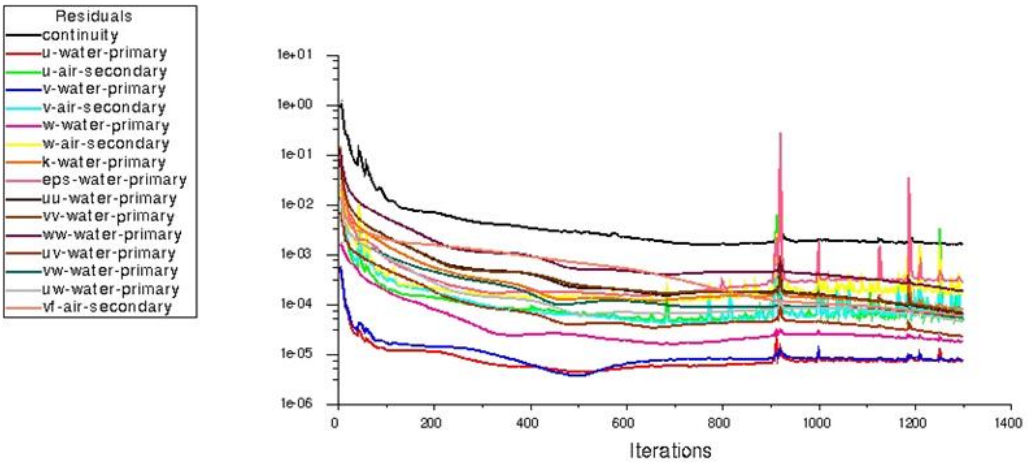

Figure 30: Tomiyama et al. Model Scaled Residual Curves

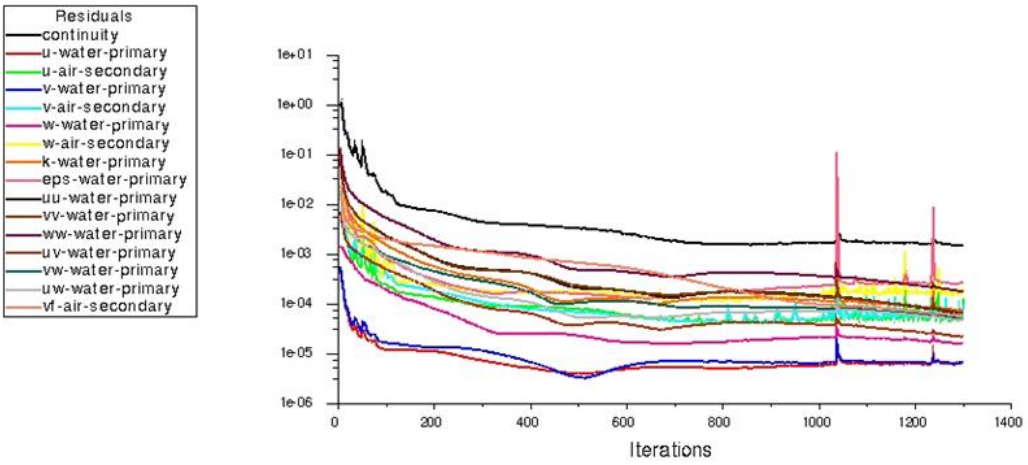

Figure 31: Universal Drag Law Scaled Residual Curves

According to scaled residual curves:

- Schiller-Naumann, Morsi-Alexander and Symmetric models showed a high frequency of oscillation with reflects to having numerical instabilities in the solution of their governing equations. The difference different between these three models and the rest is that they treat the dispersed phase (bubbles) as rigid (undistorted) spheres and do not consider any distortion that can happen when having larger bubble diameters.
- Grace et al. and Tomiyama et al. models showed more stable scaled residual curves and so better stability. These models take into consideration different bubble shapes such as spheres, ellipses, and caps by adding extra parameters such as Eotvos number (Eo) and Morton number (Mo).
- Universal Drag Law is similar to Grace et al. and Tomiyama et al. models in taking into consideration bubble distortion. However, it uses the gas void fraction instead of Eotvos and Morton in considering bubble distortion. After doing our sensitivity analysis on this model, it showed the best scaled residual curve and the fastest computational time compared to all the previous models.

Therefore, Universal Drag Law was chosen to be the best drag force model.

3.3.1.2 Wall Lubrication Force

Regarding wall lubrication force, four models are available in ANSYS Fluent:

- Antal et al. Model[26]
- Tomiyama Model[7]
- Frank Model[7]
- Hosokawa Model[27]

And so, four sub-cases were studied in which each one uses one of these wall lubrication force models while fixing the prechosen universal drag law model to describe the drag force.

Figures 32 and 33 show the comparison between different wall lubrication force models and the experimental measurements concerning both local void fraction and bubble interface velocity.

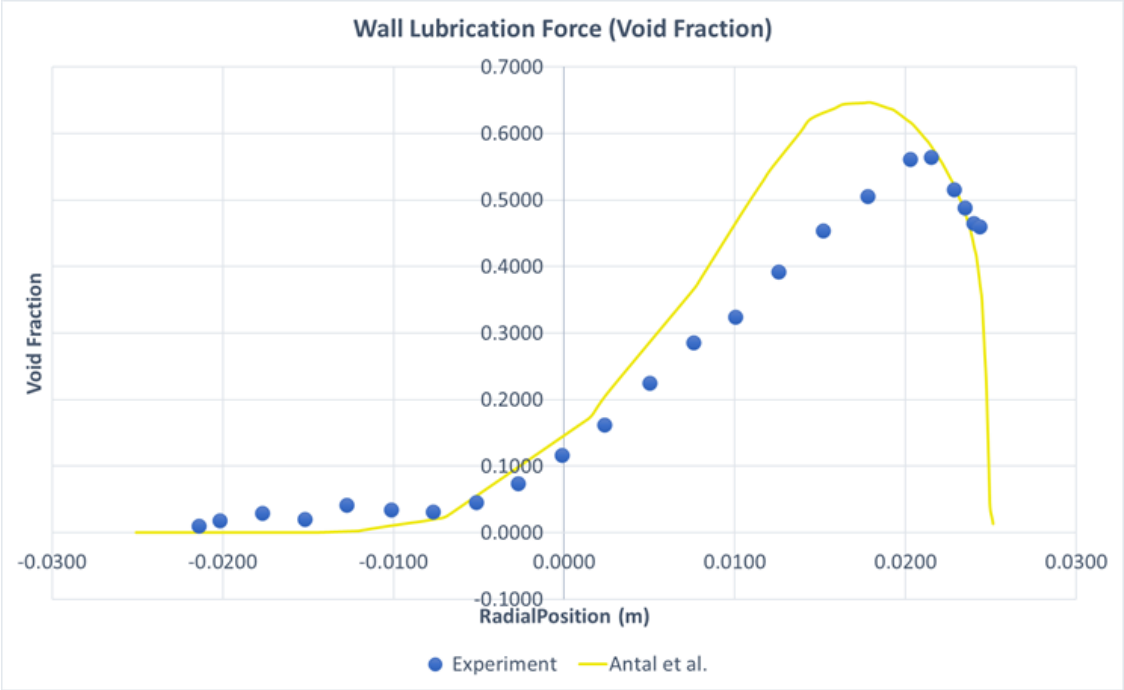

Figure 32: Comparison between wall lubrication force models and the experimental measurements concerning local void fraction.

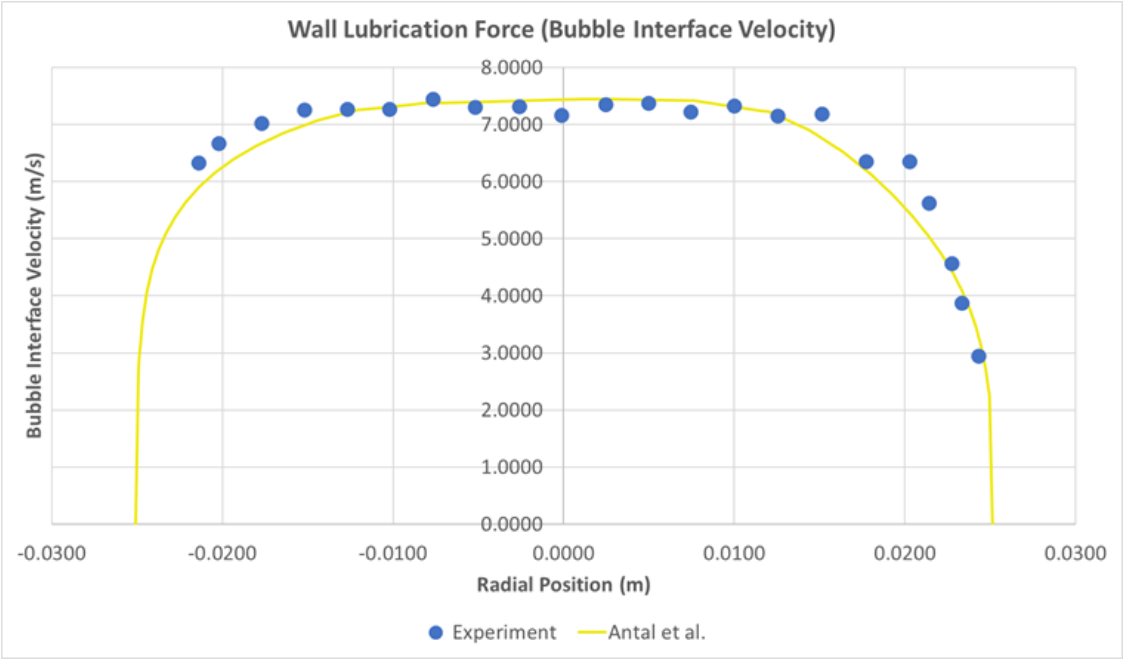

Figure 33: Comparison between wall lubrication force models and the experimental measurements concerning local bubble interface velocity.

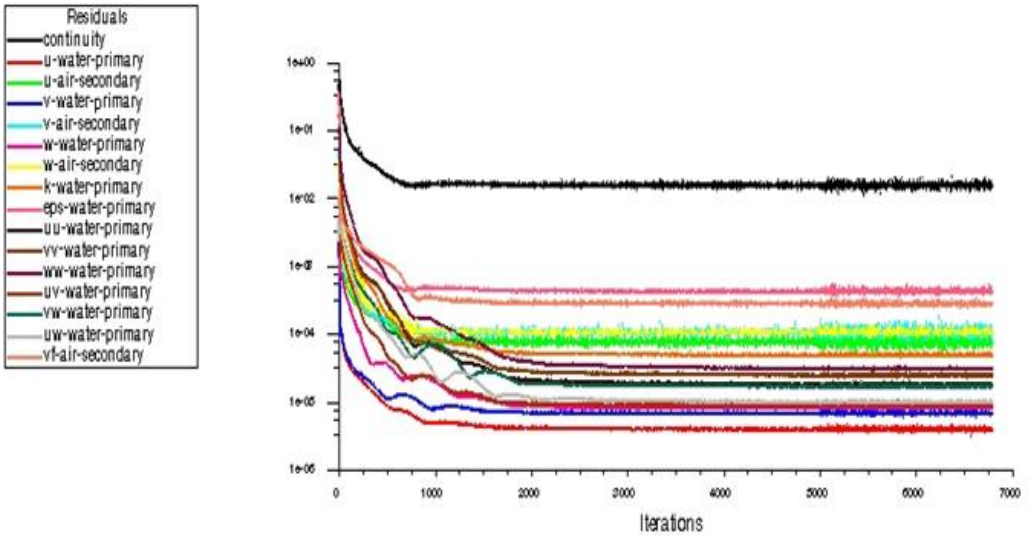

Figure 34: Antal et al. Scaled Residual Curves

According to the wall lubrication force sensitivity analysis, it was found that only Antal et al. model converged to a stable solution.

In this model, the local void fraction was slightly overpredicted (like the drag force model but with better results) while having accurate results in terms of bubble interface velocity. Moreover, it showed better stability when compared to the scaled residual curves when using only the Universal drag law model in section 3.3.1.1.

However, all the three remaining models "Tomiyama, Frank and Hosokawa Models" failed to converge, even after trying to decrease the under-relaxation factors to make the system more stable. The reason behind this divergence is unknown, but what is in common between these models and different from Antal et al. model is that they all depend on Eotvos number.

Therefore, Antal et al. model was selected to account for the wall lubrication force model.

3.3.1.3 Turbulence Dispersion Force

After choosing both drag and wall lubrication force models, turbulence dispersion force models were then investigated to find the best one.

In ANSYS Fluent, four models are available:

- Lopez de Bertodano Model[28]
- Simonin Model[29]
- Burns et al. Model[30]
- Diffusion in VOF Model[31]

Therefore, four subcases were simulated referring to these four models while fixing both Universal Drag Law and Antal et al. models for both drag and wall lubrication forces, respectively.

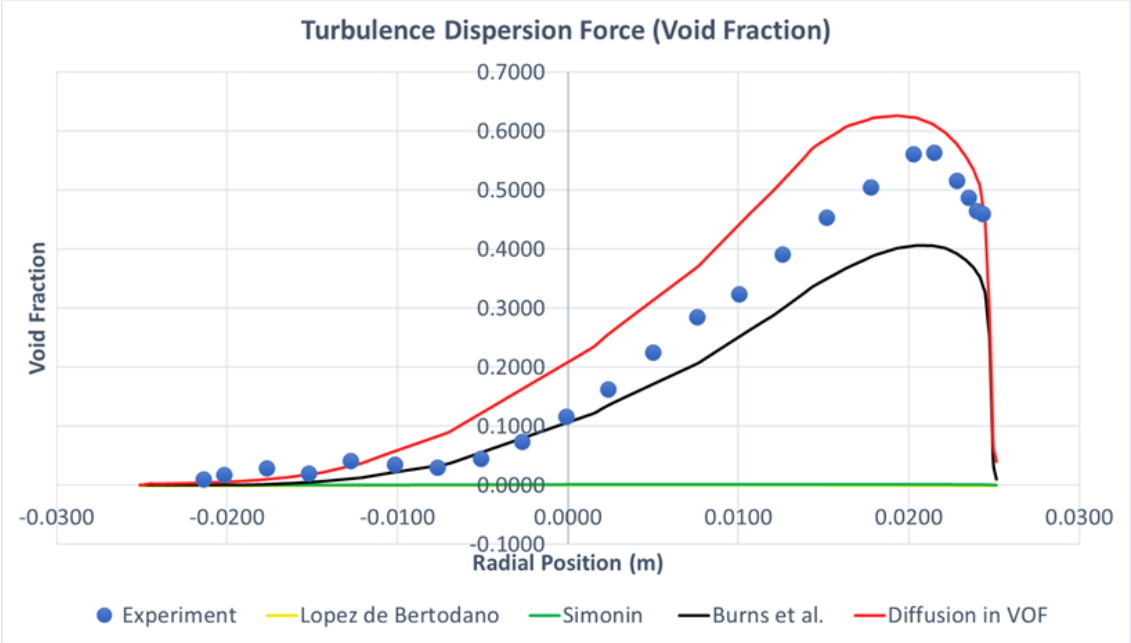

Figure 35: Comparison between turbulence dispersion force models and the experiment concerning local void fraction.

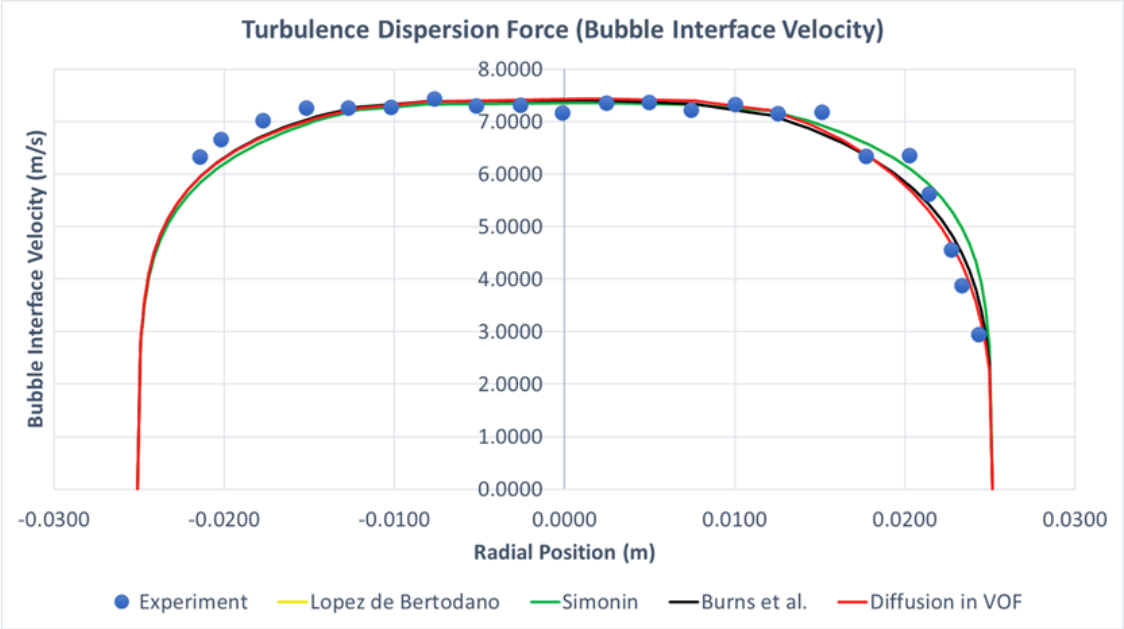

Figure 36: Comparison between turbulence dispersion force models and the experimental measurements concerning local bubble interface velocity.

When comparing local bubble interface velocity profiles (Figure 36), it was found that all the models successfully described the experiment and so no decision was taken depending on this parameter.

However, major differences occurred when comparing local void fraction profiles.

According to figure 35:

- Both Lopez de Bertodano and Simonin models had extremely low local void fractions which were unrealistic because no phase change is occurring in our system.
- Burns et al. model showed a better local void fraction profile when compared to the previous two models, but still lower than the experimental one.
- The reason for having unrealistic results when using these three models is not clear.
- However, Diffusion in VOF model showed accurate results with having a small overprediction. Moreover, it greatly improved the overall system stability (Figure 37).
- The reason for these results is not yet known, but the difference between this model and the previous three models is that the turbulence dispersion force is

not added as an explicit force term or as a drift velocity, but as a turbulence diffusion term in our continuity equation (see section 2.4.3.4.4).

Therefore, Diffusion in VOF model would be then used to simulate the turbulence dispersion force.

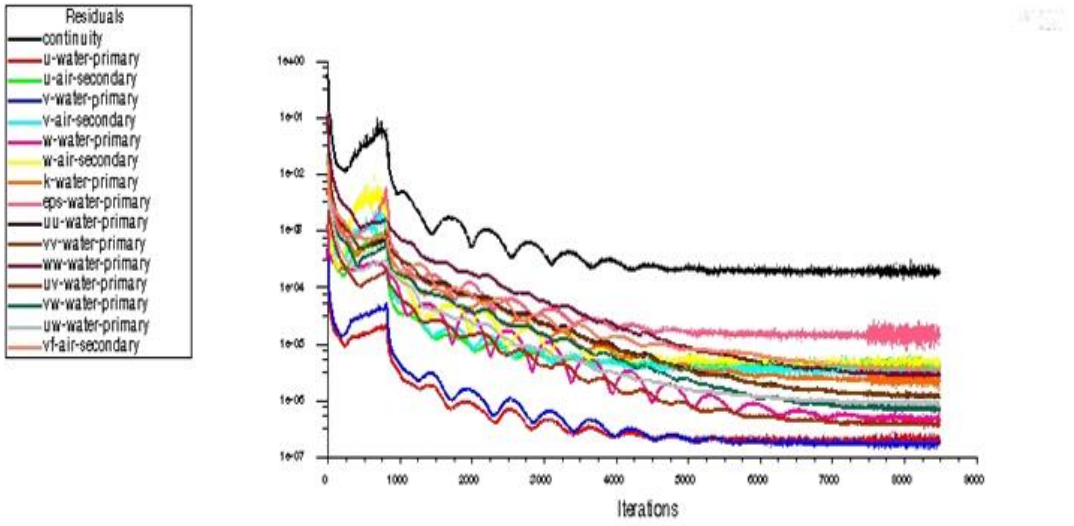

Figure 37: Diffusion in VOF Scaled Residual Curves

3.3.1.4 Turbulence Interaction Force

In ANSYS Fluent, three models are available to describe turbulence interaction force:

- Troshko-Hassan Model[43]
- Sato Model[44]
- Simonin et al. Model[42]

Therefore, three additional sub-cases were numerically investigated to study the impact of these models while having all the previously selected models fixed.

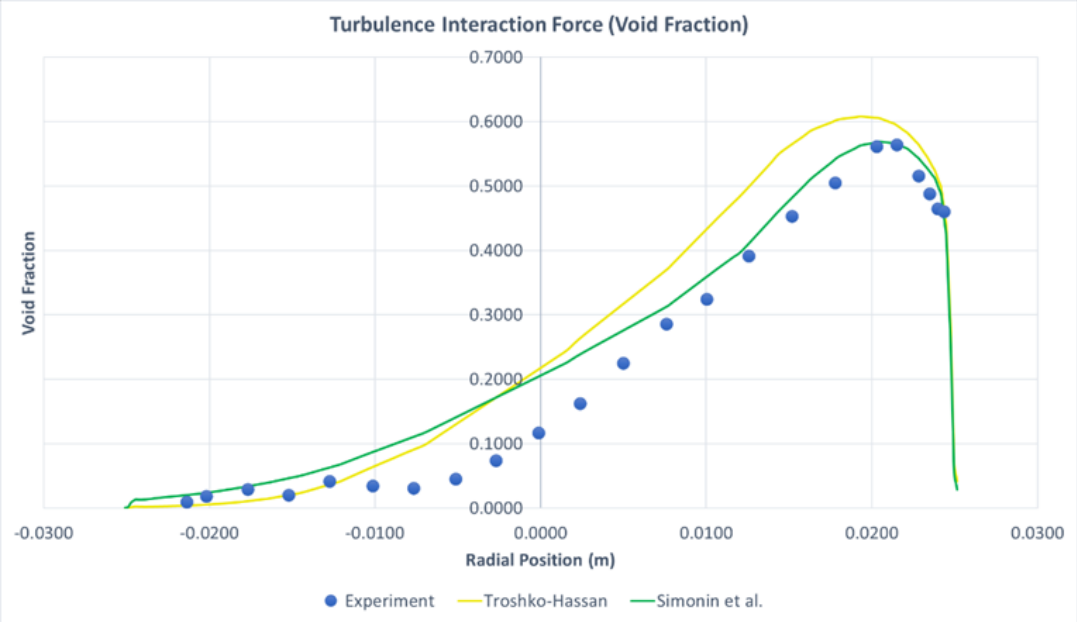

Figure 38: Comparison between turbulence interaction force models and the experimental measurements concerning local void fraction.

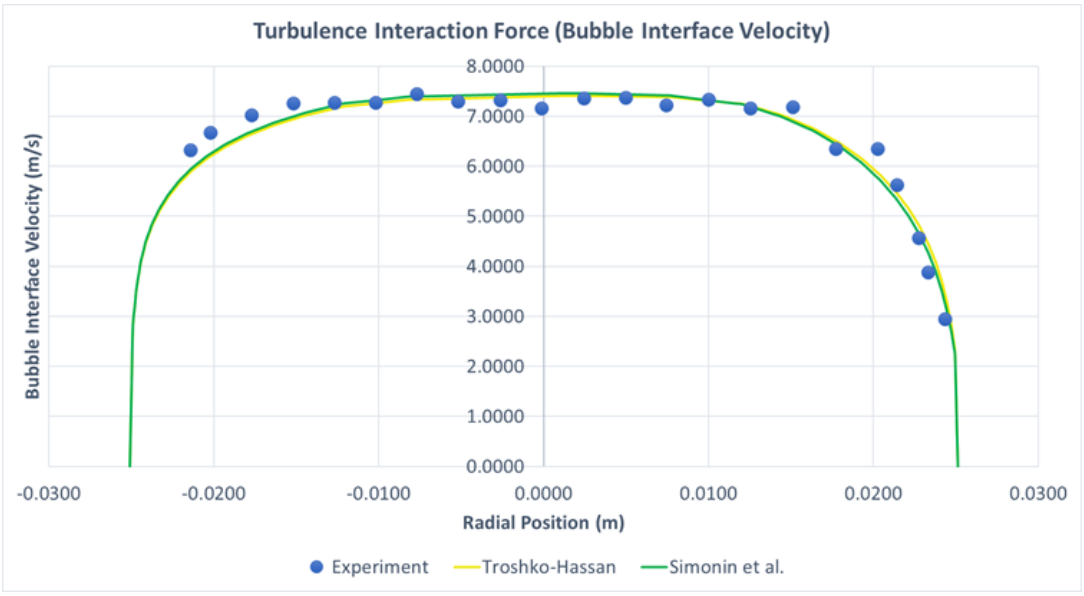

Figure 39: Comparison between turbulence interaction force models and the experimental measurements concerning local bubble interface velocity.

According to our sensitivity analysis, it was found:

- Sato model diverged even after decreasing the under-relaxation factors. Therefore, implicitly adding the effect of the random primary phase motion induced by the dispersed phase turbulence is not suitable in our steady-state model.

- Troshko-Hassan model converged to a stable solution with accurate bubble interface velocity and slightly over-predictive local void fraction results.
- Simonin model converged to a stable solution with both accurate local void fraction and bubble interface velocity profiles. However, it took a long time to converge and is only suitable for dispersed turbulence models while Troshko-Hassan is faster and can work in both dispersed and mixture turbulence models.

Therefore, Simonin model is suitable when having a small amount of dispersed phase (dispersed turbulence model) while Troshko-Hassan should be used when dealing with a large portion of the dispersed phase (mixture turbulence model).

3.3.1.5 Lift Force and Virtual Mass Force

When trying to perform sensitivity analyses for both lift force and virtual mass force models, all our cases either diverged or took a long time to converge with unstable behaviour and unrealistic results. Moreover, we got accurate results in our previous cases without adding these forces.
Therefore, we decided to ignore these forces from our model so as not to make it too complex.

Before closing this sensitivity analysis and setting out our phase interaction force model, one final comparison was done between all the previous sensitivity analyses to see how adding each force like drag, wall lubrication, turbulence dispersion and turbulence interaction improved our model with respect to the experimental results.

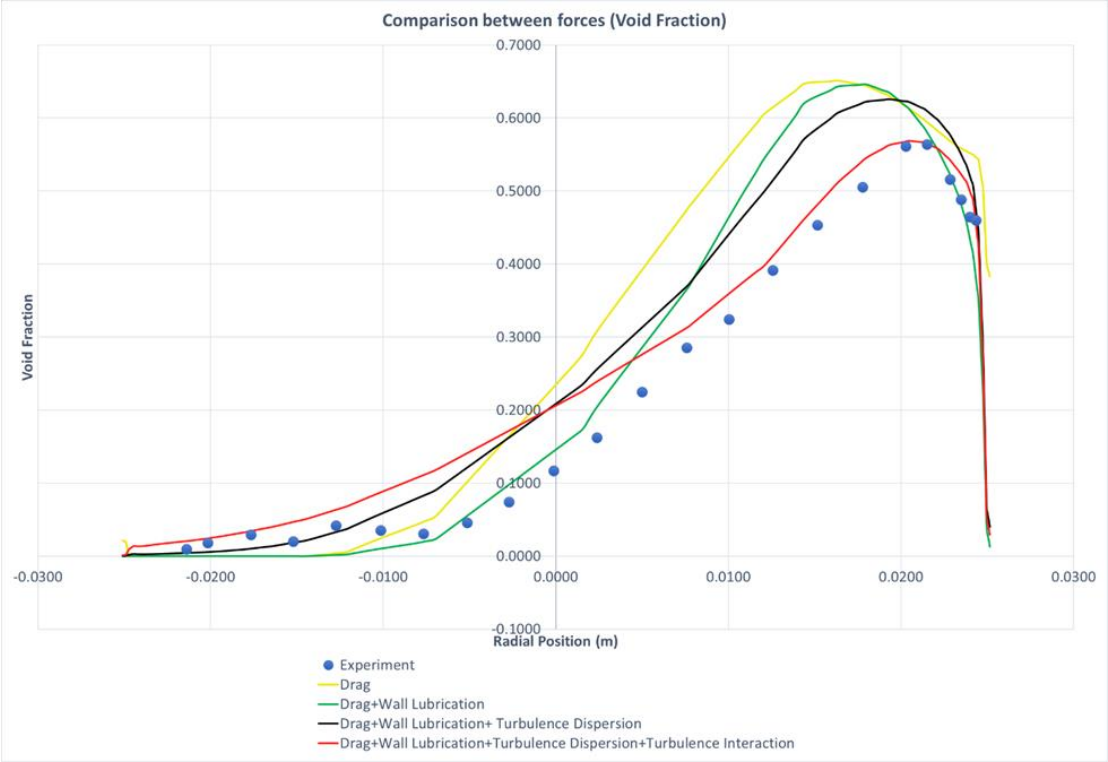

Figure 40: Comparison between phase interaction forces and the experimental measurements concerning local void fraction.

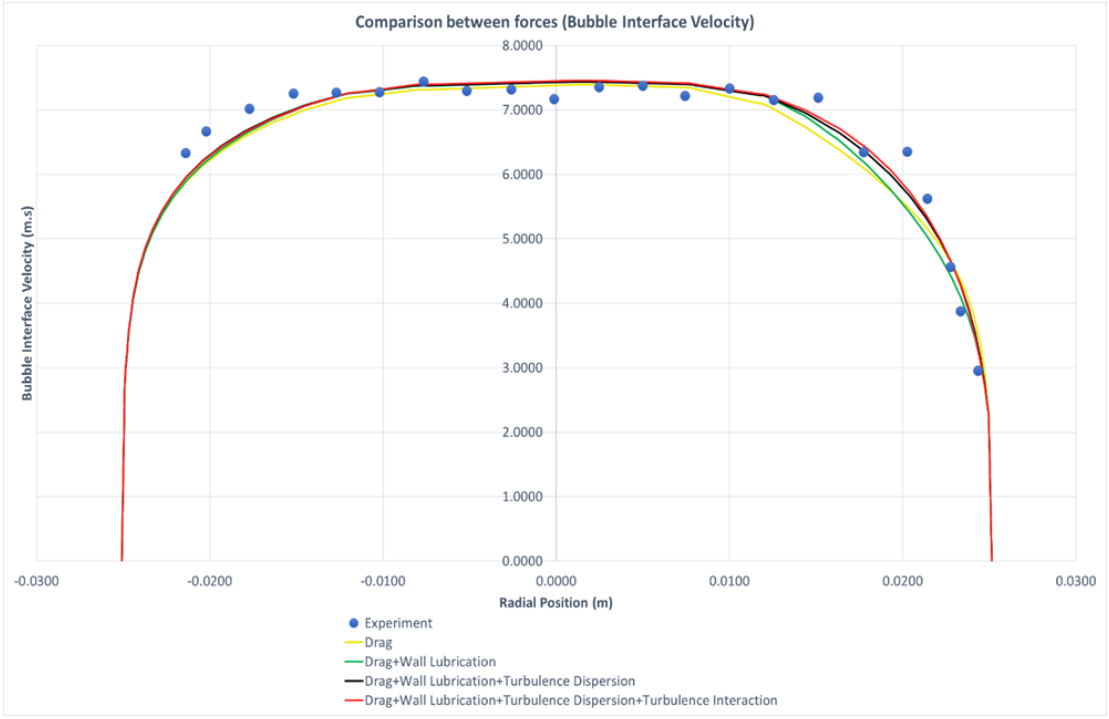

Figure 41: Comparison between phase interaction forces and the experiment concerning local bubble interface velocity.

According to Figures 40 and 41, all the forces showed accurate results regarding the bubble interface velocity. However, the local void fraction profile became more accurate concerning the experiment when adding each force (for example drag force + wall lubrication force is better than drag force only) till reaching the accurate local void fraction profile when adding all the four interaction forces.

Finally, our phase interaction forces sensitivity analysis revealed that adding these forces improves our multiphase model. Moreover, we should use the following models in describing these interaction forces:

- Drag force: Universal Drag Law
- Wall lubrication force: Antal et al. Model
- Turbulence dispersion force: Diffusion in VOF Model
- Turbulence interaction force: Sato (for dispersed turbulence model) and Troshko-Hassan (for mixture turbulence model)
- Lift force and virtual mass force: Ignored.

3.3.2 Revalidation Using Other Experimental Cases

After setting up our multiphase model and finding out what models should be used for the phase interaction forces, five extra experimental cases were modelled using our new selected model to revalidate it and make sure that it is working on multiple bubbly gas-liquid systems and not just one case.

Boundary conditions of these fixe extra cases can be found in tables 2 and 3 and figures 42 to 49 represent the comparison between experimental and modelling data in terms of local void fraction and bubble interface velocity.

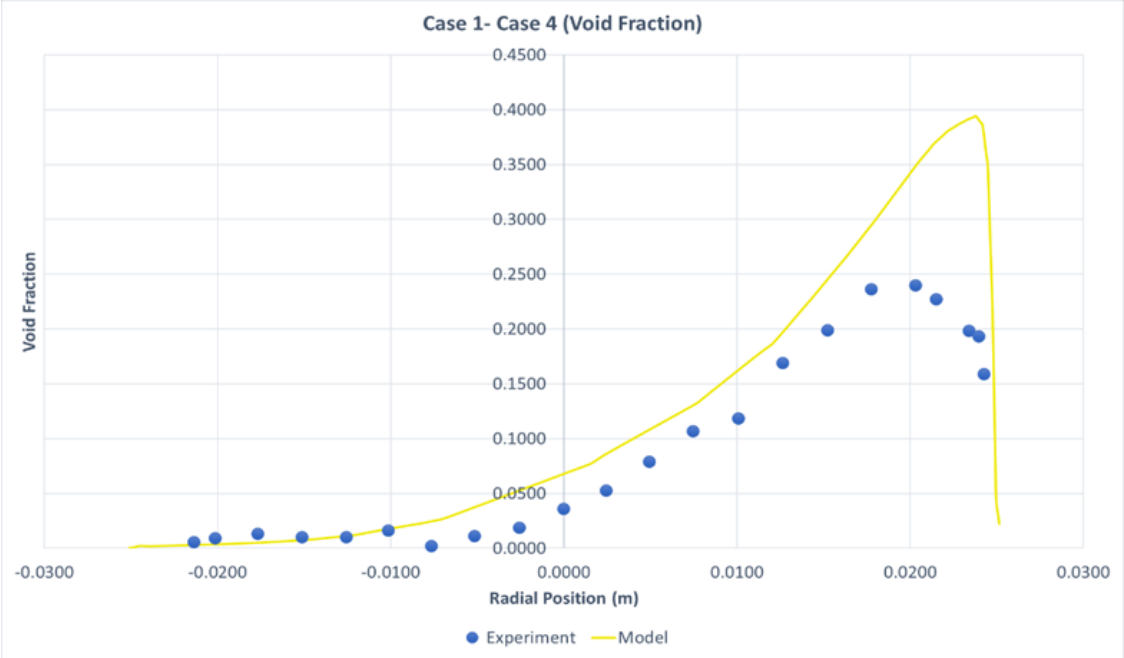

Figure 42: Case 1 and Case 4 comparison between experimental and modelling results concerning local void fraction.

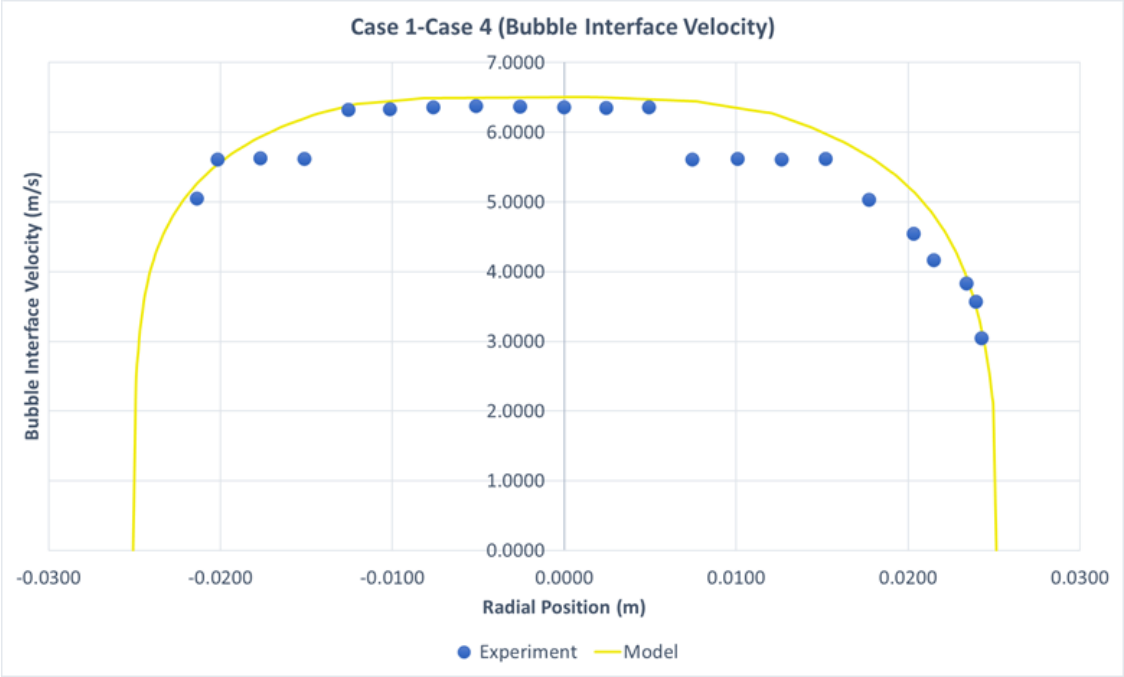

Figure 43: Case 1 and Case 4 comparison between experimental and modelling results concerning bubble interface velocity.

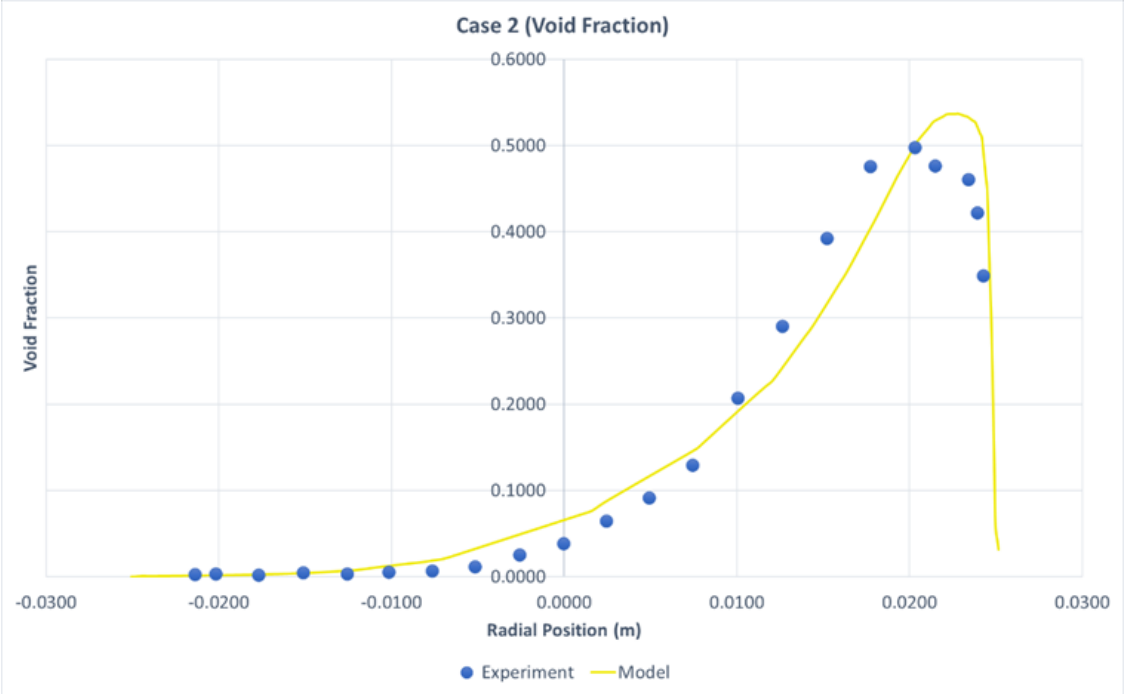

Figure 44: Case 2 comparison between experimental and modelling results concerning local void fraction.

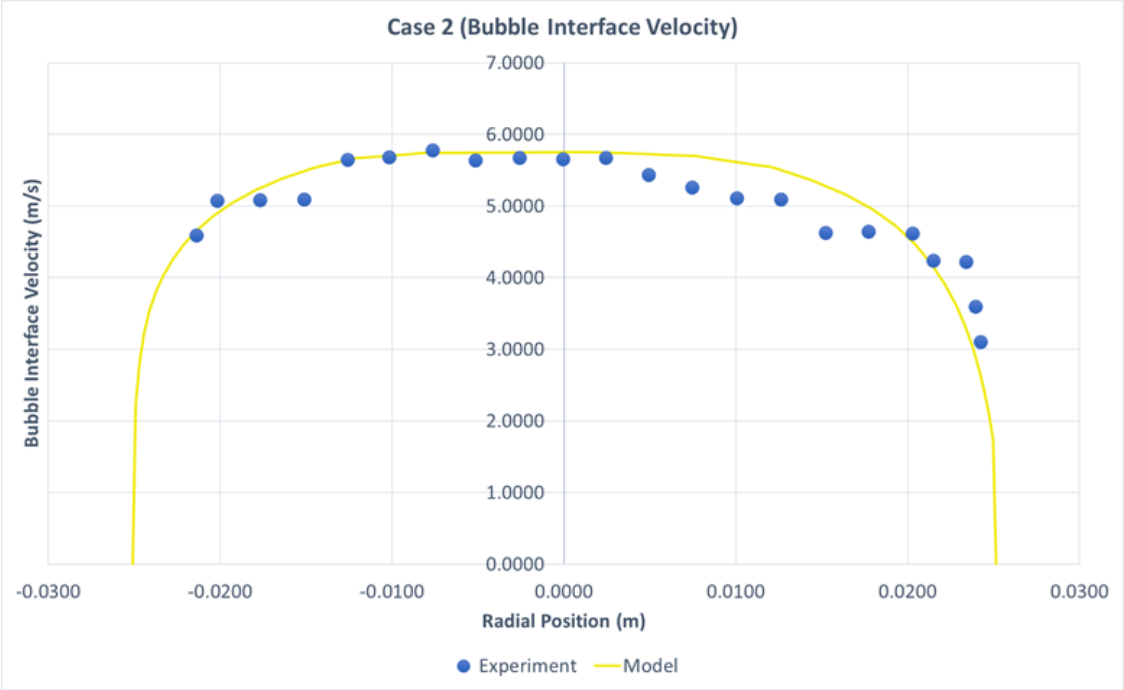

Figure 45: Case 2 comparison between experimental and modelling results concerning bubble interface velocity.

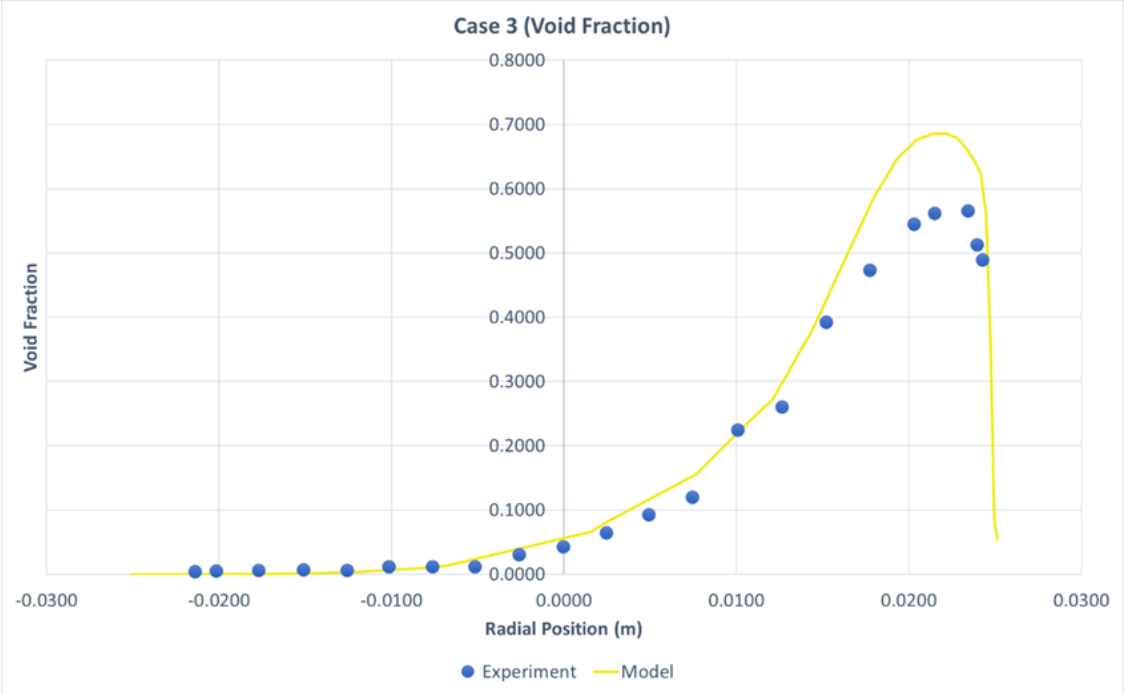

Figure 46: Case 3 comparison between experimental and modelling results concerning local void fraction.

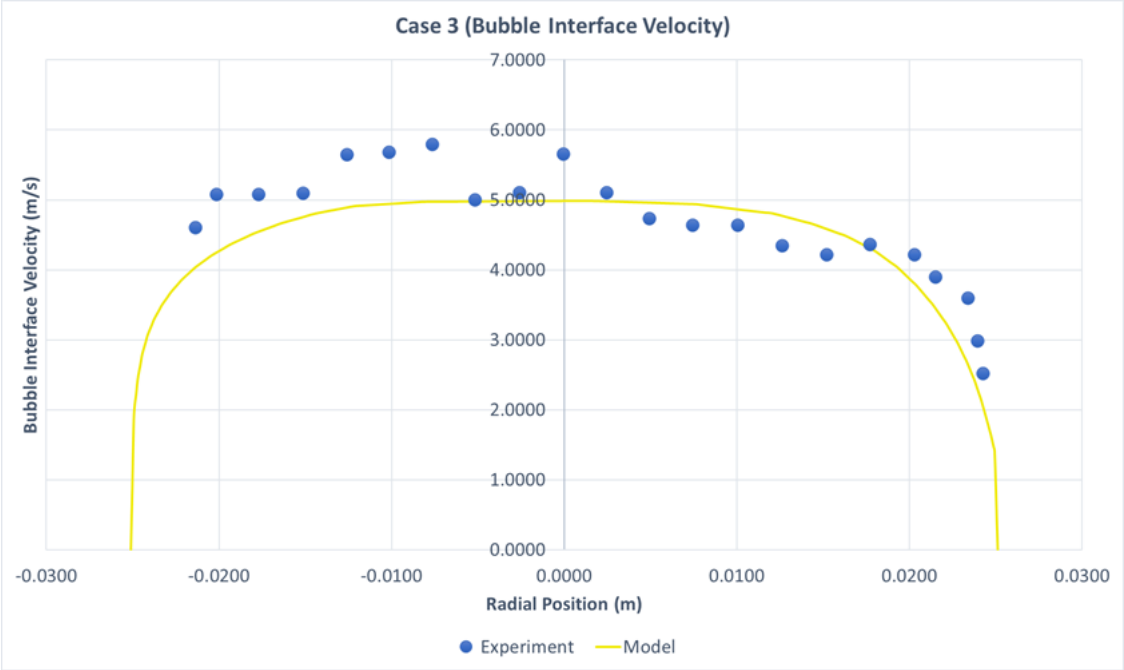

Figure 47: Case 3 comparison between experimental and modelling results concerning bubble interface velocity.

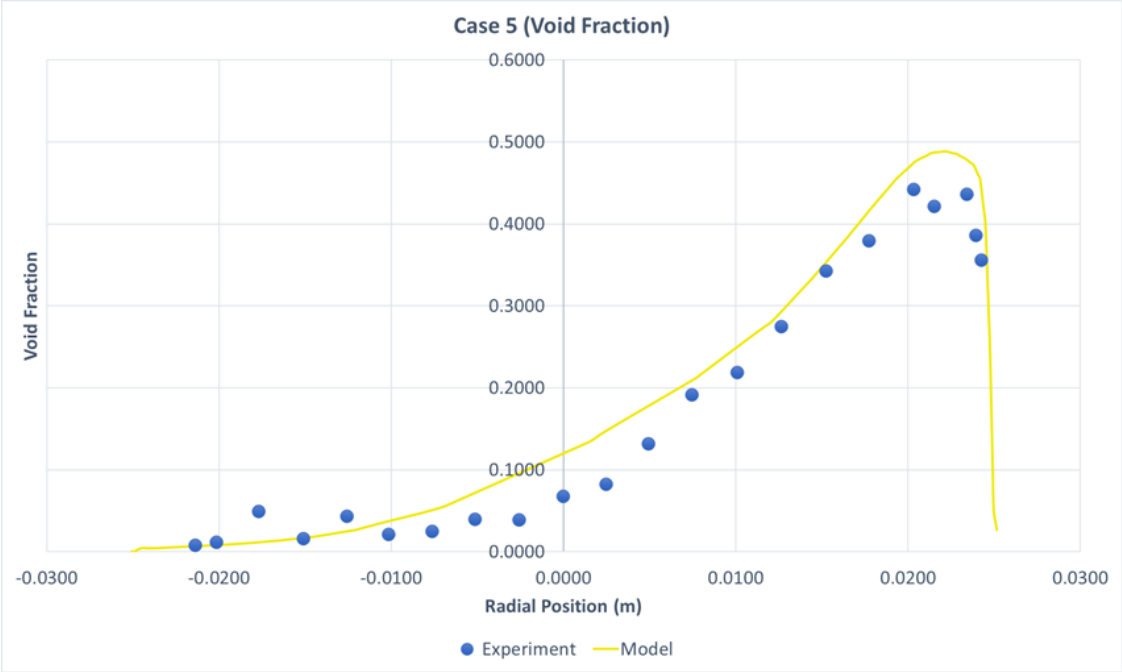

Figure 48: Case 5 comparison between experimental and modelling results concerning local void fraction.

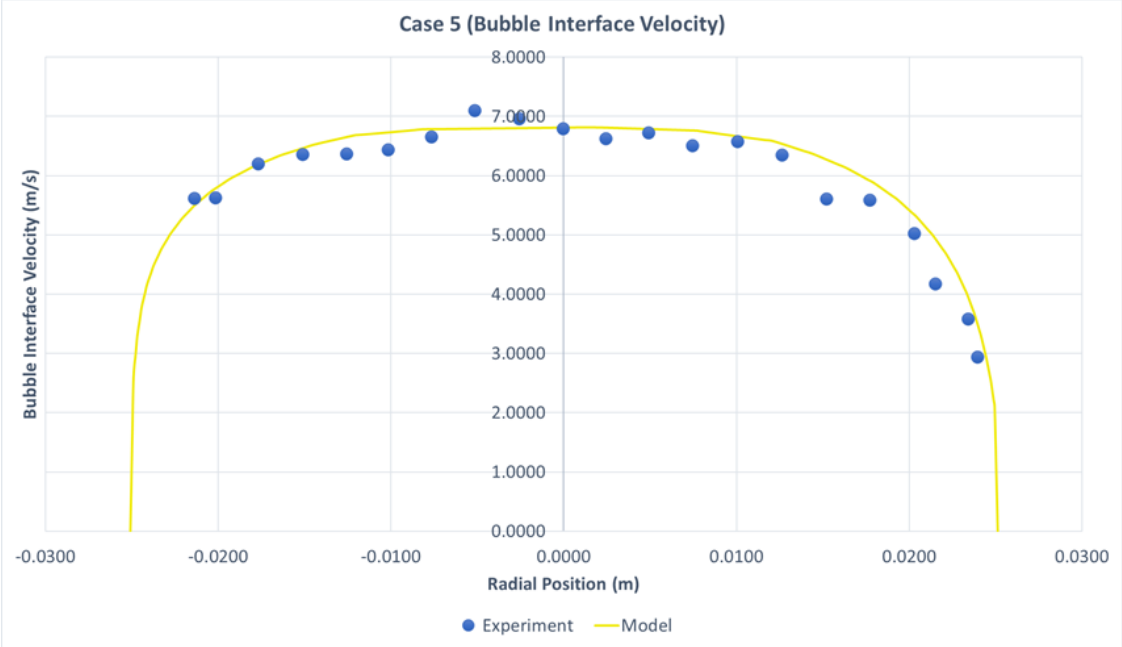

Figure 49: Case 5 comparison between experimental and modelling results concerning bubble interface velocity.

- **<u>Case Study 1 and Case Study 4:</u>**

  Our model accurately predicted the bubble interface velocity profile while having overpredicted results in terms of local void fraction. These

overpredicted results became extremely high in the profile peak by having a local void fraction of 0.4 instead of 0.25.

- **Case Study 2:**

  Our model accurately predicted both local void fraction and bubble interface velocity profiles.

- **Case Study 3:**

  Our model overpredicted the local void fraction profile by having a peak value of 0.7 instead of 0.6. However, some deviations appeared in the bubble interface velocity profile due to our uncertainty in experimental data reading and so it can be neglected.

- **Case Study 5:**

  Our model accurately predicted both local void fraction and bubble interface velocity profiles.

- **Case Study 6:**

  It was our sensitivity analysis case.

The revalidation results were quite acceptable regarding the accuracy. These deviations that occur were due to:

- Uncertainty in the experimental data is due to having complex multiphase experiments. These complex multiphase experiments and their measurements are always encountered by some sort of errors in readings although it is not mentioned in our experiment. Therefore, it should be taken into consideration.
- False prediction of the bubble diameter and having a constant bubble diameter throughout the domain is considered unrealistic. Our results could be better if we accounted for having a bubble size distribution and modelling both coalescence and breakage between these bubbles. This could be done by using a population balance model, but it would add more complexity to the system

and require a huge computational time. Besides, our focus was mainly to find the best interaction force models and validate them.

As a last step, our six cases were compared with each other to find the trend of changing both liquid and gas flow rates and their effect on both local void fraction and bubble interface velocity profiles.

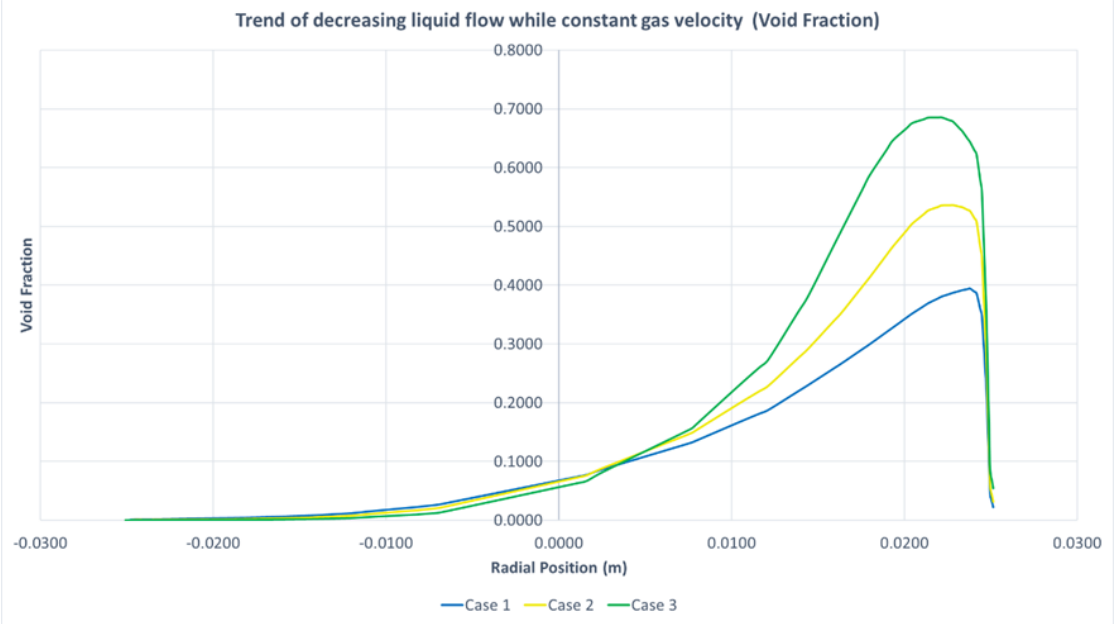

Figure 50: The trend of decreasing liquid flow rate while having constant gas velocity (local void fraction)

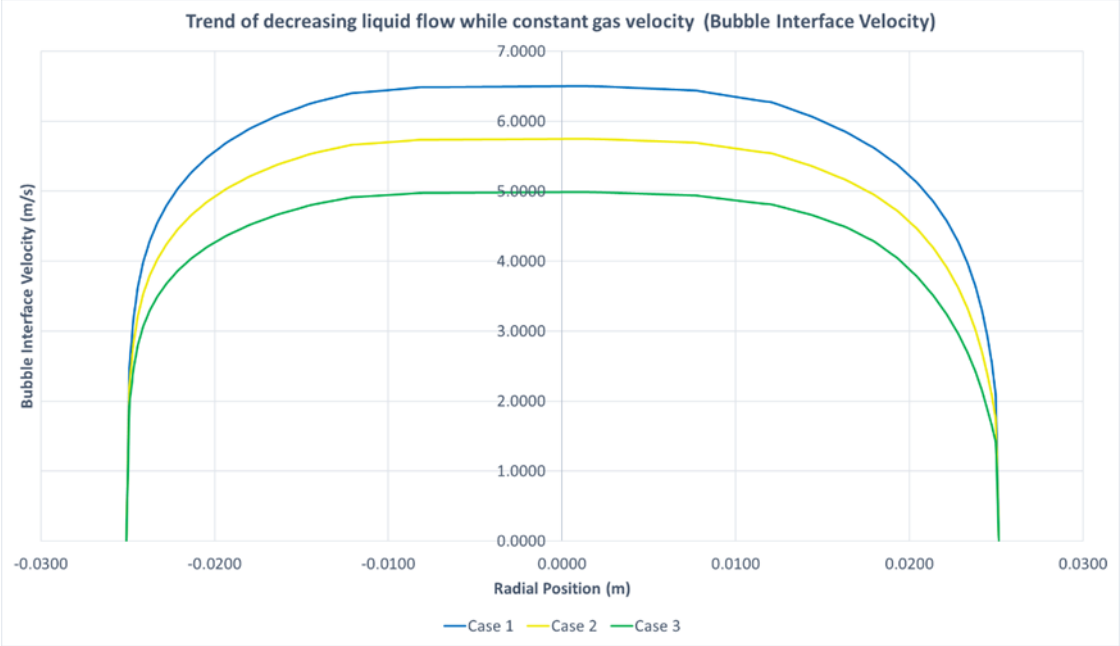

Figure 51: The trend of decreasing liquid flow rate while having constant gas velocity (bubble interface velocity)

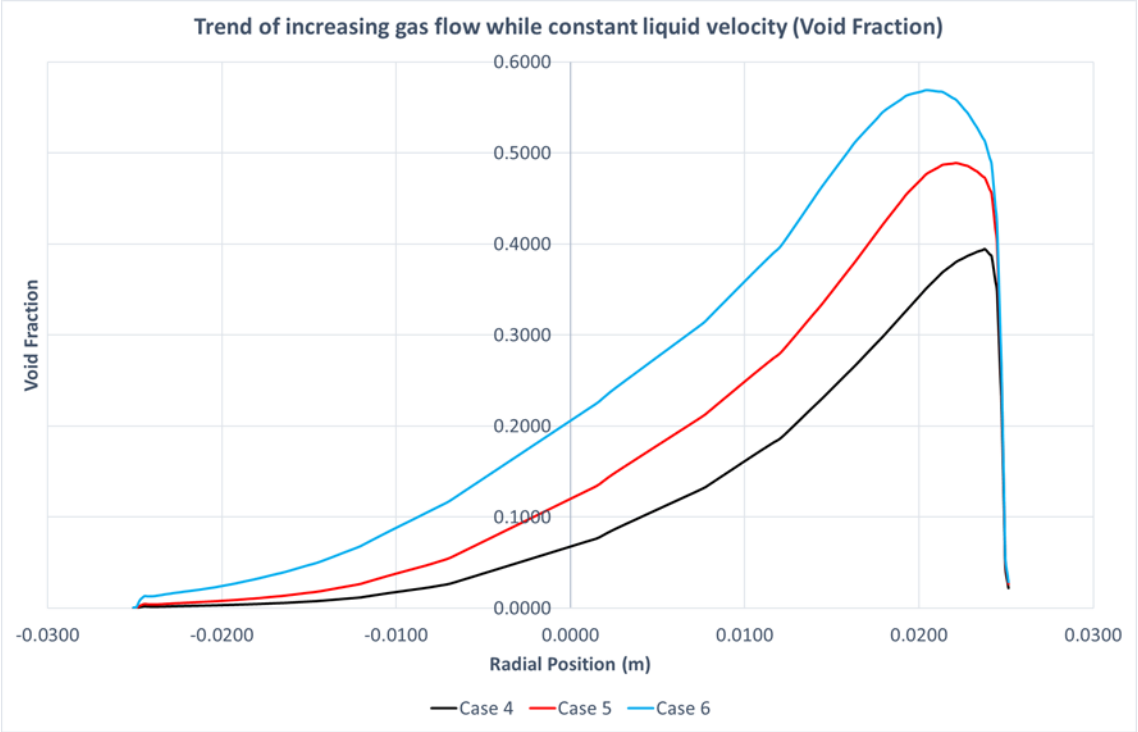

Figure 52: The trend of increasing the gas flow rate while having constant liquid velocity (local void fraction)

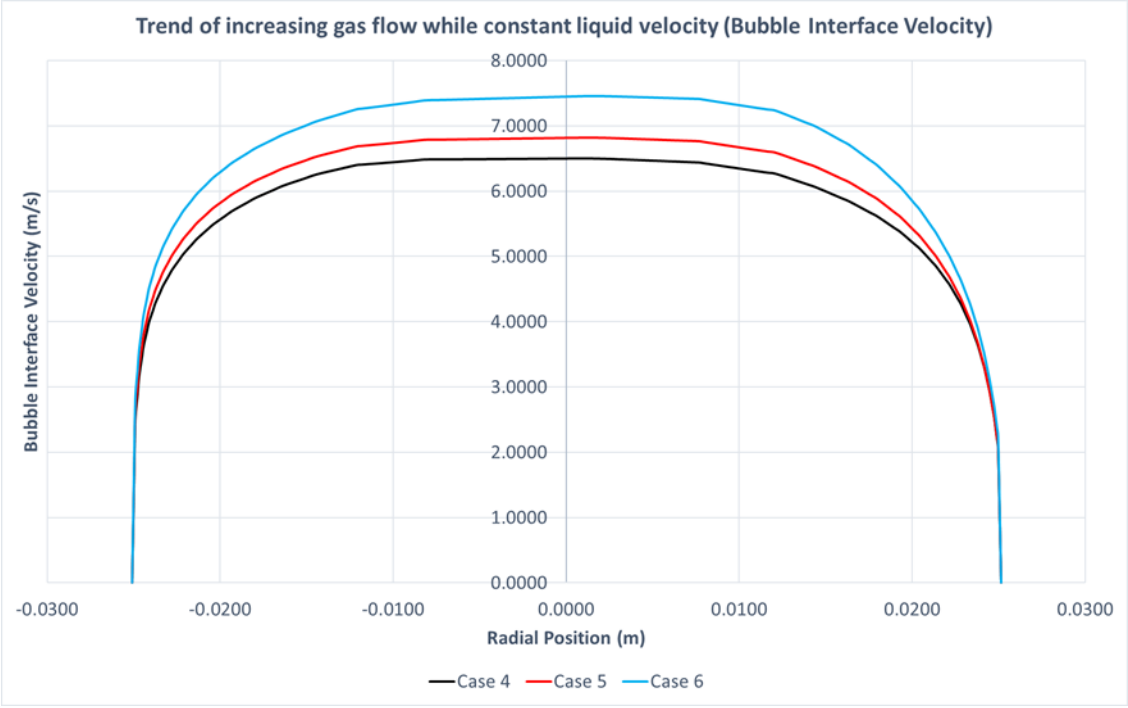

Figure 53: The trend of increasing the gas flow rate while having constant liquid velocity (bubble interface velocity)

It was found that:

- Decreasing liquid flow rate while having constant gas velocity increased the gas void fraction. Moreover, increasing gas flow rate while having constant liquid velocity leads to increasing the gas void fraction.
- Either increasing gas or liquid flow rate can increase the bubble interface velocity and vice versa.
- These trends were the same as the experimental results.

Finally, it can be concluded that our multiphase model having the phase interaction forces (refer to section 3.3.1) is suitable to simulate the complex bubbly gas-liquid flow in steady-state conditions with acceptable results and so having a preliminary estimation of its flow behaviour. Moreover, better results could be achieved by adding a population balance model but also would require significantly longer computational times.

4 CASE STUDY 2

4.1 Experimental Work

The experimental study “Two-phase flow through branching pipe junctions” by Davis and Fungtamasan studied the distribution of gas volume fraction for a bubbly air-water mixture in a vertical T-junction with a horizontal branch.

T-junctions are common parts in any pipeline system and so their study is important to know what happens to both liquid and gas in our multiphase flow when this extreme divergence in the flow happens.

In this experiment, a nearly uniform air-water mixture entered a vertical T-junction from the bottom after being mixed in a mixing chamber. This T-junction had one inlet from the bottom and two outlets, one horizontal called the branch arm and a vertical one called the run arm. This T-junction is 50 mm in diameter and has a length of 500 mm for each arm as shown in figure 54.

When an air-water bubble flow entered the T-junction and reached the splitting part, a redistribution of the phases is expected to occur in which a higher portion of the gas phase favours moving in the branch arm while most of the liquid continues its flow in the run arm. This redistribution is because of the small inertia of the gas (due to its lower density) compared to the liquid, which allows the low-density gas to easily change its direction when facing the splitting part while the high-density liquid cannot.

Several experiments were done using different inlet velocities and volume fractions in which probes (as in the previous experiment) were used to measure local and average parameters such as gas and liquid velocities and gas volume fraction at inlet, branch arm outlet and run arm outlet.

The experiment showed that a higher proportion of gas was flowing in the branch arm as expected while having a higher liquid fraction in the run arm. Moreover, most of the gas flowing in the branch arm tended to go to the upper part of the pipe due to the effect of gravity (as in case study 1).

Regarding the effect of inlet conditions on the separation phenomenon, it was found that the amount of gas that flowed into the branch arm increased with increasing either inlet volume fraction or inlet mixture velocity (as expected).

Not all the experimental results will be presented here because we take only one set of inlet conditions (intermediate conditions) to validate our previously generated CFD model.[5][12]

Selected boundary condition:

- Inlet actual gas velocity: 5 m/s
- Inlet actual liquid velocity: 6.21 m/s (corresponding liquid Reynolds number: 3.2×10^5)
- Inlet gas volume fraction: 0.52
- Outlet mass flow percentage directed to the branch: 20%
- Outlet mass flow percentage directed to the run arm: 80%

Measured outlet average parameters:

- Branch gas volume fraction: 0.77
- Run gas volume fraction: 0.35
- Branch gas flow rate / Inlet gas flow rate (Gas splitting ratio): 0.6

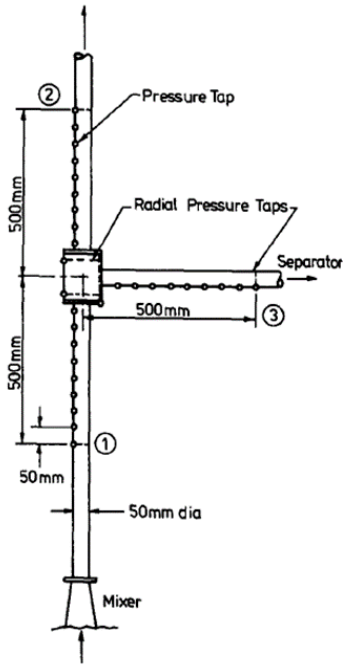

Figure 54: T-junction in the experiment conducted by Davis and Fungtamasan.[12]

4.2 Simulation Methodology

After studying the phase interaction forces and doing a sensitivity analysis to choose what forces and models to be added in our multiphase model (Case study 1), this selected model was used to investigate a new experimental case study having a more complex domain (T-Junction) to:

- Revalidate our generated model using different experimental data and make sure that it can work in different geometries (not just a horizontal pipeline).
- Try to study the effect of bubble diameter in our modelling results. This is because there are no bubble diameter profiles in this experiment as in the previous one and so we had to assume certain bubble diameters.
- Try to investigate the effect of having a bubble diameter size distribution other than setting a constant one, by coupling our multiphase model with a population balance model (refer to section 2.4.4). Moreover, the effect of different bubble sizes interaction (coalescence or breakage) should be studied and see how it can enhance our model results.

Therefore, our multiphase model was applied to this experimental case study and both gas volume fractions and gas splitting ratio were compared between our model and the experiment.

In addition, different sub-cases were studied in which different constant bubble diameters were set to see how changing the bubble diameter could affect our results.

Finally, extra sub-cases having bubble size distribution were added through the usage of the population balance model (with bubble interaction) to see how our modelling results would be enhanced.

- **Geometry and Meshing:**

  As in case study 1, the computational domain was drawn using DesignModeler software. Our domain was a vertical T-junction with a horizontal branch outlet arm (as mentioned before). It was drawn after the mixing chamber with 50 mm diameter and 500 mm for each T-split section (Figure 55).

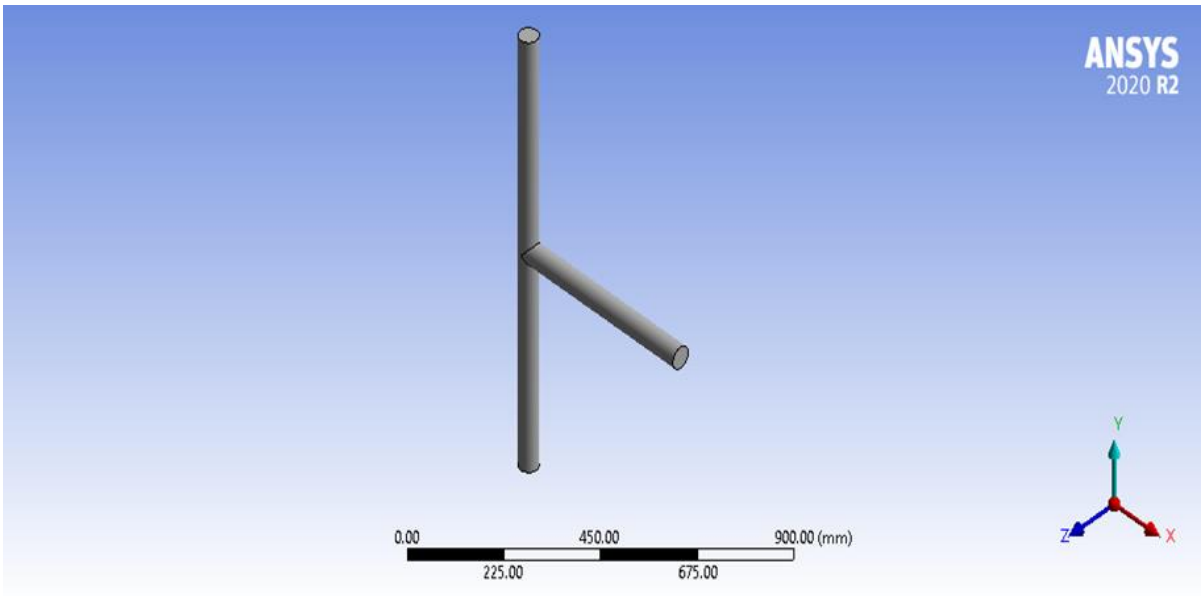

Figure 55: Case Study 2 (Computational Domain)

For meshing, a non-symmetrical mesh was created for our computational domain in which our cross-section had 15 inflation layers near the wall, with a growth rate of 10% and a first-layer thickness of 0.3 mm (to have about half of the pipe radius covered with this inflation). These inflation layers improve the accuracy of our calculation because they increase the meshing density near the walls and at the splitting part where a large number of phenomena occur (for example water velocity gradient near the wall, phase interaction forces near the walls, gas-liquid splitting in the T-junction,…etc).

For defining our mesh size, a mesh independence analysis was executed using different element sizes as shown in figure 56.

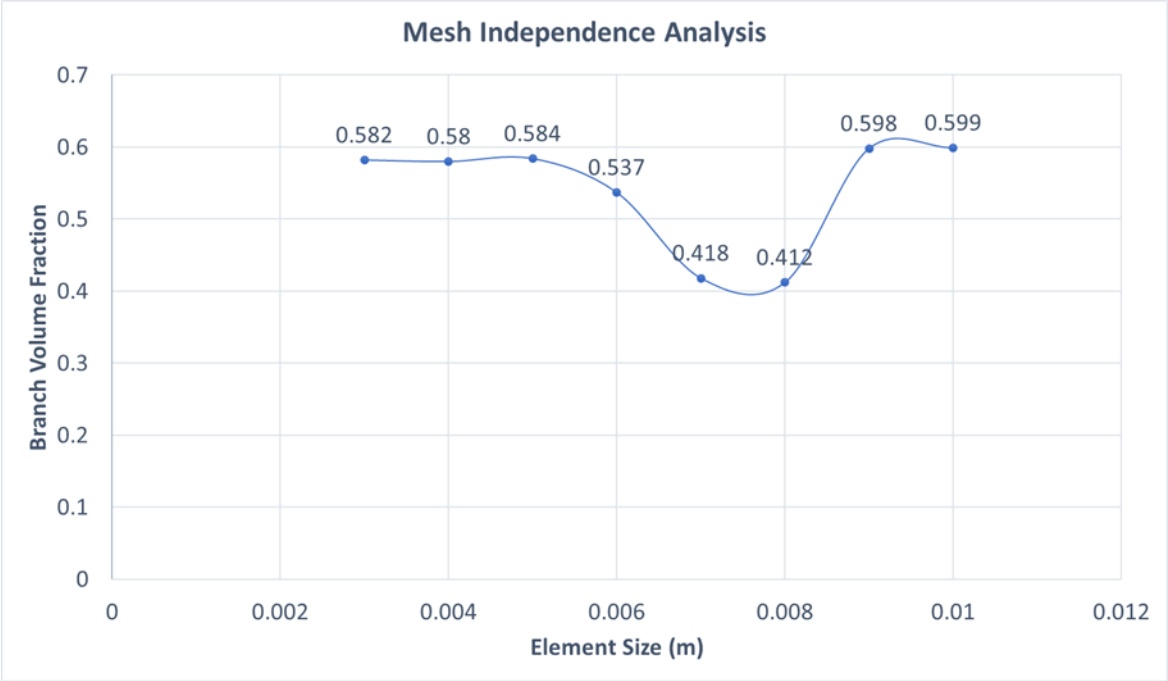

Figure 56: Mesh independence analysis of case study 2

As one can see, the branch volume fraction value is constant after having an element size of 5 mm and so this element size shall be used in all our coming simulation cases.

Our mesh, using 5 mm as an element size with 15 inflation layers of 10% growth rate, is shown in figure 57.

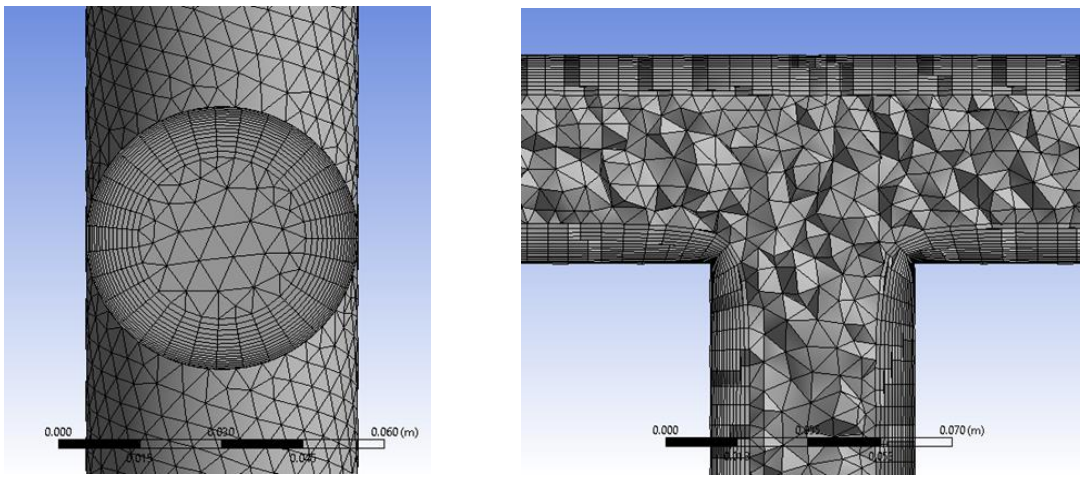

Figure 57: Mesh Distribution of Case study 2 (using 5 mm element size)

- **Simulation Settings:**

  In this case study, the previously selected model in case study 1 was used regarding the phase interaction force models and all the other fixed simulation settings.

  - **Solver Type:**

    Pressure based solver as we are dealing with an incompressible flow.

  - **Time Formulation:**

    Steady State simulation because it is significantly less time consuming than a transient one.

  - **Multiphase Model:**

    Eulerian model (refer to section 2.4.2.1) was used because it is the most accurate model (same as case study 1) in which the phase interaction force models were as follows:

    - Drag force: Universal Drag Law[18]
    - Wall lubrication force: Antal et al. Model[26]
    - Turbulence dispersion force: Diffusion in VOF Model[31]
    - Turbulence interaction force: Trosko-Hassan[43] (as we are dealing with a large dispersed phase volume fraction and so mixture turbulence model was used).
    - Lift force and virtual mass force: Ignored, as they lead to either diverged solutions or unrealistic results. Besides, they shall increase the computational time (fully explained in case study 1).

  - **Turbulence Model:**

    Reynolds Stress Model (RSM) was used with mixture model as a multiphase description of the RSM in which turbulence transport equations were normally solved, but for mixture properties that could be taken as an average of both phases.

  - **Bubble Diameter:**

    In this case study, a sensitivity analysis was performed on the effect of changing bubble diameter on our modelling results. Therefore, three

sub-cases were defined as having constant bubble diameters of 1 mm, 2 mm, and 4 mm, respectively.

- **Population Balance Model:**

  When considering having a bubble size distribution instead of constant bubble size, the population balance method was coupled with our multiphase model. In this model, the discrete method was used in which bubbles ranging from 1 mm to 10 mm diameter were equally divided into 10 classes (or bins) as shown in table 4.[13]. Regarding bubble breakage, Luo-model for breakage frequency [48] was used, while Luo aggregation kernel model[49] was used for bubble coalescence modelling.

Class (or bin)	Bubble diameter (mm)
1	1.45
2	2.35
3	3.25
4	4.15
5	5.05
6	5.95
7	6.85
8	7.75
9	8.69
10	9.55

Table 4: Diameter of each bubble in the discrete population balance model

- **Boundary Conditions:**

  The inlet velocity and volume fraction for the gas and liquid phase was known from the experimental study:

  - Inlet gas velocity: 5 m/s
  - Inlet liquid velocity: 6.21 m/s
  - Inlet gas volume fraction: 0.52

  For the outlets (branch and run arms), outflow boundary conditions were used in which the flow split for the total mass flow rate between

the run and the branch was given (20% for the branch arm and 80% for the run arm).

This is because the overall flow split was controlled in the experiment by varying the outlet pressures for the two outlets. However, these outlet pressures were not mentioned in the experimental paper and therefore the total mass flow rate split was specified as an outlet condition. Moreover, it should be noted that the complexity of our experiment and the incomplete information regarding the outlet boundary conditions should have an impact on our simulation results. These boundary conditions that were impossible to be the same as our experiment shall play a role in the agreement between simulations and experimental data.

Moreover, a stationary wall was assumed with standard roughness of 0.00045 m as it was mentioned that the T-split material was structural steel.

Additional boundary conditions had to be specified when considering a bubble size distribution instead of having a constant bubble diameter. In the Discrete population balance model, arbitrary equal initial volume fractions of 0.1 were defined for each size bin (equal bubble size distribution).

The reasons for choosing equal bubble size distribution instead of having one of the popular distributions like the Normal (Gaussian) distribution[50] are:

1. For simplicity in ANSYS Fluent as the scope of this thesis was not to work on the population balance model (PBM) and their different approaches (it shall be a future work to be done). Therefore, the usage of PBM was just preliminary and simple to just see the effect of using PBM on the simulation results.
2. These distributions can be better simulated when using the QMOM model instead of the discrete model. Because in discrete model, we must manually specify each size and so to

have this distribution, it would take a lot of bins and more computational time. However, QMOM uses the moments to shape these distributions in a much simpler way. Moreover, the reason for not using QMOM was that the study of PBM was still preliminary and not the main scope of this thesis.

- **Pressure-Velocity Coupling:**

  Phase coupled SIMPLE was used.

- **Discretization Scheme:**

  Second-order Upwind and QUICK discretization schemes were used as in case study 1.

- **Under Relaxation Factors:**

  Since we were dealing with complex geometry (T-split) compared to the previous case study (horizontal pipe), low under relaxation factors were defined because our case studied diverged when using the default ones.

  The used under relaxation factors were:

  - Pressure: 0.2
  - Density, Body forces, Momentum, Volume fraction, Turbulence kinetic energy, Turbulence dissipation rate, Turbulent viscosity, and Reynolds stresses: 0.4

  Although this made our model take much more time to reach convergence, it had a stable manner.

- **Solution Initialization:**

  Hybrid initialization was used as the previous case study.

- **Convergence Criteria:**

  As in case study 1, the scaled residuals for all the governing equations were monitored and our solution was considered converged when reaching a value below 10^{-5}. Besides, some parameters were monitored (such as branch and run average volume fractions) in which our solution was considered converged

when these parameters reached constant values over a long number of iterations.

- **Evaluation Criteria:**

  Accuracy, computational time, and stability were our three criteria in judging our modelling results.

4.3 Results and Discussion

4.3.1 Phase Separation Phenomenon

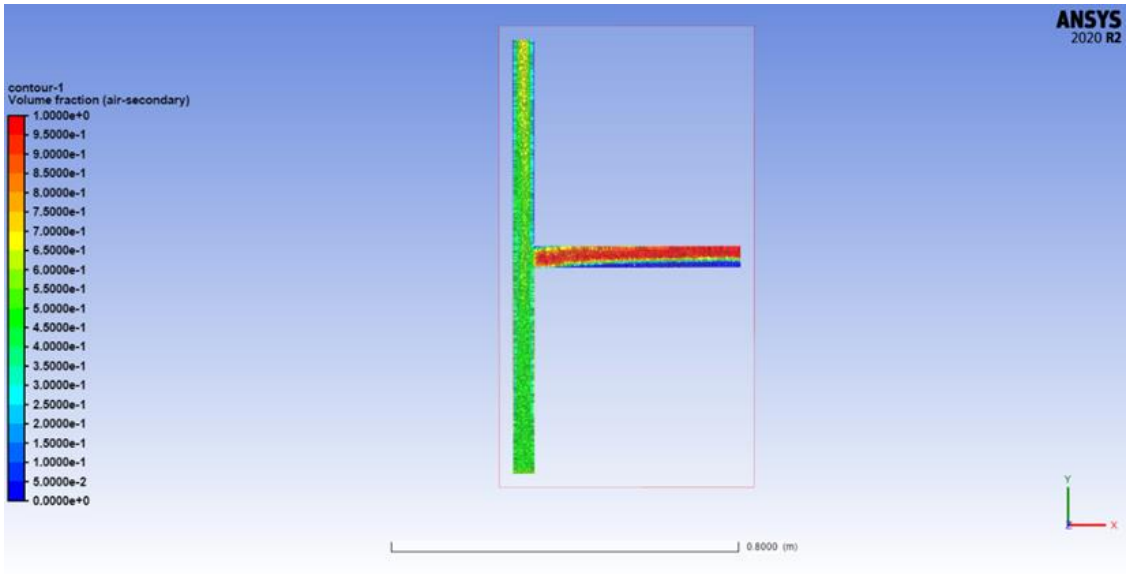

Figure 58: The contour of gas volume fraction at bubble diameter 0.004 m

According to figure 58, it was observed that most of the air is diverted to the branch arm which was represented by the red spots in the contour while having most of the water in the run arm due to the inertia difference. Moreover, most of the gas in the branch arm came to the upper part of the arm leading to a higher local gas volume fraction in the upper part. These phenomena happened exactly as in the experiment which validated that our model could simulate general flow behaviours in horizontal pipes.

4.3.2 Effect of Bubble Diameter

After our model validation of having the ability to simulate the general flow behaviours such as the separation phenomenon, the next step was to validate our

model by comparing some parametric values between our model and the experiment. These parameters were:

- Gas volume fraction at the branch arm outlet.
- Gas volume fraction at the run arm outlet.
- Gas splitting ratio

Moreover, we studied the effect of changing the bubble diameter on our simulation results.

Therefore, three sub-cases were proposed which differ in their bubble diameter:

- Sub-case 1: 0.001 m
- Sub-case 2: 0.002 m
- Sub-case 3: 0.004 m

Cases	Branch Outlet Gas Volume Fraction	Run Outlet Gas Volume Fraction	Gas Mass Splitting Ratio (branch gas mass flow/inlet gas mass flow)
Experiment	0.77	0.35	0.6
Sub-case 1	0.584	0.396	0.286
Sub-case 2	0.665	0.367	0.292
Sub-case 3	0.671	0.353	0.291
Sub-case 4	0.681	0.345	0.297

Table 5: Comparison between predicted simulation parameters and experimental data

According to table 5, when the bubble diameter increased from 1 mm to 2 mm them 4 mm the phase separation increased. This was shown in increasing the branch arm volume fraction, decreasing the run arm volume fraction, and increasing the gas splitting ratio. Moreover, all our models underpredicted the separation process, but with improving results while increasing the bubble diameter.

The main reason for increasing the phase separation when increasing the bubble diameter is the “Drag force” acting on the air bubbles.

Drag force is the frictional force created by the continuous phase (water) due to the movement of the dispersed phase (air) inside it and it plays in important role in forcing

the air bubbles to move within the water flow without any change in its direction and so having large drag force means less phase separation between water and air. When increasing the bubble diameter and having the same amount of air in our domain, it means that we are having fewer number of bubbles and so having a smaller total bubble surface area. This can then lead to smaller friction between continuous and dispersed phases and so lower drag force. Finally, lower drag force means that these bubbles are freer to move and so these bubbles can respond easily to the local pressure gradient in the junction and consequently are diverted into the branch arm. This phase separation increases with decreasing the bubble diameter can be better visualized through the gas volume fraction contours in figure 59.

However, we could not just increase our proposed bubble diameter to increase the phase separation because increasing the bubble diameter would lead to high numerical instability. This was revealed when our subcases diverged upon using a bubble diameter of 0.006 m. It is important to notice that the maximum bubble diameter in some local places in our domain is restricted to some local parameters and so having a constant bubble diameter of a certain value higher than this one can lead to divergence due to unrealistic assumptions.

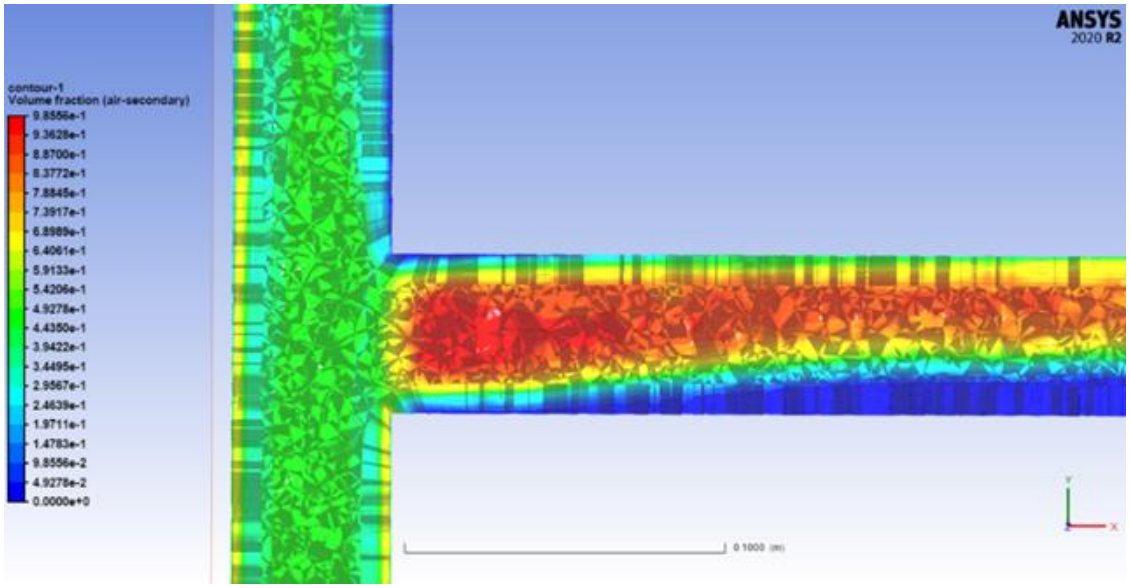

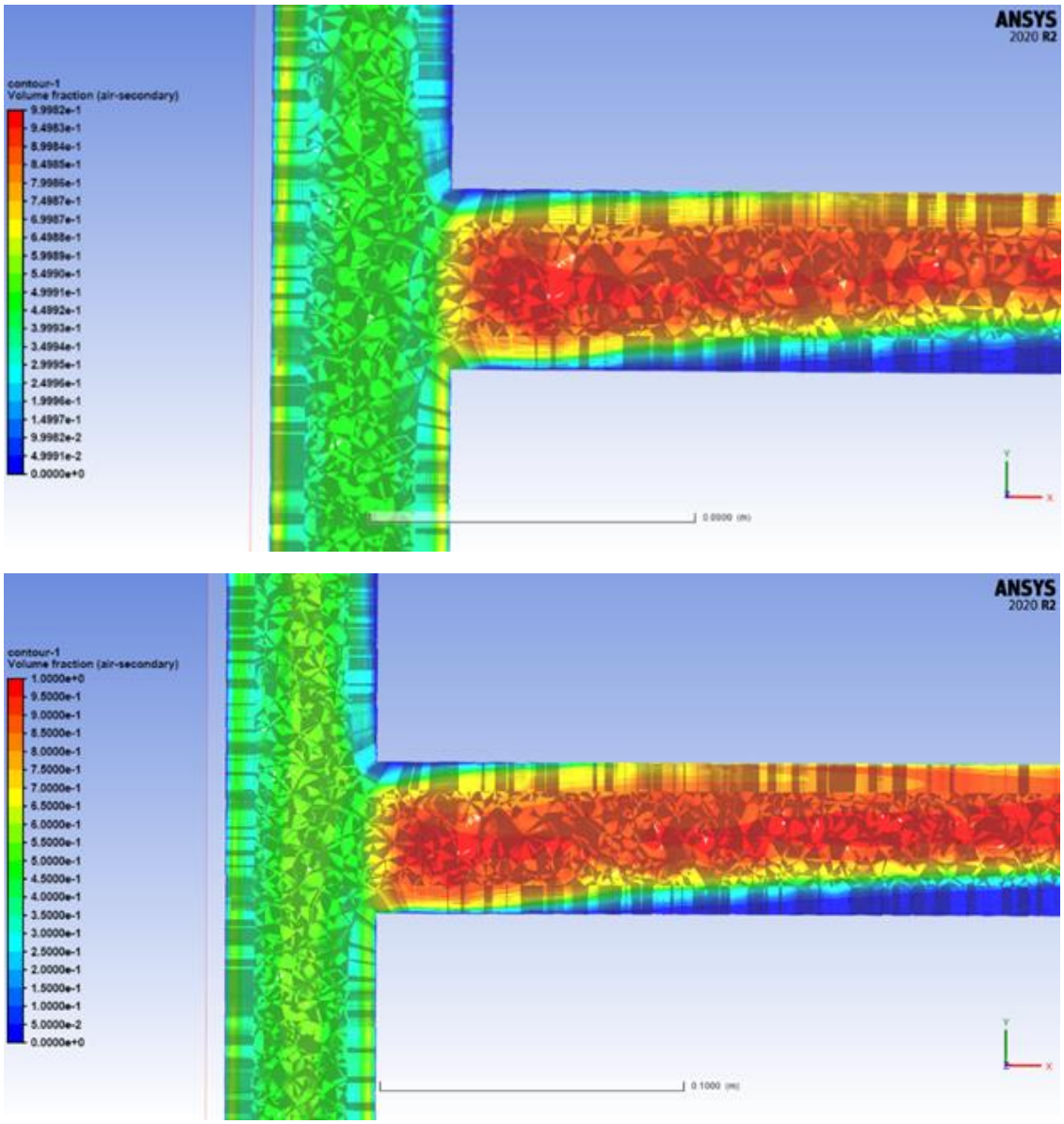

Figure 59: Gas volume fraction contour at the T-junction for sub-cases 1, 2 and 3, respectively

To increase our model accuracy, a bubble size distribution was used instead of having a constant bubble diameter and so the population balance model was suggested and so one additional subcase (Sub-case 4) was proposed.

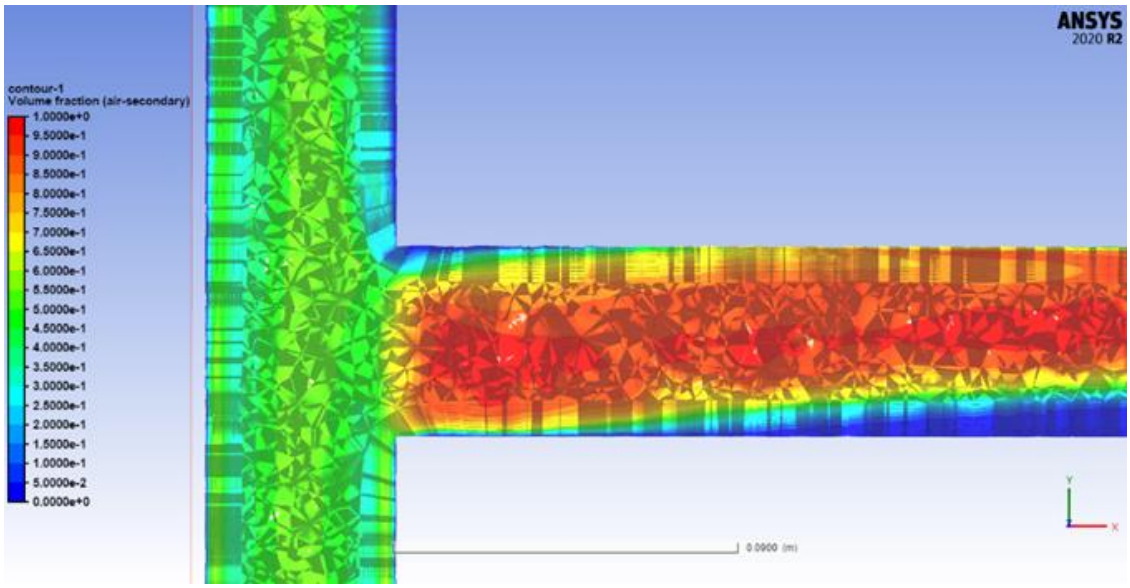

Figure 60: Gas volume fraction contours at the T-junction for sub-case 4

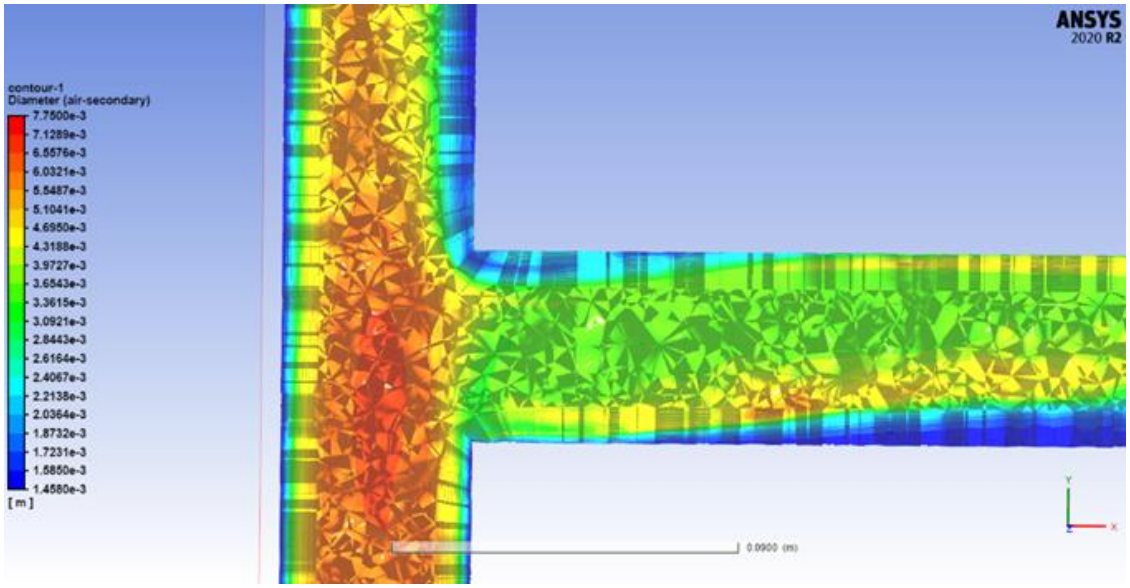

Figure 61: Bubble diameter contours of Sub-case 4

When having a bubble size distribution (sub-case 4), we got the best results in terms of gas volume fractions and gas splitting ratio (Table 5). This is because it allowed our model to have a large bubble diameter of about 0.004-0.007 m in the T-splitting part leading to stronger phase separation (Figure 60) and at the same time having smaller bubble diameters in the rest of our domain and so having more stability (Figure 61). Moreover, the model can predict the presence of bubbles with smaller diameters close to the pipe walls.

However, one main disadvantage of using a discrete population balance model with coalescence and breakage was that it needed a lot of CPU time meaning that it was computationally expensive and so using it in any industrial application would be impractical.

Other less time-consuming Population balance models like the Quadrature Method of Moment (QMOM) could be used. However, the limited timeframe of this thesis and being not the main scope of our studies led to delaying the study of these models. Therefore, more investigation on different population balance models could be done in the future to enhance our model and make it industrially applicable.

Finally, it can be concluded that our selected multiphase model can work in different complex geometries and can both show general flow trends (for example the phase separation) and give accurate results compared to the experimental data.

Moreover, changing the bubble diameter can play a vital role in our simulation results and so having a bubble size distribution with bubbles interaction (Population balance model) can enhance our model but with having a more computational time cost.

5 CASE STUDY 3 (INDUSTRIAL)

5.1 Introduction

After setting our multiphase model using analysis studies from case study 1 and validating it using both cases studies 1 and 2, it is now the time to practically explore its effectiveness industrially and how our multiphase model can accurately predict different phenomena occurring in any multiphase flow, detect any problem in the flow and be able to resolve it.

Therefore, an industrial case study having a multiphase gas-liquid flow shall be studied using our multiphase model. Moreover, this industrial case study was investigated in collaboration and during my internship in the engineering company “Maire Tecnimont”.

Our industrial case study is an oil-gas central processing plant (CPP) having two parallel working trains called (Train 3 and Train 4) in which oil-gas mixture coming from wells is being separated to both oil stream and gas stream, each one is treated separately before exporting. Therefore, we shall have multiphase flow at the beginning of the plant where both oil and gas are coupled and flowing with each other before separation.

At the beginning of this plant, slug catchers are used to receive oil-gas mixture from the off-shore wells in a gentle way using baffles to decrease the impact of having slugs in the flow and so protecting the successive equipment from damage. Moreover, they are used to preliminary separate between oil and gas before going to the phase separators.

After the preliminary separation between oil and gas in both trains’ slug catchers, liquid oil streams with minimal gas are then directed to a series of separators to extract any entrained gas in this liquid stream. Then the separated liquid is directed to the desalting unit, oil stabilization unit, purification unit, and finally storage ready for export. A block flow diagram (BFD) for the liquid oil route in the CCP is shown in figure 62.

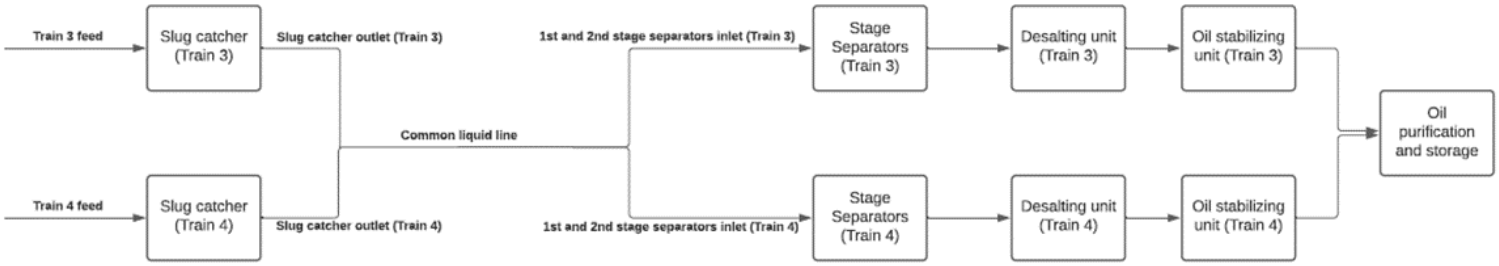

Figure 62: Block flow diagram (BFD) for oil route in the CPP

In the section between the slug catchers and stage separators, oil streams from both trains are combined in a common line before being redistributed again to both train 3 and train 4. This is because uneven flow rates can be experienced in both trains and so unifying the flow in one common line and then redistributing again in two trains helps to evenly redistribute the total flow rate to equal flowrates in both trains and so have equal capacity equipment in both trains, same operating conditions, energy requirements,…etc (symmetricity in the plant).

However, a strange phenomenon occurs in this common line which is directing most of the flow to one train and leaving the other train almost empty.

- One fast guessing of what caused this problem is the difference between downstream pressures of both train 3 and train 4 at the stage separator inlets. However, both separators have inlet pressures of 13.8 barg and so this reason was eliminated.
- Another guess was related to having asymmetrical geometry in the splitting part at the end of the common line which can plan a role in directing the flow to one train over the other.

Therefore, a 3D computational fluid dynamics study using ANSYS Fluent would be a perfect choice to better visualize this phenomenon, dig more into its causes and explore potential solutions.

5.2 Simulation Methodology

In our CFD study, a water-air system was assumed and studied instead of the oil-gas system for simplicity. Moreover, not all the common line between the slug catcher

and stage separators was simulated because it would be too big and computationally expensive. Instead, only the T-split, part of the common line (long enough to have a fully developed flow), and part of the two symmetrical pipelines entering the 1st stage separator (far enough from the T-split to avoid boundary effects on the velocity field).

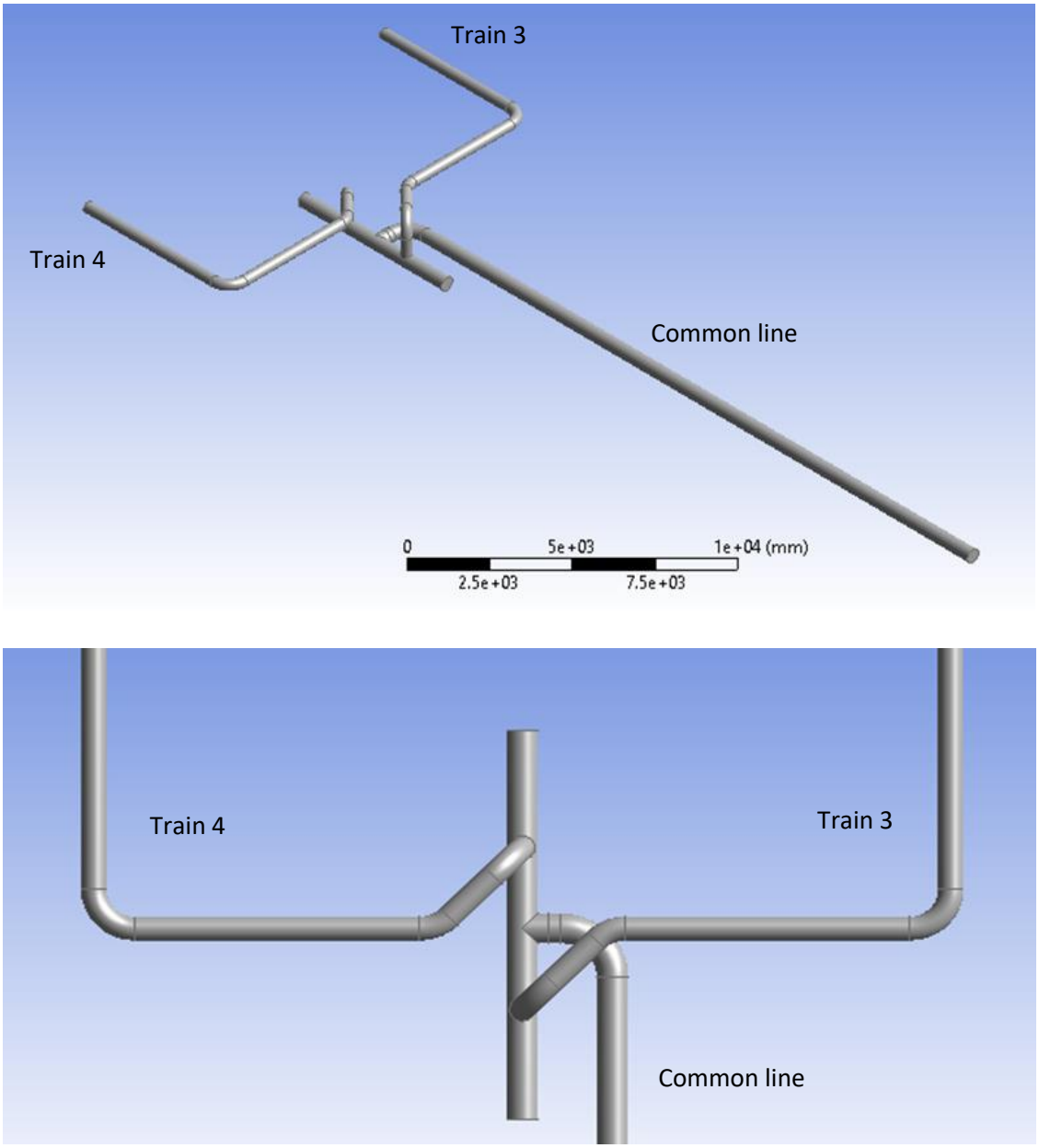

Figure 63: Case study 3 (computational domain)

At the beginning of our study, only water was considered in our system (mono-phase flow) because, in the real plant, a negligible amount of gas holdup was expected (a maximum of 4%).

After the monophasic study, an arbitrary multiphase water-air flow was studied to see if our phenomenon would be more severe when experiencing a multiphase flow.

Therefore, the following cases were studied for both mono-phasic flow (water only) and multiphase flow (water-air):

- For water only, two case studies for both maximum and turndown (minimum) flow rates with no outlet pressure difference to show the geometrical factor of the T-split when having mono-phasic flow.
- Then, three case studies (for each flow rate) having different arbitrary minimal pressure differences between both outlets (maximum 0.01 bar) to see whether an undetected small pressure difference between both outlets is going to affect the flow rate difference in the two trains or not.
- For multiphase flow, one arbitrary case study was investigated without having any outlet pressure difference to see how having a significant amount of gas can affect the flow behaviour when having our sharp geometry.
- Finally, one case study was done showing a potential solution of having a symmetrical geometry in the T-split and how it can solve this problem.

- **Geometry and Meshing:**

  As in the previous case studies, our computational domain was drawn using DesignModeler software.

  Our domain was only a part of the common line plus two small parts of the pipeline after the redistribution as shown in figure 63.

  Our common line was having a nominal diameter of 20 inches and schedule 60, meaning that its inner diameter was 18.372 inches (466.8 mm). For each train after the redistribution, the nominal diameter became 16 inches and schedule 60, meaning that its inner diameter was 14.69 inches (373.1 mm).

  However, this computational domain with these original diameters was only used in the mono-phasic cases studies (water only) and smaller diameter domains were used in multiphase simulations.

This is because our original computational domain was extremely large in diameter and so a large number of cells would have been needed to better simulate our case studies. When dealing with water only, it is not a major problem because we are dealing with only one phase and so average mesh resolution would be sufficient. However, this average resolution was not enough when simulating water-air flow as we were dealing with a complex system having extra features that needed modelling (for example the bubble diameter, phase interaction forces, turbulence in both phases,…etc) and so higher mesh resolution would be needed. This high mesh resolution would lead to having an extremely large number of nodes and so large computational time.

Therefore, two additional domains were considered having inner diameters of 50 mm, 100 mm (common line) and 40 mm, 80 mm (each train).

There was no need to have an extremely large diameter because we were only showing the asymmetric behaviour of the flow and not validating numbers and so no need to stick to the real plant dimensions. Moreover, two different domains with different inner diameters were considered to make sure that the asymmetric flow behaviour could happen in any pipe dimension regardless of its diameter.

For meshing, mesh independence analysis was done for just the original domain used for water only. This is because we were dealing with average mesh quality and so this mesh independence analysis did not take much time.

However, no mesh independence analysis was done for the other two small domains for the multiphase flow because of the limited timeframe and because we dealt with the same pipe diameter in the previous cases and so it was reasonable to take the same element size.

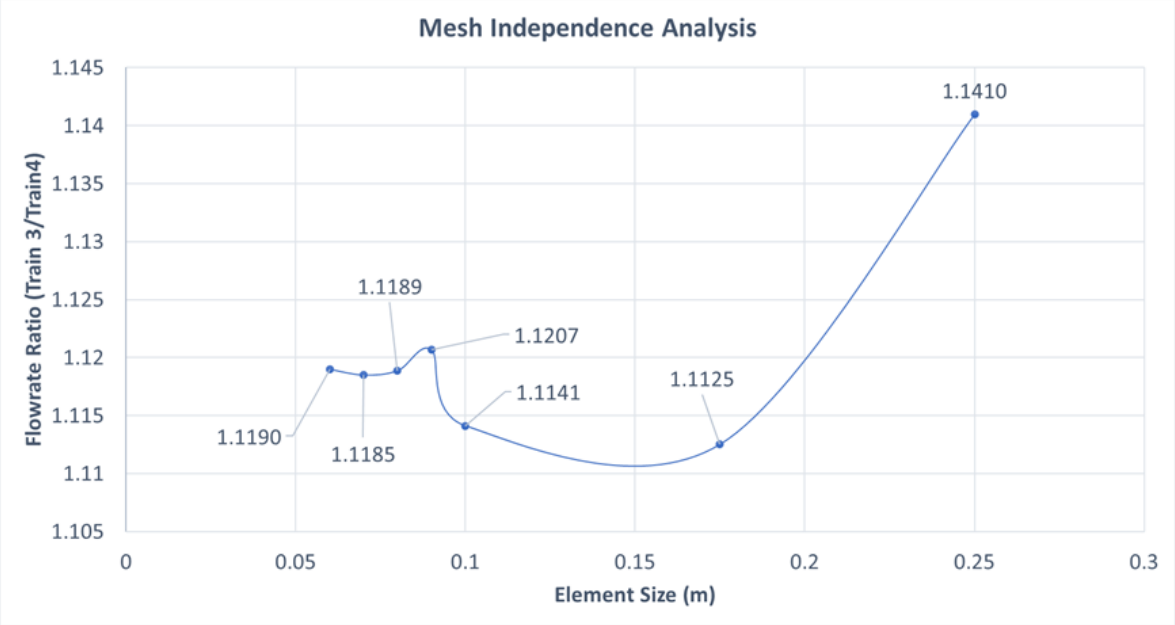

Figure 64: Mesh independence analysis of case study 3

- **Original Domain:**

  Element size: 0.08 m (According to the mesh independence analysis in figure 64)

  Inflation layers: 15 layers with 10% growth rate beside 2.5mm and 2 mm as first layer thickness for both 20 inches and 16 inches, respectively.

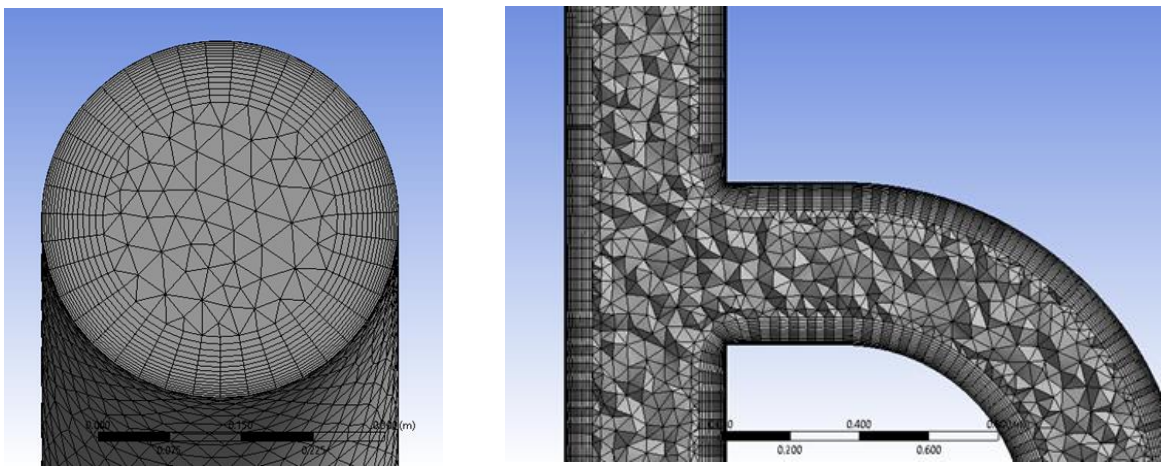

Figure 65: Mesh Distribution of Case study 3 (using 0.08 m element size)

- **50 mm Diameter Domain:**

  Element size: 0.005 m

  Inflation layers: 15 layers with 10% growth rate beside 0.3 mm and 0.25 mm as first layer thickness for both 50 mm and 40 mm, respectively.

- **100 mm Diameter Domain:**

  Element size: 0.008 m

  Inflation layers: 15 layers with a 20% growth rate beside 0.25mm and 0.22 mm as first layer thickness for both 100 mm and 80 mm, respectively.

- **Simulation Settings:**
  - **Solver Type:**

    Pressure based solver as we were dealing with an incompressible flow.
  - **Time Formulation:**

    Steady State simulation because it is considerably less time consuming than a transient one.
  - **Multiphase Model:**

    Eulerian model was used in which the phase interaction force models were as follows:
    - Drag force: Universal Drag Law[18]
    - Wall lubrication force: Antal et al. Model[26]
    - Turbulence dispersion force: Diffusion in VOF Model[31]
    - Turbulence interaction force: Trosko-Hassan Model[43]
    - Lift force and virtual mass force: Ignored.
  - **Turbulence Model:**

    Reynolds Stress Model (RSM) was used with mixture model as a multiphase description of the RSM.

- **Boundary Conditions:**
  - **Monophase flow (water only):**

    Inlet mass flow rate was defined as an inlet boundary condition for both maximum and turndown cases in which the flow rates were 226 kg/sec and 100 kg/sec, respectively.

    For the outlets (train 3 and 4), outlet pressure was defined in which both trains had 13.8 barg as an outlet pressure when simulating no pressure difference between both trains and having lower outlet pressure (for train 4) when simulating cases having outlet pressure difference.

    Moreover, a stationary wall was assumed with standard roughness of 0.00005 m as our material was carbon steel.

  - **Multiphase flow (water-air):**

    When dealing with the multiphase flow, arbitrary boundary conditions were considered in which we decided to be similar to the boundary conditions of the previous case study (as they both had the same diameter).

    Inlet velocities of 5 m/s and 6.21 m/s (corresponding liquid Reynolds number: 3.2×10^5) were considered for air and water, respectively with an inlet void fraction of 0.52. Atmospheric outlet pressure was considered for both trains and a stationary wall was assumed with standard roughness of 0.00005 m.

    Moreover, a bubble diameter of 0.001 m was set as a constant air bubble diameter. No larger bubble diameters were considered in this case study as they all diverged. Moreover, it should be noted that studying different bubble diameters and how they could influence our solution was not our scope of study because we were just studying the asymmetric flow behaviour and how it can be solved.

Case Number	Inlet Boundary conditions		Train 3 Outlet Boundary condition	Train 4 Outlet Boundary Condition	Wall roughness (m)	Bubble Diameter
	Water	Air				
1. Maximum flow-monophase-Δp=0 bar	226 kg/sec		13.8	13.8	0.00005	
2. Turndown flow-monophase-Δp=0 bar	100 kg/sec		13.8	13.8	0.00005	
3. Maximum flow-monophase-Δp= 0.01 bar	226 kg/sec		13.8	13.79	0.00005	
4. Maximum flow-monophase-Δp= 0.025 bar	226 kg/sec		13.8	13.775	0.00005	
5. Maximum flow-monophase-Δp= 0.05 bar	226 kg/sec		13.8	13.75	0.00005	
6. Turndown flow-monophase-Δp= 0.005 bar	100 kg/sec		13.8	13.795	0.00005	
7. Turbdown flow-monophase-Δp= 0.0075 bar	100 kg/sec		13.8	13.7925	0.00005	
8. Turndown flow-monophase-Δp= 0.01 bar	100 kg/sec		13.8	13.79	0.00005	
9. Multiphase flow-50 mm and 40 mm diameter	6.21 m/sec	5 m/sec	0	0	0.00005	0.001
10. Multiphase flow-100 mm and 80 mm diameter	6.21 m/sec	5 m/sec	0	0	0.00005	0.001
11. Multiphase flow-50 mm and 40 mm diameter-Modified geometry	6.21 m/sec	5 m/sec	0	0	0.00005	0.001
12. Multiphase flow-100 mm and 80 mm diameter-Modified geometry	6.21 m/sec	5 m/sec	0	0	0.00005	0.001

Table 6: Case study 3 – Boundary Conditions

- **Pressure-Velocity Coupling:**

  SIMPLE and Phase coupled SIMPLE were used for monophase and multiphase, respectively.

- **Discretization Scheme:**

  Second-order Upwind and QUICK discretization schemes were used.

- **Under Relaxation Factors:**

  For monophase flow cases, default under relaxation factors were used because we were dealing with a less complex system (water only).

  However, low under relaxation factors were defined when having a multiphase system because our system became much more complex and using defaults values would make our cases diverge.

  The used under relaxation factors were:

  - Pressure: 0.2

- Density, Body forces, Momentum, Volume fraction, Turbulence kinetic energy, Turbulence dissipation rate, turbulent viscosity, and Reynolds stresses: 0.4

Although this made our model take much more time to reach convergence, it led to stable solutions.

- **Solution Initialization:**

  Hybrid initialization was used as the previous case studies.

- **Convergence Criteria:**

  The same criteria as in the previous case studies:

  - Having scaled residuals of all the governing equations below the value of 10^{-5}.
  - Monitoring some parameters like mass flow rates and gas volume fractions in both train 3 and 4 outlets and considering our case converged when these parameters reached constant values over a long number of iterations.

- **Evaluation Criteria:**

  Same as the previous case studies: Accuracy, Computational time, and Stability.

5.3 Results and Discussion

5.3.1 Monophase Flow (Water Only)

Case Study	Train 3 mass flow rate (Kg/sec)	Train 4 mass flow rate (Kg/sec)	Ratio (Train3/Train4)	Train 3(%)	Train 4 (%)
1. Maximum flow-monophase-Δp=0 bar	119.3400	106.6600	1.1189	52.8053	47.1947
3. Maximum flow-monophase-Δp= 0.01 bar	99.3500	126.6500	0.7844	43.9602	56.0398
4. Maximum flow-monophase-Δp= 0.025 bar	75.7700	150.2200	0.5044	33.5280	66.4720
5. Maximum flow-monophase-Δp= 0.05 bar	28.8700	197.1300	0.1465	12.7743	87.2257

Table 7: CFD results of case study 3 (monophase system with maximum flowrate)

Case Study	Train 3 mass flow rate (Kg/sec)	Train 4 mass flow rate (Kg/sec)	Ratio (Train3/Train4)	Train 3(%)	Train 4 (%)
2. Turndown flow-monophase-Δp=0 bar	53.4400	46.5600	1.1478	53.4400	46.5600
6. Turndown flow-monophase-Δp= 0.005 bar	33.1900	66.8100	0.4968	33.1900	66.8100
7. Turbdown flow-monophase-Δp= 0.0075 bar	23.7600	76.2400	0.3116	23.7600	76.2400
8. Turndown flow-monophase-Δp= 0.01 bar	13.1000	86.9000	0.1507	13.1000	86.9000

Table 8: CFD results of case study 3 (monophase system with turndown flowrate)

It was observed from the results of the monophase systems simulations (Tables 7 and 8) that:

- Unbalanced flow phenomenon appeared in both maximum and turndown flowrates even with no pressure difference between both trains' outlets. Moreover, this asymmetric flow behaviour was more severe in the turndown conditions meaning that decreasing the flow rate leads to more favouring of one train over the other.
- This unbalanced flow phenomenon could be related to the sharp pipe bend close to the T-junction inlet.
- When our fluid is moving a fully developed flow inside a pipe, the velocity profile shows a higher velocity in the pipe centre while having lower velocity near the walls due to the friction. However, when our flow enters a 90-degree bend, the velocity profile becomes more complicated than the previously described profile. This is because of the centrifugal force that acts on our rotating fluid making it moves away from the centre of rotation (inner edge of the 90-degree bend) and so most of the fluid flow near the outer bend edge with a higher velocity at the outer bend edge (in an opposite manner of that the horizontal pipe). This can be better visualized in figures 66 and 67 the represent the velocity pathlines and the 90-degree bend and the velocity contour at the 90-degree bend outlet, respectively.
- When having this sharp pipe bend directly before the T-junction inlet, it leads to not having enough space for our flow to become symmetric again before entering the T-junction inlet, our fluid entered asymmetrical in our T-junction

leading to having a non-uniform split between both trains. This can be easily visualized through the velocity contour at the T-junction inlet (figure 68).

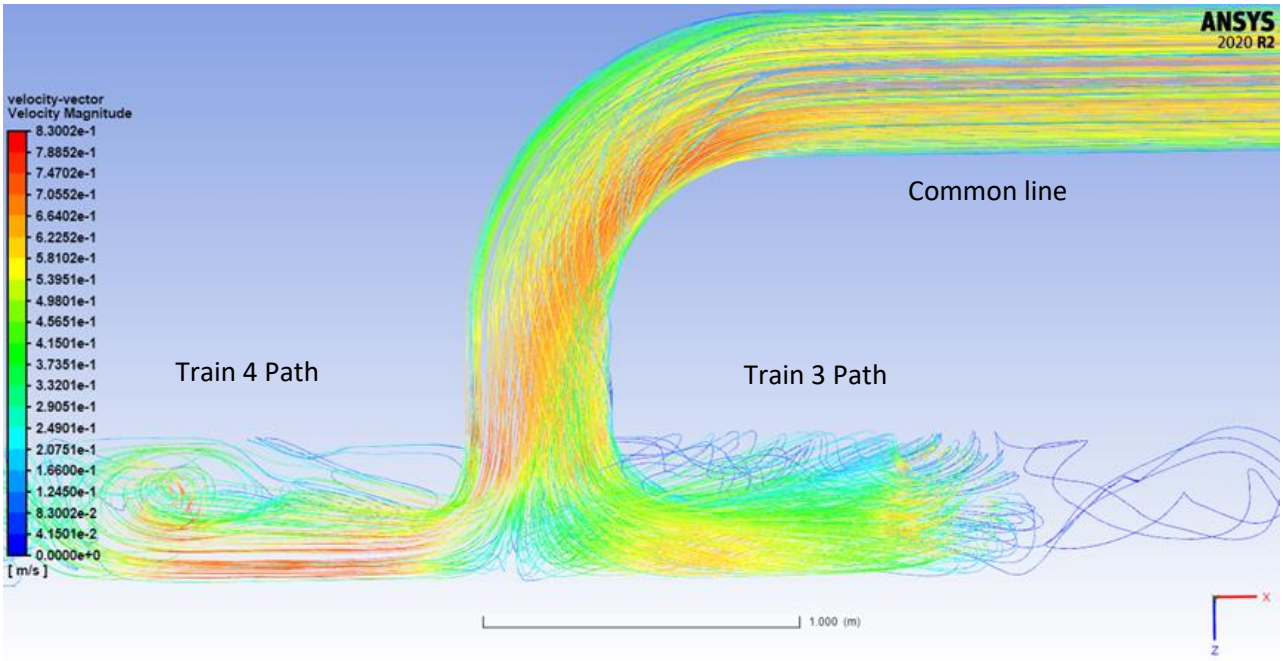

Figure 66: Pathlines of velocity vectors at the T-junction inlet (plan view)

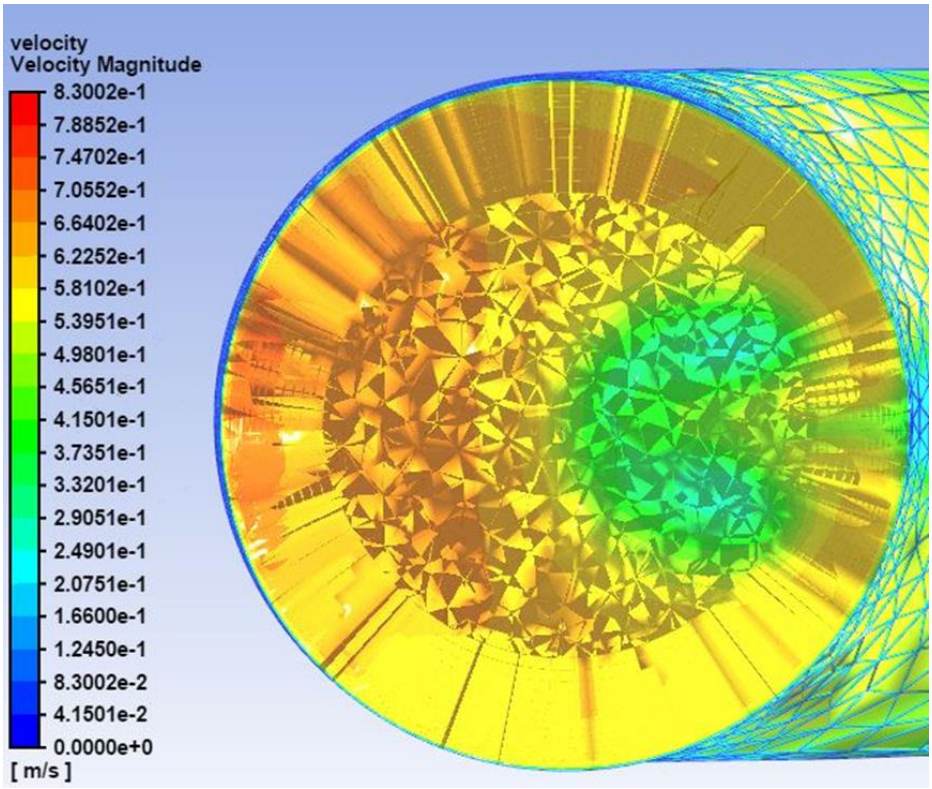

Figure 67: Velocity contour at the 90-degree bend outlet

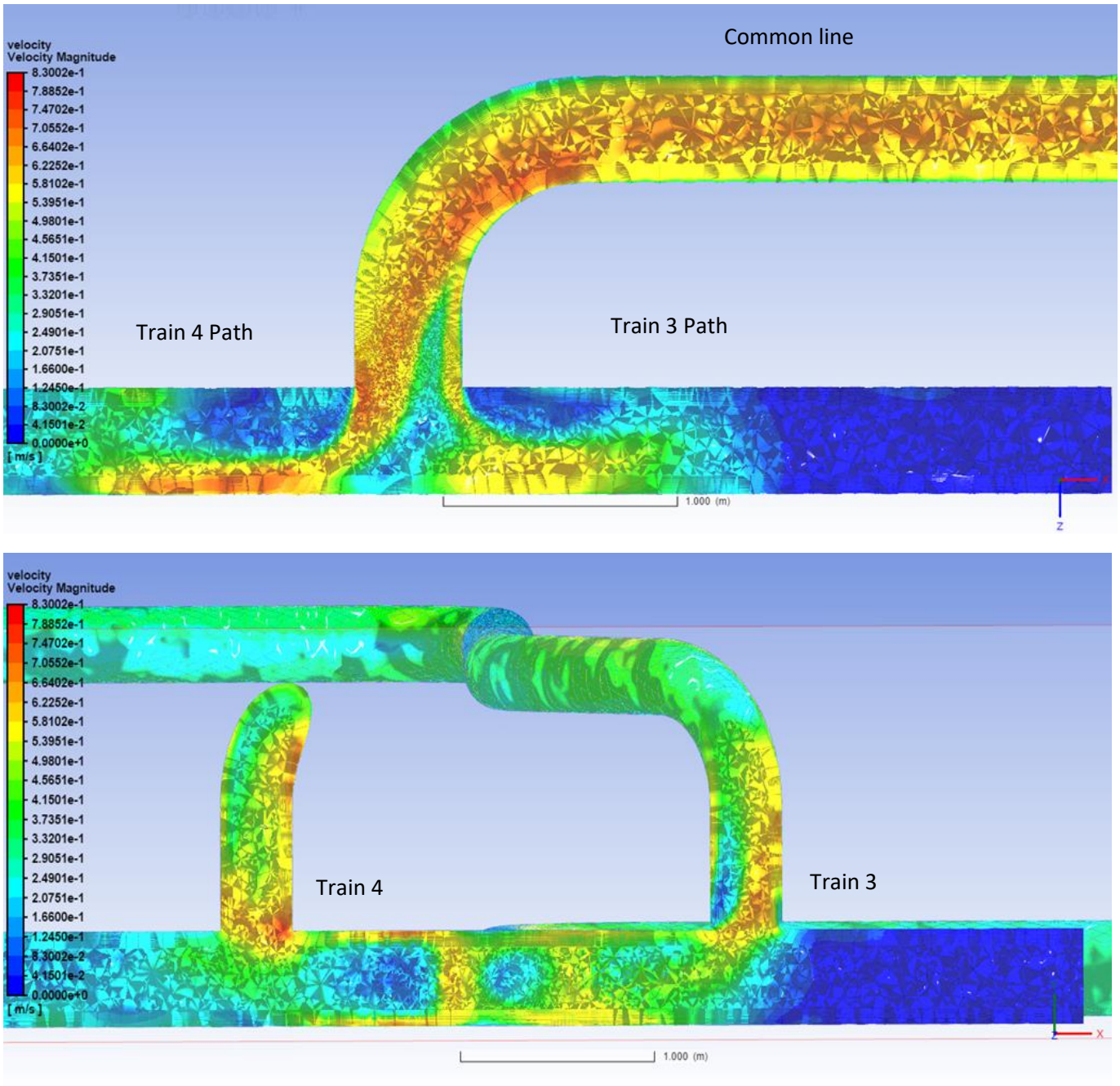

Figure 68: Velocity distribution contour at the T-junction inlet (plan and side views, respectively)

- When decreasing the flowrate (turndown case), the asymmetrical flow behaviour was enlarged due to the smaller flowrate and so more non-uniform split occurred.
- Moreover, when dealing with systems in which a small pressure difference existed between both trains, a very large difference in flow rates between both trains was observed. Only a pressure difference of 0.05 barg (which was only

0.36% of the total pressure) led to having about 87% of the flow rate flowing in one train.

- In addition, the pressure effect was magnified more in the turndown cases by having 87% of the flow rate moving through one train when only having a pressure difference of 0.01 barg (0.07% of the total pressure).
- The problem is that these pressure differences are within the acceptable error range within any industrial plant as we are talking about a maximum of less than 1%. Therefore, it is then possible to have such small deviations in the outlet pressures of both trains.
- This extremely high sensitivity could be explained through the pressure drop equations within pipes. When any fluid flows through a pipe, its pressure decreases due to:
  - Primary friction within the pipe in which the pressure loss can be calculated through Darcy-Weisbach equation:

$$\Delta P = \rho/2 \sum_i \frac{L_i}{D_i} v_i^2 f_i \tag{94}$$

    In which:

    - ΔP is the pressure drop within the pipeline due to the primary friction (pascal)
    - ρ is the fluid density (kg/m^3)
    - L_i and D_i are the pipe length and diameter in meter, respectively.
    - v_i is the fluid velocity that is directly related to its flowrate (m/s)
    - f_i is the friction coefficient that is a function of the local Reynolds number and roughness, and it is computed by using Colebrook-White equation
  - Secondary friction due to fittings (bends, elbows, sudden expansion or contraction,..etc)
  - Elevation change

Since we are having a pipe of extremely large diameter (373.1 mm in its narrowest part) and extremely low friction factor (0.00005 m pipe roughness), our pressure loss due to primary friction would be too low (refer to equation 94) and an extremely large flowrate would then be required to cause any noticeable pressure drop. However, for the same reason, any small change in the pressure drop can lead to an extremely large change in the flow rate.

When having any small pressure difference between both trains, this can lead to having a small difference in the pressure drop between both trains. This small change in the pressure drop between both trains can lead to a large change in the flow rate in both trains and so having most of the flow moving in one train over the other.

- One possible solution could be adding control valves on both trains in which these valves would add extra significant secondary pressure drop to our system making the total pressure drop within each train significant. This can then lead to stabilizing the system against any pressure fluctuations because these fluctuations would be negligible compared to the extra added pressure drop and so not affecting the flow rate in both trains.

5.3.2 Multiphase Flow (Water-Air)

	Water					Air						
Case Study	Mass flow rate (Train 3) Kg/sec	Mass flow rate (Train 4) Kg/sec	Ratio (Train 3/4)	Train 3 %	Train 4 %	Mass flow rate (Train 3) Kg/sec	Mass flow rate (Train 4) Kg/sec	Ratio (Train 3/4)	Train 3 %	Train 4 %	Train 3 volume fraction	Train 4 volume fraction
9. Multiphase flow-50 mm and 40 mm diameter	2.7664	3.0868	0.8962	47.2634	52.7366	0.0043	0.0019	2.2429	69.1638	30.8362	0.5098	0.3228
10. Multiphase flow-100 mm and 80 mm diameter	10.0580	13.3968	0.7508	42.8825	57.1175	0.0177	0.0069	2.5669	71.9645	28.0355	0.5284	0.2634

Table 9: CFD results of case study 3 (Multiphase flow)

When doing arbitrary multiphase flow simulations on different inner diameters, we found that:

- Non-uniform flow distribution occurred between trains 3 and 4 in which more liquid flowed in train 4 while most of the gas favoured train 3. As a result, more volume fraction could be observed in train 3.

- The same pattern happened in both inner diameter cases but in a more severe way of non-uniformity meaning that the asymmetric flow behaviour of both liquid and gas could happen regardless of the pipe size. Moreover, increasing the multiphase flow rate by increasing the diameter with the same inner velocity (as our case study) can lead to increasing the separation phenomenon of bot phases and so more non-uniformity.
- The reason behind favouring both liquid and gas different trains could be better explained through gas volume fraction contour at the T-junction inlet (figure 69)

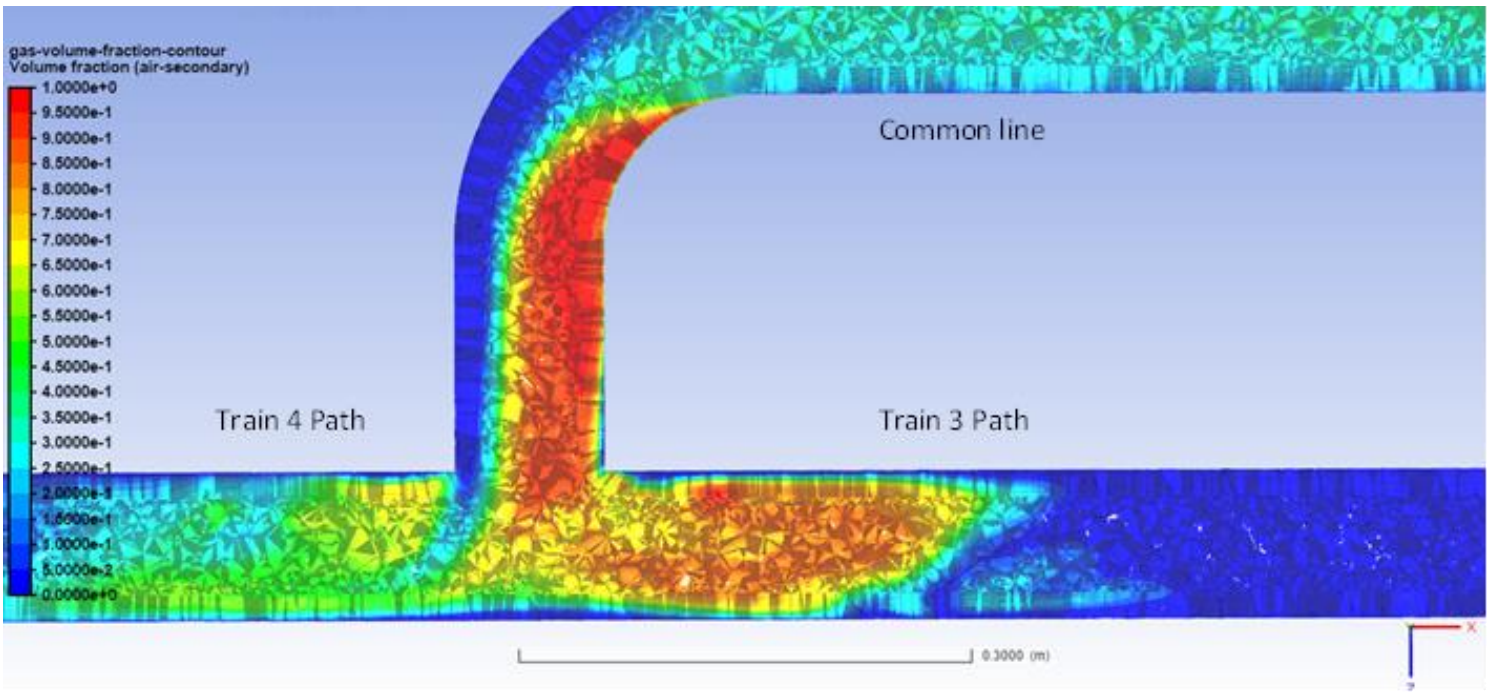

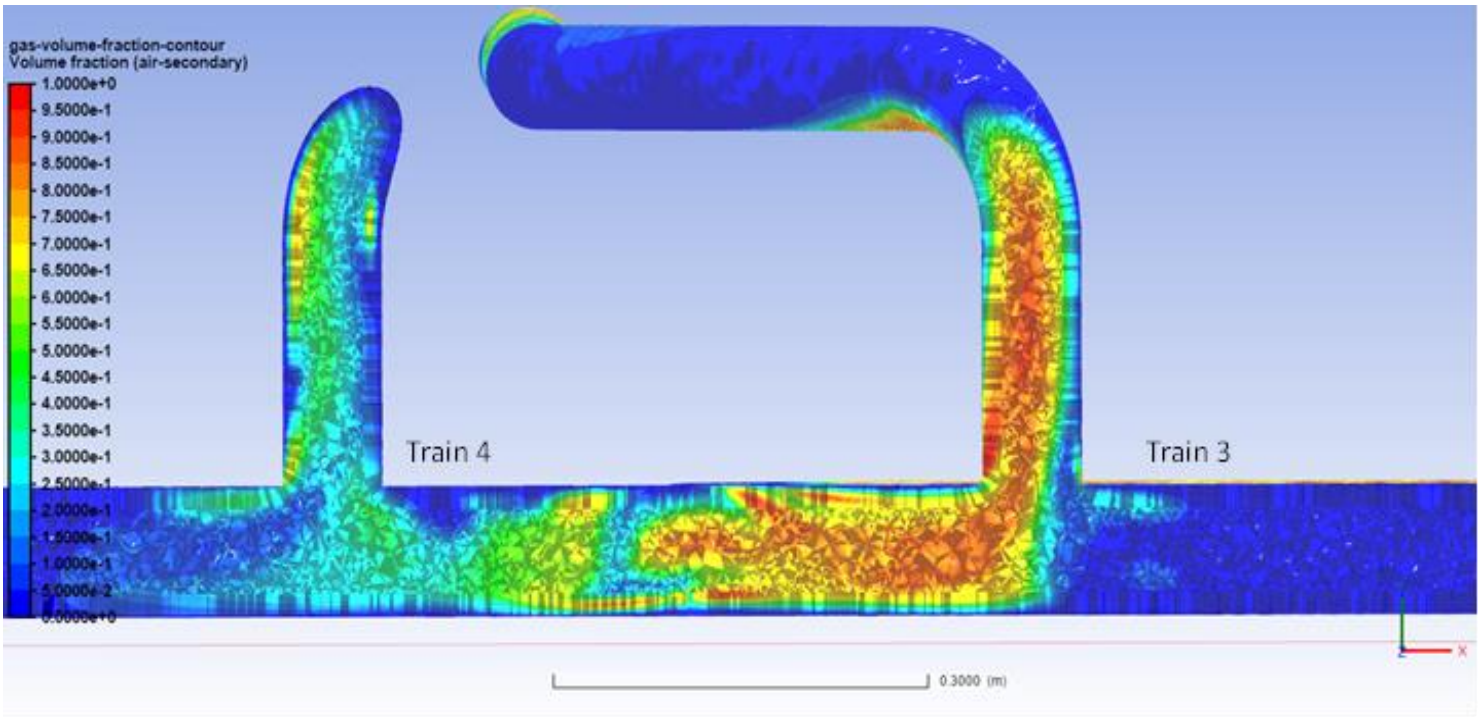

Figure 69: Gas volume fraction contour at the T-junction inlet (Plan and side views, respectively)

- As one can see from figure 69, more gas is found at the inner corner of the bend before the T-junction inlet while most of the liquid is concentrated at the outer corner.
- This is because of the large inertia difference between water and air in which water has much higher inertia than that of the air. The large water inertia makes it hard for it to rapidly change its flow direction when moving through the bend and so most of the water would then be concentrated away from the bend inlet. This is the opposite when dealing with air because its low inertia makes it easy for the air to deal with sudden flow changes. Therefore, most of the air could be found in the inner corner of the bend near its inlet.
- This local separation between both phases remained till the T-junction inlet because there was not much space between the bend and the T-junction for our multiphase flow to return into the uniform flow again. Therefore, most of the liquid moved to the left side of figure 69 which is the train 4 inlet while a larger air portion moved to the opposite direction which is train 3 inlet.
- Our proposed way to solve this problem was to remove the sharp bend that was located directly before the T-junction inlet as shown in figure 70. In this

way, we would be able to prevent the local phase separation at the bend due to the inertia difference and hence prevent any asymmetric flow between trains 3 and 4.

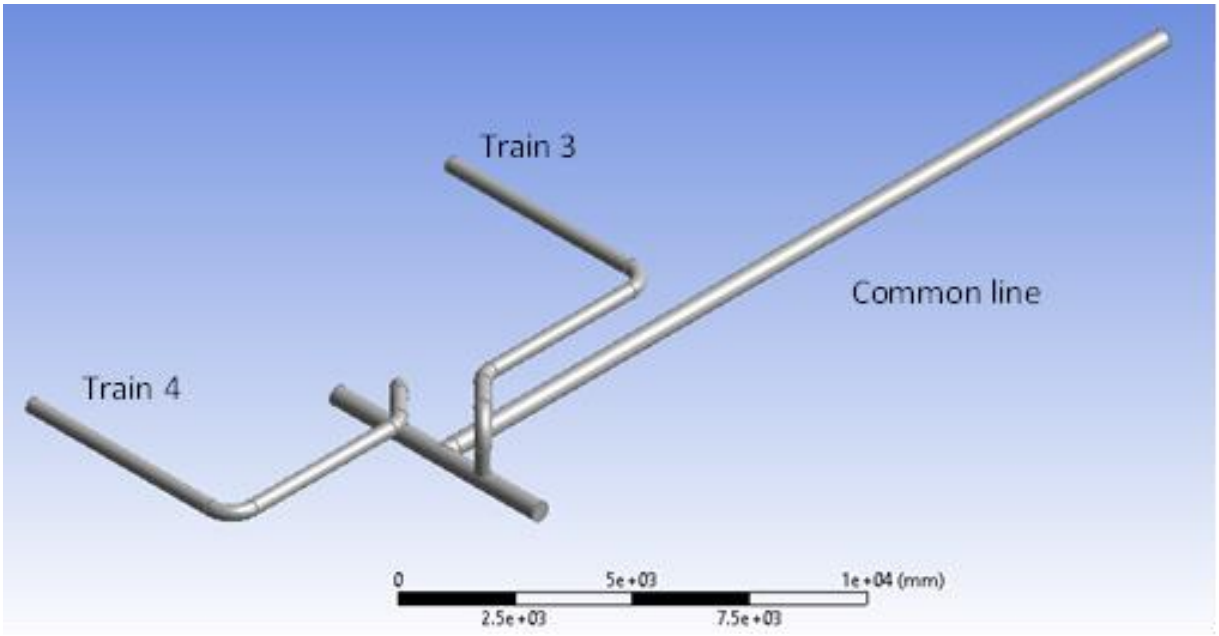

Figure 70: Proposed modified geometry for case study 3 to prevent the asymmetric flow distribution.

	Water					Air						
Case Study	**Mass flow rate (Train 3) Kg/sec**	**Mass flow rate (Train 4) Kg/sec**	**Ratio (Train 3/4)**	**Train 3 %**	**Train 4 %**	**Mass flow rate (Train 3) Kg/sec**	**Mass flow rate (Train 4) Kg/sec**	**Ratio (Train 3/4)**	**Train 3 %**	**Train 4 %**	**Train 3 volume fraction**	**Train 4 volume fraction**
11. Multiphase flow-50 mm and 40 mm diameter-Modified geometry	2.9674	2.9268	1.0139	50.3448	49.6552	0.0031	0.0030	1.0121	50.3007	49.6993	0.4324	0.4361
12. Multiphase flow-100 mm and 80 mm diameter-Modified geometry	11.8448	11.5377	1.0266	50.6569	49.3431	0.0122	0.0125	0.9697	49.2320	50.7680	0.4143	0.4396

Table 10: CFD results of case study 3 (Multiphase flow after the geometric modification)

- According to table 10, both water and air were redistributed equally between both trains in which their flow rates were almost equal. Moreover, the gas volume fractions in trains 3 and 4 were similar.
- The symmetric behaviour in both trains was due to the absence of any sudden changes in the flow direction before the T-junction inlet which would lead to phase separation. Therefore, both phases uniformly entered the T-junction and so symmetric redistribution to trains 3 and 4 occurred. The homogeneous multiphase flow at the inlet and the symmetric redistribution in both trains can

better be visualized through the gas volume fraction contour at the T-junction inlet (figure 71).

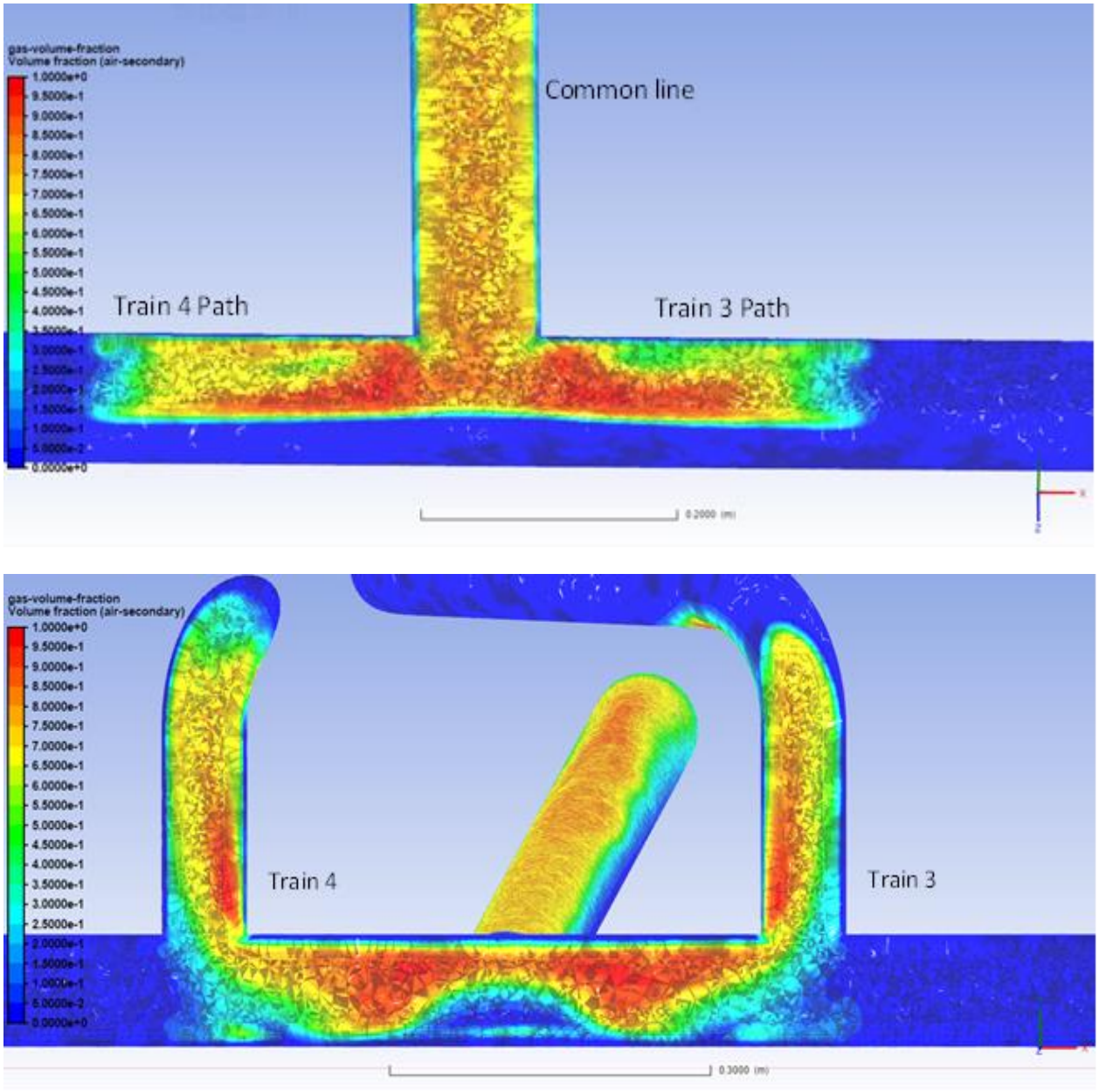

Figure 71: Gas volume fraction at the T-junction inlet for the modified geometry (plan and side views, respectively)

Finally, it can be concluded that our selected multiphase model proved its efficiency by both predicting problems in any multiphase flow through complex industrial geometries and being able to solve these problems.

6 CONCLUSION

The purpose of this thesis was to deeply study multiphase flow systems using the Computational Fluid Dynamics (CFD) technique and especially the plank areas that were not investigated before. the description of this kind of system is challenging because of lots of different physical phenomena that have to be taken into account. This complexity made it difficult to study multiphase flows using CFD approaches until recent years. Moreover, multiphase flow systems are very common in many industries, especially oil and gas, and so design improvements through CFD simulations would lead to a major impact in these sectors.

In this thesis study, gas-liquid flow systems were studied, with particular attention on the investigation of the different phase interaction forces, whose models are available in ANSYS Fluent. Our scope was to analyse all these forces and their related models and select an overall multiphase model that had the best combination of these forces and models.

Our research was executed using the Eulerian Model, which is the most accurate approach. Besides, Reynolds Stress Model was used as a turbulence model for the same reason (the most accurate one adopting a RANS approach). This is because our area of investigation was to study the interaction between different phases in the flow and so it was decided to adopt the best models to describe the other physical phenomena.

Our first step (Case study 1) was to analyse the phase interaction forces and select the new model based on a sensitivity analysis to select the models that best fit with the experimental data from G. Kocamustafaogullari and Z. Wang .

From our work in case study 1, it was concluded that:

- Having phase interaction forces like drag, wall lubrication, turbulence dispersion and turbulence interaction forces can increase the accuracy of the selected multiphase model, while the forces of lift and virtual mass would either make the numerical solution of this system unstable or inaccurate.

- The analysis showed that for the drag force, the Universal Drag Law is the best model, while Antal et al. model should be preferred to describe the wall lubrication force. Diffusion in VOF model is the most accurate one to simulate the turbulence dispersion force. Finally, Troshko-Hassan (mixture turbulence model) and Simonin (Dispersed turbulence model) are suitable models for the turbulence interaction forces.

Our next step (Case study 2) was to revalidate our selected model using another experimental data from Davis and Fungtamasan that worked on more complex geometry (T-junction instead of the horizontal pipe as in case study 1).

It was concluded from this case study that:

- Our selected model can work accurately on different complex geometries showing the general flow trends like the phase separation and giving accurate results, compared to the experimental data.
- Bubble diameter size has a major impact on the simulation results and so accurately predicting it would play a vital role in the model's accuracy.
- Using the Population balance model instead of having a constant bubble diameter would enhance simulation results as it both assumes a distribution of bubbles sizes, instead of having a constant one, and simulates the bubbles' interactions (coalescence and breakage). However, it would lead to much more computational time.

Our final step (Case study 3) was to apply the selected model to an industrial application to find its ability to simulate the case, monitor any problem and resolve it using ANSYS Fluent.

Our industrial case study was an oil and gas plant in which the pipeline between the slug catcher and the phase separators had a strange phenomenon of having an asymmetric flow distribution between two trains after flowing in a common line.

Our selected model was able to reproduce this asymmetric flow distribution in both monophase and multiphase flow scenarios. Moreover, it accurately explained this

behaviour and finally allowed to simulate a proposed geometrical modification showing how it can accurately solve this problem.

New scopes to study:

Our proposed next step would be to continue the work on multiphase flow systems and extend our study to the following points:

- **Dispersed Phase Particle Distribution:**

  Constant particle diameter was estimated for most of the experiments. However, one sub-case study was done in case of study 2 by assuming bubble size distribution (Population Balance Model) and it showed better simulation results, but with a significantly longer computational time. Therefore, we would propose to deeply study the coupling between Population Balance Model and Multiphase Model and try to compare between these three models (Discrete, SMM and QMOM) to find which one is better in terms of accuracy and reliability in computational time (to fit more in the industrial field). This can be done by having a previously investigated multiphase experiment and reproducing it through CFD modelling. However, this experiment shall include the study of the particle size distribution.

- **Mass Transfer Between Different Phases:**

  No mass transfer between different phases of chemical reactions was assumed in our selected model. However, this is not the case in many industrial applications as many chemical reactions involving mass transfer between different phases can occur.

  In these reacting systems, chemical reactions, or mass transfer from one phase to the other can become the limiting step. Therefore, extending our model to be able to study these reactive systems would be very helpful. Moreover, multiphase CFD can be considered a powerful tool in studying non-ideal multi-phase.

7 REFERENCES

1) ANSYS-FLUENT 12.0 Theory Guide, ANSYS Inc., USA.
2) Crowe, C. T. *Multiphase Flow Handbook*. Taylor & Francis/CRC Press, 2006.
3) De Schepper, Sandra C.K., et al. “CFD Modeling of All Gas–Liquid and Vapor–Liquid Flow Regimes Predicted by the Baker Chart.” *Chemical Engineering Journal*, vol. 138, no. 1-3, 2008, pp. 349–357., doi:10.1016/j.cej.2007.06.007.
4) Azzopardi, B.J. “Multiphase Flow.” *Chemical Engineering and Chemical Process Technology: Fundamentals of Chemical Engineering*, by Ryzhard Pohorecki, vol. 1, Eolss Publishers Co., Ltd., 2010.
5) STENMARK, ELIN. “On Multiphase Flow Models in ANSYS CFD Software.” *CHALMERS UNIVERSITY OF TECHNOLOGY Göteborg, Sweden* , 2013.
6) Ekambara, K., et al. “CFD Modeling of Gas-Liquid Bubbly Flow in Horizontal Pipes: Influence of Bubble Coalescence and Breakup.” *International Journal of Chemical Engineering*, vol. 2012, 2012, pp. 1–20., doi:10.1155/2012/620463.
7) ANSYS-FLUENT 2020 R2 Theory Guide, ANSYS Inc., USA.
8) Lote, Dhiraj A., et al. “COMPARISON OF MODELS FOR DRAG AND NON-DRAG FORCES FOR GAS-LIQUID TWO-PHASE BUBBLY FLOW.” *Multiphase Science and Technology*,vol.30,no.1,2018,pp.31–6., doi:10.1615/multscientechn.2018025983.
9) Sultan, Rasel A., et al. “Validation of CFD Model of Multiphase Flow through Pipeline and Annular Geometries.” *Particulate Science and Technology*, vol. 37, no. 6, 2018, pp. 685–697., doi:10.1080/02726351.2018.1435594.
10) Paladino, E. and C. Maliska. “Virtual mass in accelerated bubbly flows.” (2003).
11) Kocamustafaogullari, G., and Z. Wang. “An Experimental Study on Local Interfacial Parameters in a Horizontal Bubbly Two-Phase Flow.” *International Journal of Multiphase Flow*, vol. 17, no. 5, 1991, pp. 553–572., doi:10.1016/0301-9322(91)90024-w.
12) Davis, M.R., and B. Fungtamasan. “Two-Phase Flow through Pipe Branch Junctions.” *International Journal of Multiphase Flow*, vol. 16, no. 5, 1990, pp. 799–817., doi:10.1016/0301-9322(90)90005-4.

13) Athulya, A.S., and R. Miji Cherian. “CFD Modelling of Multiphase Flow through T Junction.” *Procedia Technology*, vol. 24, 2016, pp. 325–331., doi:10.1016/j.protcy.2016.05.043.

14) L. Schiller and Z. Naumann. *"Z. Ver. Deutsch. Ing*. 77. 318. 1935.

15) S. A. Morsi and A. J. Alexander. "An Investigation of Particle Trajectories in Two-Phase Flow Systems". *J. Fluid Mech*. 55(2). 193–208. September 26 1972

16) Clift, Grace, and Weber. "Bubbles, Drops, and Particles". *Technical Report*. Academic Press. 1978

17) T. Takamasa and A. Tomiyama. . “Three-Dimensional Gas-Liquid Two-Phase Bubbly Flow in a C-Shaped Tube”. *Ninth International Topical Meeting on Nuclear Reactor Thermal Hydraulics (NURETH-9)*. San Francisco, CA. 1999

18) N. I. Kolev. *Multiphase Flow Dynamics 2: Thermal and Mechanical Interactions*. Springer, Berlin, Germany, 2nd edition. 2005

19) D. A. Drew and R. T. Lahey. *In Particulate Two-Phase Flow*. Butterworth-Heinemann. Boston, MA509–566. 1993

20) P. G. Saffman. "The Lift on a Small Sphere in a Slow Shear Flow". *J.Fluid Mech*. 22. 385–400. 1965

21) P. G. Saffman. Corrigendum to: "The Lift on a Small Sphere in a Slow Shear Flow". *J.Fluid Mech*. 31. 624. 1968

22) D. Legendre and J. Magnaudet. “The Lift Force on a Spherical Bubble in a Viscous Linear Shear Flow”. *J. Fluid Mech*. 368. 81–126. 1998

23) F. J. Moraga, R. T. Bonetto and R. T. Lahey. "Lateral forces on spheres in turbulent uniform shear flow". *International Journal of Multiphase Flow*. 25. 1321–1372. 1999

24) Tomiyama. "Struggle with computational bubble dynamics". *Third International Conference on Multiphase Flow, Lyon, France*. June 8–12, 1998

25) Th. Frank, J. M. Shi, and A. D. Burns. "Validation of Eulerian Multiphase Flow Models for Nuclear Safety Applications". *Third International Symposium on Two-Phase Flow Modeling and Experimentation, Pisa, Italy*. Sept. 22–24, 2004

26) S. P. Antal, R. T. Lahey, and J. E. Flaherty. "Analysis of phase distribution in fully developed laminar bubbly two-phase flow". *International Journal of Multiphase Flow*. 17. 5. 635–652. 1991

27) S. Hosokawa, A. Tomiyama, S. Misaki, and T. Hamada. "Lateral Migration of Single Bubbles Due to the Presence of Wall". *ASME 2002 Joint U.S.-European Fluids Engineering Division Conference, Montreal, QC, Canada*. July 14–18, 2002

28) M. Lopez de Bertodano. "Turbulent Bubbly Flow in a Triangular Duct". *Ph.D. Thesis*. Rensselaer Polytechnic Institute, Troy, New York. 1991

29) O. Simonin and P. L. Viollet. "Modeling of Turbulent Two-Phase Jets Loaded with Discrete Particles". *Phenomena in Multiphase Flows*. 259–269. 1990

30) D. B. Burns, Th. Frank, I. Hamill, and J.-M. Shi. The Favre Averaged Drag Model for Turbulent Dispersion in Eulerian Multi-Phase Flows. *Fifth International Conference on Multiphase Flow, ICMF-2004, Yokohama, Japan*. 2004

31) Sokolichen, G. Eigenberger, and A. Lapin. "Simulation of Buoyancy Driver Bubbly Flow: Established Simplifications and Open Questions". *Journal Review, AIChE Journal*. 50:1. 24–45. January 2004

32) D. A. Drew and R. T. Lahey. *In Particulate Two-Phase Flow*. Butterworth-Heinemann. Boston, MA509–566. 1993

33) M. J. Hounslow, R. L. Ryall, and V. R. Marshall. A Discretized Population Balance for Nucleation, Growth, and Aggregation. *AIChE Journal*, 34(11):1821-1832, 1988

34) J. D. Litster, D. J. Smit, and M. J. Hounslow. Adjustable Discretization Population Balance for Growth and Aggregation. *AIChE Journal*, 41(3):591-603, 1995

35) D. Ramkrishna. *Population Balances: Theory and Applications to Particulate Systems in Engineering*. Academic Press, San Diego, CA, 2000.

36) D. Randolph and M. A. Larson. *Theory of Particulate Processes: Analysis and Techniques of Continuous Crystallization*. Academic Press, San Diego, CA, 1971.

37) R. McGraw. Description of Aerosol Dynamics by the Quadrature Method of Moments. *Aerosol Science and Technology*, 27:255-265, 1997.

38) M. M. Gibson and B. E. Launder. "Ground Effects on Pressure Fluctuations in the Atmospheric Boundary Layer". *J. Fluid Mech*. 86. 491–511. 1978.

39) E. Launder. "Second-Moment Closure: Present... and Future?". *Inter. J. Heat Fluid Flow*. 10(4). 282–300. 1989.

40) E. Launder, G. J. Reece, and W. Rodi. "Progress in the Development of a Reynolds-Stress Turbulence Closure". *J. Fluid Mech*. 68(3). 537–566. April 1975.

41) Cokljat, M. Slack, and S. A. Vasquez. "Reynolds-Stress Model for Eulerian Multiphase". In Y. Nagano K. Hanjalic and M. J. Tummers, editors. *Proceedings of the 4th International Symposium on Turbulence Heat and Mass Transfer*. Begell House, Inc. 1047–1054. 2003

42) O. Simonin and P. L. Viollet. "Predictions of an Oxygen Droplet Pulverization in a Compressible Subsonic Coflowing Hydrogen Flow". *Numerical Methods for Multiphase Flows*. FED91. 65–82. 1990

43) Troshko and Y. A. Hassan. "A Two-Equation Turbulence Model of Turbulent Bubbly Flow". *International Journal of Multiphase Flow*. 22(11). 1965–2000. 2001.

44) Y. Sato and K. Sekoguchi. "Liquid Velocity Distribution in Two-Phase Bubbly Flow". *Int. J. Multiphase Flow*. 2. 79. 1979.

45) J. O. Hinze. *Turbulence*. McGraw-Hill Publishing Co., New York. 1975.

46) "Turbulence Models in CFD - RANS, DES, LES and DNS." *IdealSimulations*, 26 Sept. 2020, www.idealsimulations.com/resources/turbulence-models-in-cfd/.

47) Lo, Simon, and Dongsheng Zhang. "Modelling of Break-up and Coalescence in Bubbly Two-Phase Flows." *The Journal of Computational Multiphase Flows*, vol. 1, no. 1, 2009, pp. 23–38., doi:10.1260/175748209787387106.

48) H. Luo and H. F. Svendsen. "Theoretical Model for Drop and Bubble Breakup in Turbulent Dispersions". AIChE Journal. 42(5). 1225–1233,. 1996.

49) H. Luo. "Coalescence, Breakup and Liquid Circulation in Bubble Column Reactors". PhD thesis from the Norwegian Institute of Technology. Trondheim, Norway1993.

50) "Normal Distribution" *From Wolfram MathWorld*, mathworld.wolfram.com /NormalDistribution.html.

8 APPENDICES

8.1 List of Figures

Figure 1: X-ray absorption Probability Density Functions of a void fraction by Jones and Zuber (1975).....7
Figure 2: Flow patterns in vertical gas-liquid flow.[4].....9
Figure 3: Flow patterns in Horizontal gas-liquid flow.[3].....11
Figure 4: A modified form of the flow pattern map of Hewitt and Roberts (1969) – vertical flow.[4].....12
Figure 5: Baker Chart.[3].....13
Figure 6: The concept of virtual mass.[10].....37
Figure 7: Flowchart representing the phase interaction forces and their available models.....38
Figure 8: Flowchart representing how to choose between different multiphase models.....44
Figure 9: Laminar, Transitional and Turbulent flow.....45
Figure 10: Double-Sensor Electrical Resistivity Probe Design.[11].....54
Figure 11: Schematic of the experimental flow loop.[11].....55
Figure 12: Air-Water mixing chamber.[11].....55
Figure 13: Mounting and traversing in double-sensor resistivity probe.[11].....57
Figure 14: Gas Void fraction versus radial position for different gas flow rates at a constant liquid velocity.[11].....58
Figure 15: Gas Void fraction versus radial position for different liquid flow rates at a constant gas velocity.[11].....58
Figure 16: Bubble diameter versus radial position for different liquid flow rates at a constant gas velocity.[11].....59
Figure 17: Bubble diameter versus radial position for different gas flow rates at a constant liquid velocity.[11].....59
Figure 18: Local bubble interface velocity versus radial position for different liquid flow rates at a constant gas velocity.[11].....60

Figure 19: Local bubble interface velocity versus radial position for different gas flow rates at a constant liquid velocity.[11] 60
Figure 20: The sensitivity analysis methodology 62
Figure 21: Case Study 1 (Computational Domain).....63
Figure 22: Mesh independence analysis of case study 1.....64
Figure 23: Mesh Distribution of case study 1 (using 5.5 mm element size).....65
Figure 24: Comparison between drag force models and the experimental measurements concerning local void fraction. 70
Figure 25: Comparison between drag force models and the experimental measurements concerning bubble interface velocity. 71
Figure 26: Schiller-Naumann Model Scaled Residual Curves 72
Figure 27: Morsi-Alexander Model Scaled Residual Curves 72
Figure 28: Symmetric Model Scaled Residual Curves.....72
Figure 29: Grace et al. Model Scaled Residual Curves.....73
Figure 30: Tomiyama et al. Model Scaled Residual Curves 73
Figure 31: Universal Drag Law Scaled Residual Curves.....73
Figure 32: Comparison between wall lubrication force models and the experimental measurements concerning local void fraction. 75
Figure 33: Comparison between wall lubrication force models and the experimental measurements concerning local bubble interface velocity.....75
Figure 34: Antal et al. Scaled Residual Curves 76
Figure 35: Comparison between turbulence dispersion force models and the experiment concerning local void fraction. 77
Figure 36: Comparison between turbulence dispersion force models and the experimental measurements concerning local bubble interface velocity. 78
Figure 37: Diffusion in VOF Scaled Residual Curves 79
Figure 38: Comparison between turbulence interaction force models and the experimental measurements concerning local void fraction. 80
Figure 39: Comparison between turbulence interaction force models and the experimental measurements concerning local bubble interface velocity. 80

Figure 40: Comparison between phase interaction forces and the experimental measurements concerning local void fraction. 82
Figure 41: Comparison between phase interaction forces and the experiment concerning local bubble interface velocity. 82
Figure 42: Case 1 and Case 4 comparison between experimental and modelling results concerning local void fraction.....84
Figure 43: Case 1 and Case 4 comparison between experimental and modelling results concerning bubble interface velocity. 84
Figure 44: Case 2 comparison between experimental and modelling results concerning local void fraction.....85
Figure 45: Case 2 comparison between experimental and modelling results concerning bubble interface velocity. 85
Figure 46: Case 3 comparison between experimental and modelling results concerning local void fraction.....86
Figure 47: Case 3 comparison between experimental and modelling results concerning bubble interface velocity. 86
Figure 48: Case 5 comparison between experimental and modelling results concerning local void fraction.....87
Figure 49: Case 5 comparison between experimental and modelling results concerning bubble interface velocity. 87
Figure 50: The trend of decreasing liquid flow rate while having constant gas velocity (local void fraction) 89
Figure 51: The trend of decreasing liquid flow rate while having constant gas velocity (bubble interface velocity) 89
Figure 52: The trend of increasing the gas flow rate while having constant liquid velocity (local void fraction).....90
Figure 53: The trend of increasing the gas flow rate while having constant liquid velocity (bubble interface velocity) 90
Figure 54: T-junction in the experiment conducted by Davis and Fungtamasan.[12] ..93
Figure 55: Case Study 2 (Computational Domain).....95
Figure 56: Mesh independence analysis of case study 2.....96

Figure 57: Mesh Distribution of Case study 2 (using 5 mm element size) 96
Figure 58: The contour of gas volume fraction at bubble diameter 0.004 m 101
Figure 59: Gas volume fraction contour at the T-junction for sub-cases 1, 2 and 3, respectively 104
Figure 60: Gas volume fraction contours at the T-junction for sub-case 4 105
Figure 61: Bubble diameter contours of Sub-case 4.....105
Figure 62: Block flow diagram (BFD) for oil route in the CPP 108
Figure 63: Case study 3 (computational domain).....109
Figure 64: Mesh independence analysis of case study 3.....112
Figure 65: Mesh Distribution of Case study 3 (using 0.08 m element size) 112
Figure 66: Pathlines of velocity vectors at the T-junction inlet (plan view) 118
Figure 67: Velocity contour at the 90-degree bend outlet.....118
Figure 68: Velocity distribution contour at the T-junction inlet (plan and side views, respectively).....119
Figure 69: Gas volume fraction contour at the T-junction inlet (Plan and side views, respectively).....123
Figure 70: Proposed modified geometry for case study 3 to prevent the asymmetric flow distribution.....124
Figure 71: Gas volume fraction at the T-junction inlet for the modified geometry (plan and side views, respectively) 125

8.2 List Of Tables

Table 1: Experimental conditions in G. Kocamustafaogullari and Z. Wang experiment.[11] 56
Table 2: Case studies having constant gas superficial velocity.....66
Table 3: Case studies having constant liquid superficial velocity.....67
Table 4: Diameter of each bubble in the discrete population balance model.....98
Table 5: Comparison between predicted simulation parameters and experimental data 102
Table 6: Case study 3 – Boundary Conditions.....115
Table 7: CFD results of case study 3 (monophase system with maximum flowrate) 116
Table 8: CFD results of case study 3 (monophase system with turndown flowrate) 117
Table 9: CFD results of case study 3 (Multiphase flow).....121
Table 10: CFD results of case study 3 (Multiphase flow after the geometric modification).....124